

MASTER

Silicon rich nitride (SRN) for optical waveguide applications

Mertens, H.

Award date:
2002

[Link to publication](#)

Disclaimer

This document contains a student thesis (bachelor's or master's), as authored by a student at Eindhoven University of Technology. Student theses are made available in the TU/e repository upon obtaining the required degree. The grade received is not published on the document as presented in the repository. The required complexity or quality of research of student theses may vary by program, and the required minimum study period may vary in duration.

General rights

Copyright and moral rights for the publications made accessible in the public portal are retained by the authors and/or other copyright owners and it is a condition of accessing publications that users recognise and abide by the legal requirements associated with these rights.

- Users may download and print one copy of any publication from the public portal for the purpose of private study or research.
- You may not further distribute the material or use it for any profit-making activity or commercial gain

**Silicon rich nitride (SRN)
for optical waveguide
applications**

Hans Mertens

Master's Thesis
October 2001 – August 2002

Supervisors:

Associate Professor W. E. Svendsen (COM)
Professor H. W. M. Salemink (TUE)

HIGF

COM
Technical University of Denmark (DTU)
DTU - Building 345 west
DK-2800 Kgs. Lyngby
Denmark
Telephone: +45 4525 6352
Telefax: +45 4593 6581
www.com.dtu.dk

COBRA Inter-university Research Institute
Eindhoven University of Technology
Physics Department
Semiconductor Physics
P.O. Box 513
5600 MB Eindhoven
The Netherlands
Telephone: +31 (0)40 247 4852
Telefax: +31 (0)40 246 1339
www.cobra.tue.nl/groups/hf/hf_main.html



Abstract

This work is a contribution to a research project concerning the development of a material system for high-density integrated optics based on silicon rich nitride (SRN) waveguides. Three opportunities motivate the interest in SRN for this purpose: SRN has a relatively high refractive index (~ 2), SRN films have low mechanical stress (< 100 MPa) and SRN is compatible with scalable, in semiconductor industry developed fabrication methods. The relatively high refractive index enables the fabrication of waveguides with small bending radii (~ 40 μm) compared to conventional silica-on-silicon material systems (bending radii: ~ 5 mm), which enables to increase the integration density of optical devices considerably. The low mechanical stress facilitates device fabrication, and the compatibility with mainstream semiconductor processing industry offers a low-cost perspective.

The research performed includes the analysis of a number of SRN thin film and waveguide properties to investigate the suitability of SRN for optical waveguide applications. The investigation of the refractive index and thickness uniformity of SRN films by prism coupling resulted in the conclusion that the spread in both refractive index (< 0.03 %) and thickness (< 0.8 %) of the LPCVD-grown SRN films per wafer is good enough for device applications. From the investigation of N-H related absorption by Fourier transform infrared (FTIR) spectroscopy it has been concluded that the N-H related absorption loss in the SRN films is below 2 dB/cm in the 1550-nm region. The detection limit of the equipment used is too low to obtain more accurate information. The measurement of propagation loss in SRN slab waveguides by dual prism coupling demonstrates a propagation loss of SRN films within a range from 0.6 to 1.3 dB/cm in the 1550-nm region, which is regarded to be promising for future applications. The propagation loss can partly be attributed to N-H related absorption (peak height is 0.5-0.8 dB/cm), which implies an improvement could be realized by avoiding the formation of N-H bonds or by their removal. Two methods are proposed to realize this: improved anneal treatments and the application of deuterium.

<<confidential>>

Preface

The current thesis presents the work done for the examination project to obtain the Master of Science degree in Applied Physics at the *Eindhoven University of Technology* (TUE) in The Netherlands. The project has been carried out at *Education & Research Center COM* at the *Technical University of Denmark* (DTU) in Kongens Lyngby, Denmark, in the period from October 2001 to August 2002. The performed work is a contribution to a research project concerning the development of a material system and technology platform for high-density integrated optics. This project is referred to as *high-index project* and it is one of the research projects of the *Integrated Lightwave Circuits* (ILC) group of the *Glass Components and Materials* competence area of COM.

COM is an autonomous education and research center on telecommunications and optical technologies. It is affiliated with the Technical University of Denmark. The acronym *COM* stands for *Communications, Optics and Materials*. The current high-index project is a continuation of a project in which COM research assistants Peter Carøe Nielsen and Karin Nordström Andersen started the development of a waveguide technology for high-density integrated optics. In the period from October 2001 to August 2002 the project team consisted of four people: Associate Professor Winnie Svendsen (project leader), research assistant Karin Nordström Andersen, Ph. D. student Hugh Philipp and myself.

The master project was performed under supervision of Associate Professor Winnie Svendsen (COM) and Professor H. W. M. Salemink (TUE).

Hans Mertens
Kongens Lyngby, Denmark
July 2002

Acknowledgements

I would like to thank my supervisors Winnie Svendsen (COM) and Huub Salemink (TUE) for advice and support. Karin Nordström Andersen is acknowledged for her vital help in the cleanroom. Furthermore, I'm grateful to Hugh Philipp, Mikael Svalgaard, Christian Mikkelsen, Lasse Leick, Peter Carøe Nielsen and Rasmus Kousbelt Sandberg for their contributions and suggestions. Mogens Rysholt Poulsen is thanked for offering me the possibility to do my master project at COM, and J. C. Jacobsen (1811-1887) is acknowledged for providing inspiration.

Alfred Driessen of the *Lightwave Devices Group* (LDG) at the *University of Twente* in The Netherlands is acknowledged for giving permission to use this group's dual prism coupling setup for optical loss measurements of thin films. Chris Roeloffzen and Anton Hollink are thanked for their assistance in performing these measurements.

Finally, the complete ILC group is acknowledged for being a pleasant and inspiring working environment.

Contents

Abstract	i
Preface	iii
Acknowledgements	iv
Contents	v
1 Introduction	1
1.1 Optical communications	1
1.2 Integrated optics	1
1.3 Research objective	2
1.4 Thesis outline	3
2 Optical waveguiding	5
2.1 Light confinement by total internal reflection	5
2.2 Electromagnetic theory of light	6
2.3 Single-mode criteria	7
2.4 Mode size	7
2.5 Waveguide bending	8
2.6 Fiber-to-chip coupling efficiency	9
2.7 Summary	9
3 Silicon-related material systems for integrated optics	11
3.1 Material systems for integrated optics	11
3.1.1 Comparison between key material systems for integrated optics	11
3.1.2 Scope of the high-index project	12
3.2 Classification of silicon-related material systems	12
3.2.1 Doped silica	13
3.2.2 Silicon oxynitride	14
3.2.3 Silicon	15
3.3 Concept of the high-index project	16
3.3.1 Silicon rich nitride	16
3.3.2 Fiber-to-chip coupling efficiency	16
3.4 Summary	17
4 Applications of high-contrast material systems	19
4.1 Optical filters	19
4.1.1 Working principle of optical filters	19
4.1.2 Bandpass filtering	20
4.1.3 Dispersion compensation	21
4.2 Resonators	23
4.2.1 Optical switching	23
4.2.2 Lasing	24
4.2.3 Device miniaturization	24
4.3 Photonic bandgap structures	25
4.4 Optical interconnects for electronic devices	25
4.5 Summary	26

5	Analysis of silicon rich nitride film and waveguide properties	29
5.1	Background	29
5.1.1	Arguments for the choice of silicon rich nitride	29
5.1.2	Motivation for the performance of the described experiments	30
5.2	Refractive index and thickness uniformity of silicon rich nitride films	31
5.2.1	Introduction	31
5.2.2	Measurement principle	31
5.2.3	Experimental setup	31
5.2.4	Experiment	32
5.2.5	Results	32
5.2.6	Discussion	33
5.2.7	Conclusions	34
5.3	N-H related absorption in silicon rich nitride waveguides	34
5.3.1	Introduction	34
5.3.2	Measurement principle	34
5.3.3	Experimental setup	35
5.3.4	Experiment.	35
5.3.5	Results	35
5.3.6	Discussion	37
5.3.7	Conclusions	37
5.4	Propagation loss of silicon rich nitride waveguides	37
5.4.1	Introduction	37
5.4.2	Measurement principle	37
5.4.3	Experimental setup	38
5.4.4	Experiment.	39
5.4.5	Results	39
5.4.6	Discussion	41
5.4.7	Conclusions	42
5.5	Particles in silicon rich nitride films	42
5.6	Further research	42
5.6.1	Opportunity	42
5.6.2	Recommendations	43
5.6.3	Remaining questions	44
5.6.4	Conclusions	44
5.7	Summary	44
6	Silicon rich nitride ring resonator coupled to UV written waveguide	47
6.1	Introduction.	47
6.2	Fabrication.	47
6.2.1	Cleanroom processing	47
6.2.2	UV writing of straight waveguides	48
6.2.3	Resulting device structures	48
6.3	Characterization	49
6.3.1	Experiment	49
6.3.2	Results	49
6.3.3	Analysis	49
6.4	Discussion.	51
6.4.1	Fabrication	51
6.4.2	Characterization	51
6.5	Conclusions	52
7	Conclusions and recommendations	53
7.1	Concept of the high-index project	53
7.2	Analysis of SRN film and waveguide properties	53
7.3	SRN ring resonator coupled to UV written waveguide	55

A	Mathematical analogy between waveguide theory and quantum mechanics	57
	A.1 Light confinement according to the variational theorem	57
	A.2 Single-mode criteria	58
B	Numerical analysis of buffer thickness requirements	61
	B.1 Introduction	61
	B.2 Calculation method	61
	B.3 Experiment	63
	B.4 Results	65
	B.5 Discussion	65
	B.6 Conclusions	66
C	COM's waveguide fabrication process	67
D	Ring resonator modeling software	69
	D.1 Mathematical model	69
	D.2 Computer program	71
E	Poster and conference papers	73
	<i>Optical loss analysis of silicon rich nitride (SRN) waveguides and their applications, DFS..</i>	73
	<i>Optical loss analysis of silicon rich nitride waveguides, ECOC.....</i>	74
	<i>High-index ring resonator coupled to UV-written waveguide, ECOC.....</i>	76
	Bibliography	79

1 Introduction

1.1 Optical communications

The remarkable growth of the Internet and telecommunication markets poses growing demands on network requirements. Optical communications will in the long term be the cost-effective, technically superior solution to improve network performance to the level required by market needs. The main reason for this is the fact that optical signals (with carrier frequencies of ~ 100 THz) can be transmitted in fibers with very low loss (0.1 dB/km [7]). For electrical equivalents carrier frequencies have to be kept below a few GHz to avoid unacceptably high impedance in copper wires. The efficient transmission of high-frequency signals is the essential advantage of optical communications since it enables the use of a high bandwidth, which enhances transmission capacity [1]. Table 1.1 summarizes the differences and similarities between electrical and optical signal transmission.

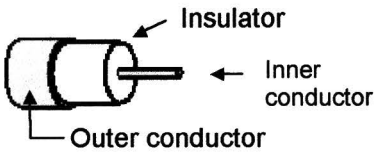
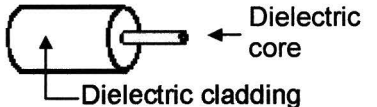
Transmission medium	Structure	Type of signal	Carrier frequency	Bandwidth	Velocity
Coaxial cable		Electromagnetic wave	~ 10 GHz	~ 0.5 GHz	$\sim 2.7 \cdot 10^8$ m/s
Optical fiber		Electromagnetic wave	~ 100 THz	~ 50 THz ¹	$\sim 2.1 \cdot 10^8$ m/s

Table 1.1: Comparison between signal transmission by coaxial cables and optical fibers. The signal types are the same, but the bandwidths differ significantly (factor of 10^5). In contrast to what is sometimes suggested (in reference 2 for example), the velocities are of the same order of magnitude and don't make the difference.

The way in which the bandwidth of a transmission medium affects transmission capacity is expressed by the *Shannon capacity theorem* [3]:

$$C = B \cdot C'_{SH} = B \cdot \log_2 \left(1 + \frac{S}{N} \right), \quad (1.1)$$

where C is the achievable capacity of the transmission medium (in bit/s), B is the bandwidth of the transmission medium (in Hz), C'_{SH} is the maximal spectral efficiency² and S/N is the signal-to-noise ratio. In the context of this section, the essential part of the theorem is that it gives a quantitative expression for the importance of bandwidth, which emphasizes the benefits of optical communications. The maximum achievable capacity C of an optical fiber is 150 Tbit/s [6].

1.2 Integrated optics

To exploit the bandwidth opportunities that are offered by optical communications a higher degree of *optical integration*³ is required than what can be achieved with current, commercially available technologies. The reason for this is that advanced integrated optical devices enable the implementation of optical multiplexing technologies in communication networks. Optical multiplexing technologies are inevitable to utilize the huge, physical data capacity of fibers. They are especially relevant for backbone networks, where the amount of data traffic is biggest and electrical devices are the bottleneck for network performances [4] due to the bandwidth

¹ The intrinsic loss mechanisms in silica-based optical fibers (Rayleigh scattering and IR absorption) limit the spectral bandwidth to about 50 THz, corresponding to a wavelength range from 1.2 to 1.6 μm [5].

² The expression for the maximal spectral efficiency, $\log_2(1+S/N)$, is only valid for linear transmission media. The influence of non-linear effects in optical fibers is complex. Reported calculations that take these effects into account predict a maximal spectral efficiency of 3 [6]. As a consequence, the theoretical transmission capacity of an optical fiber is about 150 Tbit/s.

³ The concept *optical integration* refers to the incorporation of several optical components for the generation, focusing, splitting, combining, switching, modulation and detection of light on a single substrate [7].

limitation of electronics, as is illustrated in figure 1.1. It is beyond the scope of this thesis to describe optical multiplexing technologies and their essential role in high-capacity communication networks. This information can be found elsewhere [8]. Additional, up-to-date information on technology trends in optical communications, integrated optics included, can be found on the website of the IST Thematic Network project OPTIMIST [9].

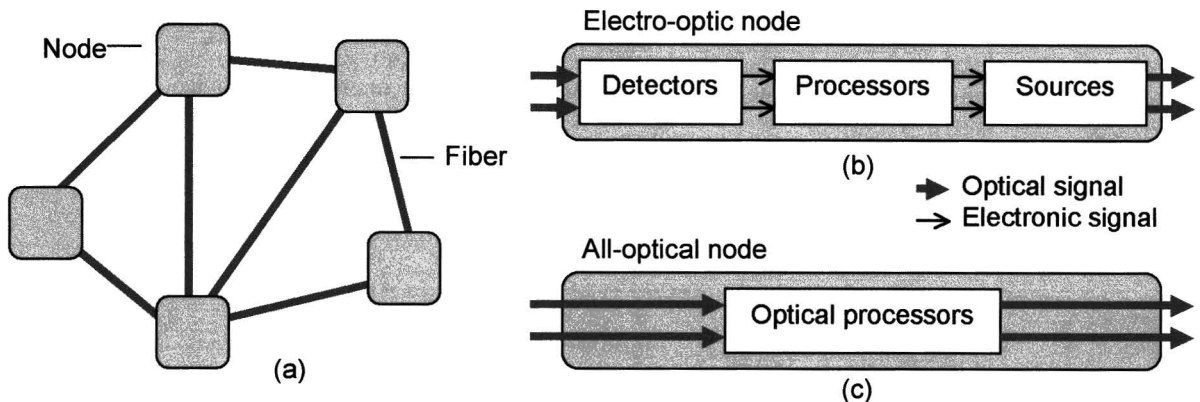


Figure 1.1: (a) Arbitrary fiber-optic network configuration. (b) Network node based on electronic data processing which acts as a bandwidth bottleneck. (c) All-optical node in which the electronic bottleneck has been removed.

In short, the realization of advanced integrated optical devices is highly desirable because of performance improvements and cost reductions of communication networks. This objective is the motivation behind research activities in the field of integrated optics.

Although optical communications can be classified as a real *killer technology*¹ [2], it is still in an early stage of its development, which is illustrated by the fact that the used data capacity of optical fibers in current communication networks is on the order of tens of Gigabits per second, far below the theoretical limit of 150 Tbit/s. Because of this and because of the fundamental scientific aspects, optical communications remains an attractive area for advanced university research that is focused on investigating the feasibility of new concepts and technologies.

1.3 Research objective

In the context of the situation described in section 1.2, COM's *high-index project* aims to develop a material system and technology platform for high-density integrated optics. The primary goal is to enable the potentially scalable realization of low-loss passive integrated optical devices for wavelength division multiplexing (WDM) networks (e.g., add/drop multiplexers, dispersion compensators, gain equalizers) with a higher degree of integration and complexity than what can be achieved with current, state-of-the-art technologies based on discrete components. Other applications might become available as research continues.

The concept under investigation comprehends the implementation of two types of waveguides on the same silicon substrate to benefit from the best properties of both types. In particular, these two types of waveguides are high-contrast Silicon Rich Nitride (SRN)² and low-contrast germanium-doped silica waveguides. The concept is described in detail in this thesis.

Contributions of the current master project to the high-index project are related to several aspects. The reason why it is not focused on one specific issue is because the state of the high-index project did not allow defining a narrow assignment. Contributions include the analysis of SRN thin film properties, cleanroom processing of waveguides and test components and the implementation of a method to characterize optical ring resonators. Besides, attention has been paid to the issue of transferring light between different types of waveguides. Substantial results are related to the optical loss analysis of SRN waveguides.

¹ In reference 2, a killer technology is defined as a technology that delivers enhanced system performance of a factor of at least a hundred-fold per decade.

² In the literature various abbreviations are used to refer to silicon rich nitride: SRN, SiRN and SiN. *SRN* is used in this thesis because it is the common abbreviation used at COM.

1.4 Thesis outline

The thesis has been divided in two main parts: chapters 2, 3 and 4 present a general analysis of the concept under investigation in the high-index project, while chapters 5 and 6 describe the experimental work performed during this master project. The exact structure is as follows:

Chapter 2 gives an overview of waveguide-theoretical aspects that are relevant for the high-index project. Especially the influence of the index contrast of waveguides on their optical properties is explained because this is an important issue for the concept under investigation. **Chapter 3** discusses the quantitative consequences of the application of particular material systems on the waveguide theory described in chapter 2. The added value of the material system under development in the high-index project is explained on the basis of a comparison with alternative material systems. The comparison is mainly focused on silicon-related material systems. **Chapter 4** lists a number of potential applications of the material system under development. The objective of this chapter is to explore to what extent the functionality of optical devices can be expanded by using high-contrast material systems (e.g., the material system under development) instead of conventional low-contrast silicon-related material systems.

Chapter 5 describes the experiments done to investigate the suitability of silicon rich nitride (SRN) for optical waveguide applications. This chapter contains the description of three experiments: index and thickness uniformity measurements of SRN films, the investigation of N-H related absorption in silicon rich nitride by Fourier transform infrared spectroscopy and the investigation of propagation loss in SRN waveguides by dual prism coupling. Besides, a number of possible process improvements are discussed. **Chapter 6** describes an experiment in which an SRN ring was coupled to a UV written waveguide. The objective of this experiment was to investigate an essential part of the concept of the high-index project: the integration of low- and high-contrast waveguides on the same substrate. Parts of this experiment were performed within the framework of the current master project.

Chapter 7 summarizes the conclusions and recommendations and five appendices contain secondary information: **Appendix A** describes a mathematical analogy between waveguide theory and quantum mechanics. The analogy gives insight in the mathematical similarity between the confinement of a particle-wave in a quantum well and the confinement of an optical mode in a waveguide. **Appendix B** presents an analysis of buffer thickness requirements of various silicon-related material systems. The objective of this analysis was to investigate to what extent the buffer fabrication time could be reduced for components based on silicon rich nitride waveguides compared to components based on germanium-doped silica waveguides. **Appendix C** gives an overview of COM's waveguide fabrication technology. This overview is background information for chapters 5 and 6. **Appendix D** describes a mathematical model of a ring resonator that can be used to investigate the behavior of ring resonators as function of the parameters optical loss in the ring and coupling ratio between ring and straight waveguide. The model provides insight in the applications of ring resonators. Besides, the model provides the possibility to deduce the optical loss in the ring and coupling ratio between ring and straight waveguide from the transmission spectra of fabricated ring resonators. **Appendix E** shows the poster that has been presented at the annual meeting of the Danish Physical Society as well as the papers that have been accepted for ECOC 2002.

2 Optical waveguiding

This chapter presents an overview of the main concepts of optical waveguide theory. The aim is to provide a theoretical basis to facilitate the reading of this work. Comprehensive accounts on optical waveguide theory can be found elsewhere [10], [11], [12]. The role of the *relative index difference* Δ is explained extensively because this parameter is important for the concept of the high-index project. The definition of the relative index difference of a waveguide, which is sometimes referred to as *height profile parameter* [10], is given by:

$$\Delta = \frac{n_{co}^2 - n_{cl}^2}{2n_{co}^2} = \frac{1}{2} \left(1 - \frac{n_{cl}^2}{n_{co}^2} \right), \quad (2.1)$$

where n_{co} and n_{cl} are the refractive indices of the core and the cladding of the waveguide under consideration. See the next section for an explanation of the terms *core* and *cladding*.

2.1 Light confinement by total internal reflection

Light is usually described in one of three ways: as rays, as waves or as photons. Some phenomena in optical communications can be described by the simple model of ray optics which is also referred to as geometrical optics. The most important one is the effect that light can be confined in a medium with a certain refractive index (core) that is imbedded in a medium with a lower refractive index (cladding). This confinement effect forms the basis of waveguiding in optical communications. It can be explained by total internal reflection as is illustrated in figure 2.1 for a waveguide geometry that can be encountered in integrated optics.

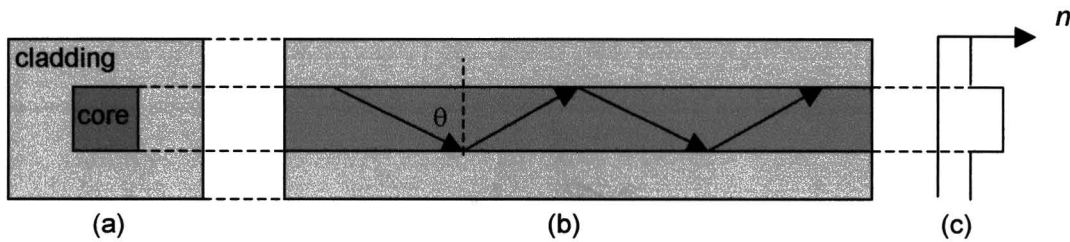


Figure 2.1: (a) Cross section of an optical waveguide. (b) Longitudinal section of the waveguide which illustrates the confinement of light by total internal reflection. (c) Refractive index profile of the waveguide.

According to the model of total internal reflection, a ray of light is reflected completely at the interface between core and cladding if the angle of incidence θ is larger than the critical angle θ_c . The critical angle is dependent on the relative index difference, as can be derived from Snell's law [7]:

$$\theta_c = \sin^{-1} \left(\frac{n_{cl}}{n_{co}} \right) = \frac{1}{2} \cos^{-1} (1 - 4\Delta). \quad (2.2)$$

Because of the fact that the angle of incidence decreases in waveguide bends, it can be deduced from formula 2.2 that an increase in relative index difference enables the reduction of bending radii of waveguides, as is illustrated in figure 2.2. To quantify this effect and to describe optical waveguiding in a better way¹, it is necessary to switch from the limited description of ray optics to the more general, electromagnetic theory of light (see section 2.2).

¹ The electromagnetic description is better in the sense that it is able to deal with substantial changes in the refractive index on a length scale that is comparable to the wavelength of light, in contrast to ray optics.

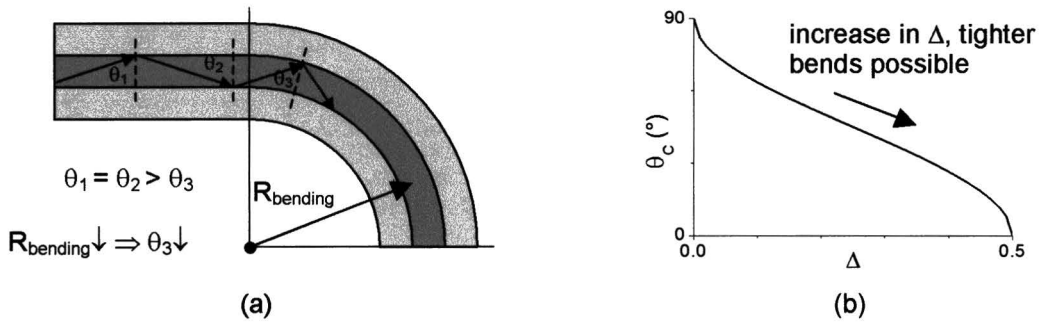


Figure 2.2: (a) Guiding of light rays in a bent optical waveguide, which illustrates that the minimal angle of incidence θ decreases as the bending radius decreases. (b) Influence of the relative index difference Δ on the critical angle θ_c according to formula 2.2.

2.2 Electromagnetic theory of light

In the context of optical communications, the best way of regarding light is to think of it as an electromagnetic wave. The reason is that the length scale of the structures that are involved is comparable to the wavelength of light. Therefore, the Maxwell equations are in principle the starting point for any optical waveguiding analysis. However, the complexity of this set of coupled equations makes it very complicated [13]. As a result there are very few exact analytical solutions, which do not include the types of cross-sectional geometries and refractive index profiles encountered in integrated optics. As a consequence, detailed descriptions of optical waveguiding in integrated optics rely on approximations and numerical methods. The mathematical complexity of the mode profiles under consideration is illustrated in figure 2.3.

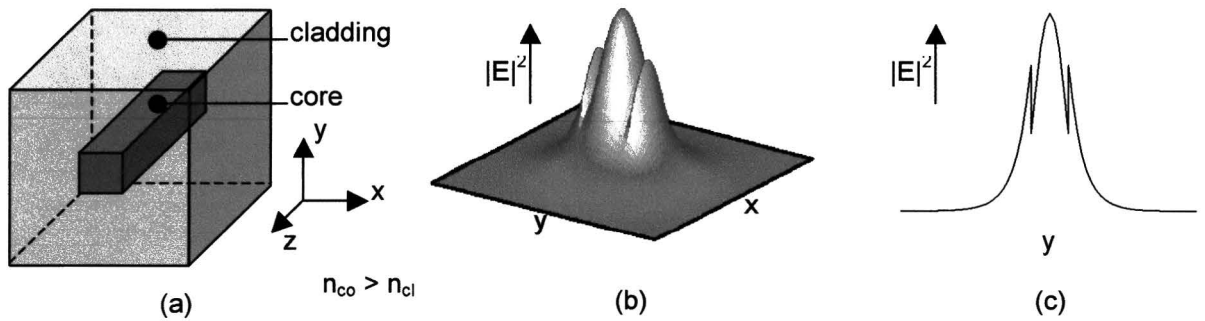


Figure 2.3: (a) Typical geometry for waveguides encountered in integrated optics. (b) Cross-sectional profile of the fundamental mode for one polarization on a linear scale. (c) Two-dimensional view of the profile. The discontinuities (see side-lobes) illustrate the mathematical complexity of the solutions of the Maxwell equations.

The discontinuities in the displayed intensity profile originate from the fact that the Maxwell equations require that the *electric displacement* \mathbf{D} is continuous (see reference 13 for exact conditions for this to be true). As a consequence the boundary condition for the electric field \mathbf{E} at the interface between core and cladding is given by:

$$E_{co,\perp} = \frac{\epsilon_{cl}}{\epsilon_{co}} E_{cl,\perp} = \frac{n_{cl}^2}{n_{co}^2} E_{cl,\perp} = (1 - 2\Delta) E_{cl,\perp} \Leftrightarrow \frac{E_{co,\perp}}{E_{cl,\perp}} = 1 - 2\Delta. \quad (2.3)$$

Formula 2.3 shows that an increase in relative index difference results in an increase in step size of the discontinuity.

As in general the mathematics of electromagnetism is complicated, the next sections describe optical waveguiding in a qualitative way with the objective to provide physical insight. The attention is focused on the influence of the relative index difference of a waveguide on single-mode criteria, mode size, bending radius and fiber-to-chip coupling efficiency. All these aspects are relevant for the high-index project. The quantitative consequences of the application of particular material systems, including the material system under development in the high-index project, are presented in chapter 3.

2.3 Single-mode criteria

One of the consequences of increasing the relative index difference of waveguides in order to enable the reduction of bending radii is that it is required to reduce the core dimensions of waveguides to maintain single-mode operation. The reason why single-mode operation of waveguides is necessary is that the propagation properties of various modes differ significantly (i.e. different propagation constants and difference in confinement), which makes it practically impossible to fabricate useful devices for telecommunication purposes based on multi-mode waveguides.

The relation between core dimensions, relative index difference Δ and single-mode operation can be expressed based on the dimensionless *waveguide parameter* V which is an important parameter in the electromagnetic description of optics:

$$V = \frac{2\pi}{\lambda} \rho n_{co} \sqrt{2\Delta}, \quad (2.4)$$

where ρ is the characteristic dimension of the cross-section of the core (i.e., diameter for a fiber, width for a square waveguide) [11].

The waveguide parameter V , which is also known as *degree of guidance* [11] or *normalized frequency* [17], needs to be below a certain cutoff value V_c for a waveguide to be single moded [11]:

$$V < V_c. \quad (2.5)$$

For fibers, V_c is equal to 2.405. A detailed analysis is required to find an appropriate value of V_c for rectangular waveguides with a high relative index difference. The performance of such an analysis is beyond the scope of this thesis. However, it is clear from formulas 2.4 and 2.5 that the characteristic dimension of a waveguide core needs to be reduced to maintain single-mode operation when the relative index difference is increased.

An alternative way to understand the relationship between relative index difference and core dimensions, which is based on a mathematical analogy between waveguide theory and quantum mechanics, is described in appendix A. In chapter 3 attention is paid to the values of the core dimensions of single-mode waveguides for a number of material systems with various relative index differences.

2.4 Mode size

In contrast to what the description of total internal reflection suggests (see section 2.1) an optical mode is partly located outside the core of a waveguide. This could already be seen in figure 2.3. The extent of optical modes in the cladding of waveguides has important consequences for the waveguide fabrication process. In particular, optical modes have to be kept away from the substrate (if the substrate has a refractive index higher than the cladding) to avoid leakage to the substrate. This leakage effect is a result of the fact that light tends to localize itself in regions with a high refractive index. This phenomenon can be understood on the basis of the electromagnetic variational theorem, as is described in appendix A.

The technological consequence of this leakage effect is that the thickness of the buffer layer of a waveguide, indicated with d_{buffer} in figure 2.4, should be made sufficiently large. The required value for the buffer thickness increases with the extent of the mode profile in the cladding which decreases with relative index difference. So, increasing the relative index difference Δ relaxes the requirements for the buffer thickness:

$$\Delta \uparrow \Rightarrow d_{buffer, min} \downarrow \quad (2.6)$$

It is beyond the scope of this thesis to derive an analytical relationship between relative index difference and required buffer thickness for rectangular waveguides in an analytical way. However, appendix B presents a numerical analysis of the required buffer thickness for various material systems.

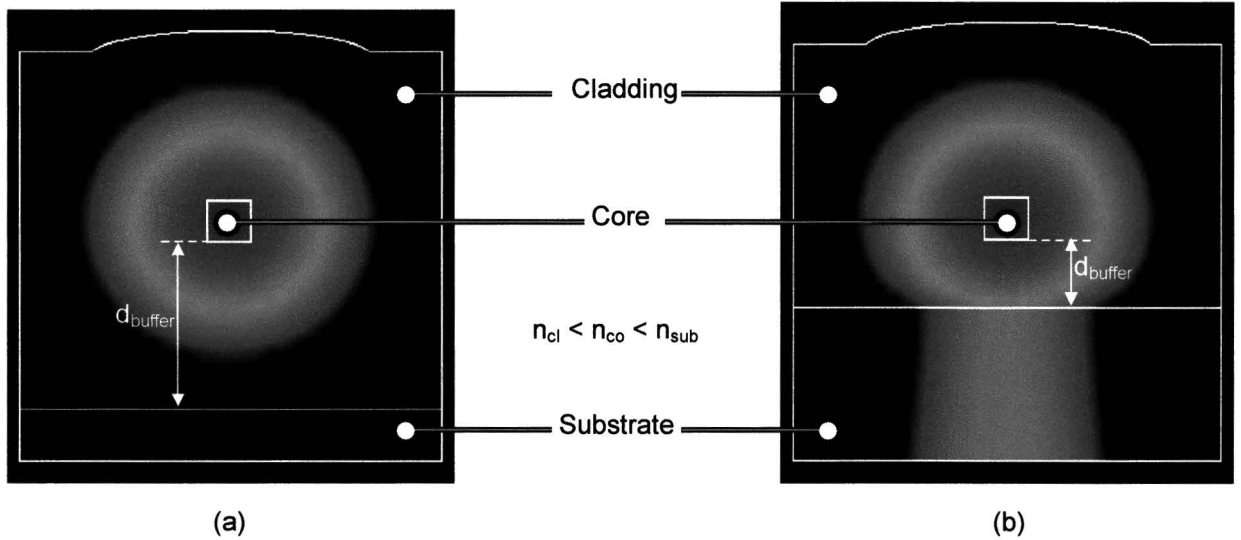


Figure 2.4: Mode profiles a properly designed waveguide (a). Mode profile of a waveguide which buffer thickness is a too small (b). The displayed intensity profile represents the size of $|E|^2$. It can be seen how buffer thickness affects substrate leakage.

2.5 Waveguide bending

The physical picture of wave propagation in a bent waveguide is that the wavefront of the mode has to travel a larger distance on the outer side of the bend than on the inner side to maintain a constant phase over the cross section of the waveguide. This situation corresponds to a straight waveguide with a tilted refractive index profile, since both increasing the refractive index n and increasing the physical length $l_{physical}$ result in an increase in optical path length ($l_{optical} = n \cdot l_{physical}$). This analogy, which is illustrated in figure 2.7, can be used to calculate the mode profiles of a bent waveguide.

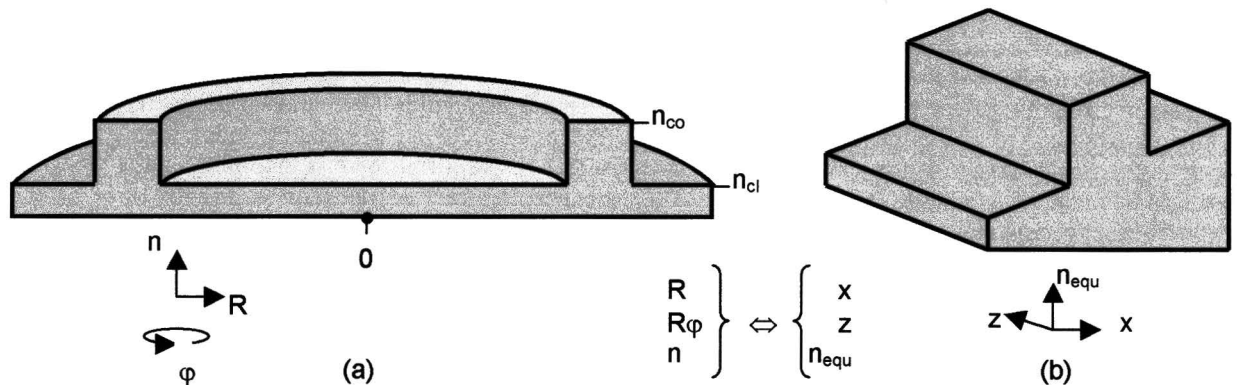


Figure 2.7: (a) Refractive index profile of a bent waveguide and (b) the equivalent refractive index profile for a straight waveguide. The analogy between these two descriptions, which is based on the equation of optical path length, has been indicated. Notice that the structures are not waveguide geometries but refractive index profiles.

If the resulting mode profile has a significant overlap with the cladding of the equivalent refractive index profile, next to the mark that has been indicated with *breaking point* in figure 2.8, then that part of the field is radiated into the cladding. This effect is similar to substrate leakage which has been described in section 2.4. From figure 2.8 it can be deduced that two effects of increasing the relative index difference have positive consequences for the configuration depicted in figure 2.8: the potential trap increases and the extent of the tail in the cladding decreases (see appendices A and B respectively). Therefore, the profile can be tilted more, without the optical mode having an overlap with the cladding. However, an issue that should be considered in the design is that the optical mode should not have a low effective index, because that would move the breaking point towards the core.

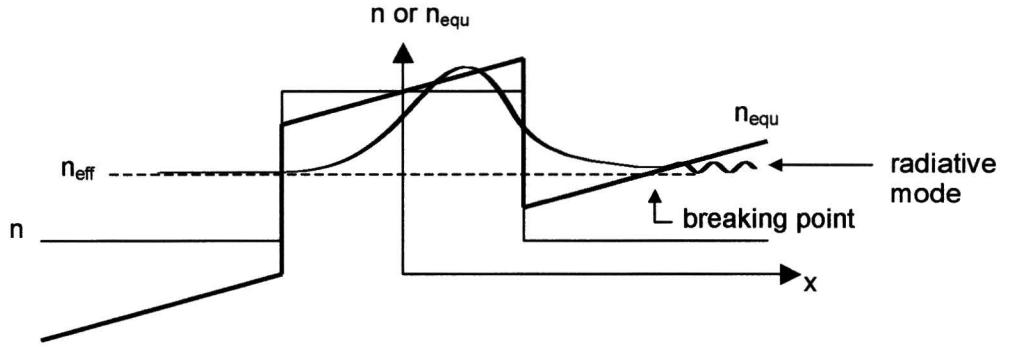


Figure 2.8: Illustration of bend loss that is based on optical tunneling in an equivalent index profile.

An additional conclusion that can be drawn from the shape of the equivalent index profile from figure 2.7 is that the index profile of a waveguide with a perfectly square cross section is not symmetrical in a bend. This means that wave propagation in a bent waveguide is polarization dependent. The dependence is stronger for tight bends because the tilt of the equivalent index profile increases with decreasing bending radius.

2.6 Fiber-to-chip coupling efficiency

The size of the mode in an optical waveguide decreases when the relative index difference increases (and the core dimensions are reduced to preserve single-mode operation), see for example the mode profiles in figure B.2 in appendix B. A consequence is that the fiber coupling loss ($L_{coupling}$) of an integrated optical waveguide decreases with increasing relative index difference Δ :

$$\Delta \downarrow \Rightarrow L_{coupling} \uparrow \quad (2.7)$$

This effect can be attributed to the growing mismatch in the spatial dependence between the modes in fiber and waveguide, where the mode size of standard fibers (FWHM $\sim 15 \mu\text{m}$) is large compared to integrated optical waveguides (see also figure B.2 in appendix B). The coupling loss $L_{coupling}$ (in dB) between two modes is given by the overlap integral:

$$L_{coupling} = -10 \log \left(\frac{\left(\int_{area} \phi_1 \phi_2 dA \right)^2}{\int_{area} \phi_1^2 dA \int_{area} \phi_2^2 dA} \right), \quad (2.8)$$

where the normalized electric fields of fiber and waveguide are denoted by ϕ_1 and ϕ_2 and the integrals are over the waveguide cross-section [11], [17].

As the profiles of optical modes in rectangular waveguides are complicated (see figure 2.3), it is difficult to derive a more detailed expression of relative-index-difference dependence of the coupling loss than formula 2.7 analytically. An approximation that is often used to overcome this problem is to describe the modes as Gaussian functions [11]. However, this approximation is not applicable on waveguides with a large relative index difference, because the discontinuity (see figure 2.3) in the electric field is not negligible (see chapter 3). Therefore, the relevance of such an approximation is very limited in the context of the high-index project. As an alternative, the overlap integrals for waveguides with various relative index differences have been calculated numerically. This analysis has been enclosed in appendix B.

2.7 Summary

In this chapter the main concepts of optical waveguiding have been described briefly to present a theoretical basis to facilitate the reading of this work. Attention has been paid to two different formalisms by which light can be described: ray optics and electromagnetism (sections 2.1 and 2.2). It has been shown that the simple model of ray optics can explain some important phenomena, like the confinement of light, but that it does not give an accurate description of optical waveguiding in general.

The electromagnetic theory of light has been used to explain the index contrast dependence of single-mode criteria, mode size, bending radius and fiber coupling efficiency of integrated optical waveguides. In summary, it

can be said that to be able to decrease the bending radius of waveguides, it is necessary to increase the relative index difference (sections 2.2 and 2.5). As a consequence, the dimensions of the core need to be reduced to preserve single-mode operation (section 2.3). Furthermore, the fiber-to-chip coupling efficiency decreases (section 2.6), which asks for concepts and components that can eliminate this negative effect. Another phenomenon is that the mode size decreases (section 2.4) which is positive for the relaxation of the requirements for the thickness of the buffer layer. Quantitative consequences of increasing the relative index difference are presented in chapter 3. More extensive waveguide-theoretical explanations can be found in the references specified in this chapter.

3 Silicon-related material systems for integrated optics

The current chapter presents a review of silicon-related material systems for integrated optics, where the term *silicon-related*¹ refers to material systems that incorporate the element silicon. Involved materials include silica (SiO₂), silicon oxynitride (SiON), silicon nitride (SiN) and silicon (Si). The concept of the high-index project is related to the differences between the various silicon-related material systems, which clarifies why the review has been included in this thesis.

First, silicon-related material systems are compared to other material systems to place their pros and cons in a larger context. Subsequently, the similarities and the differences between the various silicon-related material systems are described, and finally the concept of the high-index project is explained.

3.1 Material systems for integrated optics

A *material system for integrated optics* is the combination of materials that is used for the fabrication of integrated optical circuits. A material system forms the link between optical waveguide theory described in chapter 2 and the actual realization of devices. It is closely related to an associated *technology platform* which is the equipment that is applied in the fabrication process. The choice of a material system has technological and waveguide-theoretical consequences for both performance and cost of devices.

In integrated optics there is a wide variety of technologies available and there is not yet a dominant manufacturing process. In comparison: in mainstream semiconductor industry, silicon is the material, CMOS is the fabrication technology and transistors are the building blocks. This difference is an indication of the early stage of development of integrated optics.

3.1.1 Comparison between key material systems for integrated optics

Key material systems for integrated optics include III-V semiconductors, silicon-related material systems (especially doped silica) and polymers. Every material system has its specific pros and cons. The main differences are summarized in table 3.1. The comparison is based on more extensive reviews which can be found elsewhere [18], [19].

Property	Doped silica	III-V semiconductors	Polymers
Availability of light-emitting components	Limited (rare-earth doping required)	Yes (direct bandgap)	Limited (rare-earth doping required)
Insertion loss (demonstrated)	Low	High (due to the low fiber-to-chip coupling efficiency)	Low
Integration density (demonstrated)	Low	High	Low
Availability of non-linear structures	Limited	Good	Good
Scalability / low cost perspective	Good	Less good	Very good
Maturity of manufacturing methods	Very good	Good	Less good

Table 3.1: Overview of the differences between some key material systems for integrated optics. The comparison is based on a number of sources [18] - [22]. Due to the shortness of the comparison, the table gives a simplified picture of reality.

¹ The term *silicon-based* has been avoided because this term, which is often used in the literature, doesn't cover materials like silica, silicon oxynitride and silicon nitride.

In general, it can be said that doped silica is the dominant technology for passive components (e.g., optical bandpass filters, dispersion compensators and gain equalizers). The low integration density and the lack of both highly nonlinear and compact active structures are major disadvantages of this technology.

III-V semiconductors (e.g., indium phosphide) allow the monolithic integration of electronic functions as well as both active and passive optical functions, which is a big pro. Disadvantages include the low fiber-to-chip coupling efficiency and the fact that the technology relies on crystalline instead of amorphous materials, which limits the scalability of the fabrication process. Consequently, the economy of scale is not as applicable to III-V semiconductors as it is to silicon-related material systems. Some of the most advanced integrated optical devices, however, have been realized in III-V semiconductors [23], [24] which indicates the opportunities of this technology.

The third category that is mentioned in table 3.1 is polymer-based integrated optics. The attractiveness of polymers includes the wide range of pronounced properties that can be encountered in these materials (e.g., strong thermo-optic effects) and the fact that the involved processing equipment is ultralow cost. Current disadvantages include the poor long-term temperature stability of devices and the relative immaturity of polymer device manufacturing methods [21].

For the sake of completeness, it should be mentioned that so-called *speciality fibers* also have the capability to perform an increasingly wide range of tasks in optical networks (e.g., dispersion compensation) [25].

3.1.2 Scope of the high-index project

The future will decide which material systems for integrated optics will become industry standards. Important criteria are device performance, manufacturability and cost. Silicon-related material systems have a large potential on account of their compatibility with conventional semiconductor processing industry. However, the issues of low integration density and lack of both highly nonlinear and compact active structures limit their applications significantly.

In the context of these deficiencies, the high-index project aims to increase the integration density of devices that are based on established silicon-related material systems, particularly doped silica, while maintaining their positive features. Besides, the high-index project opens up possibilities to improve the performance of active and nonlinear components based on silicon-related material systems. This subject is discussed in chapter 4.

Before the primary concept of the high-index project is described in section 3.3, a classification of silicon-related material systems and an overview of the status of silicon-related integrated optics are presented in section 3.2. These descriptions enable to clarify and contrast the concept of the high-index project in a better way.

3.2 Classification of silicon-related material systems

Waveguides that are based on silicon-related material systems have a structure as is depicted in figure 3.1. The base is a silicon ($n = 3.45^1$) substrate with on top of it a silica (SiO_2 , $n = 1.45$) buffer layer. The waveguide cores are positioned on top of the buffer layer with a cladding of borophosphosilicate glass (BPSG) above them. The refractive index of the BPSG is matched to the refractive index of silica, which is indicated by the dashed line and the correspondence of both colors in figure 3.1. An overview of the fabrication process used at COM is given in appendix B.

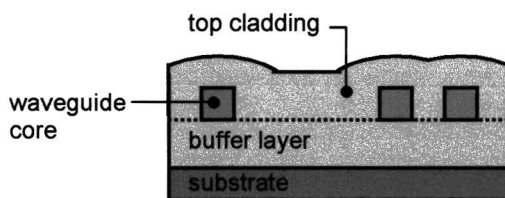


Figure 3.1: Cross-sectional geometry of an arbitrary component that is based on a silicon-related material system. Three waveguide cores are visible.

The essential difference between waveguides based on the various silicon-related material systems is the core material which can either be doped silica², silicon oxynitride, silicon nitride or silicon. These materials have significantly different refractive indices, which implies that waveguide properties as bending radius, core dimensions, mode size and fiber-to-chip coupling efficiency are considerably different because of the arguments that have been explained in chapter 2. In addition to these waveguide-theoretical consequences, there are also

¹ All refractive indices n in this thesis are specified for a wavelength of 1550 nm, unless specified otherwise.

² Dopants that can be used to induce an increase in refractive index include germanium, phosphorus and titanium [26]. At COM, germanium is the main dopant material. Therefore, this chapter concentrates on germanium-doped silica to explain the properties of doped silica waveguides and components.

differences in material properties that affect optical waveguiding. Both aspects are discussed in the next subsections.

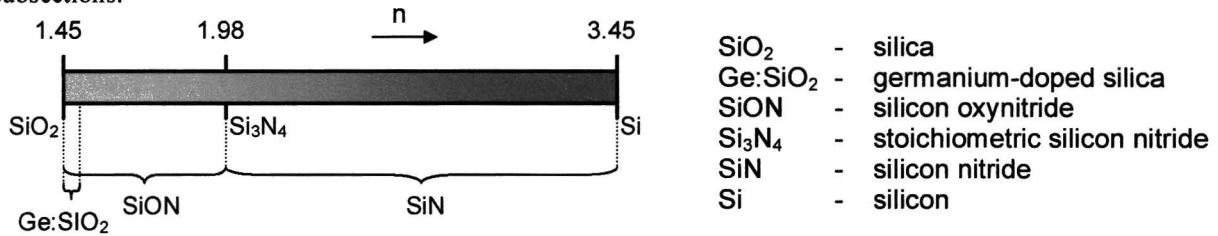


Figure 3.2: Overview of the refractive index values of a number of silicon-related materials. It is illustrated that the refractive index can be adjusted between 1.45 and 3.45.

Figure 3.2 shows a classification of silicon-related materials that is based on refractive index. Germanium-doped silica has a refractive index between 1.45 and about 1.48, depending on the germanium concentration. The maximum value is determined by the maximum achievable doping concentration. Silicon oxynitride can have a refractive index between 1.45 and 2.0. The exact value can be tuned by varying the oxygen-nitrogen ratio [27]. Because nitrogen is not a dopant but a part of the material matrix, the atomic nitrogen fraction is not limited to a few percent. The refractive index of silicon oxynitride can be increased even further (> 3) if the relative silicon content is increased [28]. Above a value of 2.0 the refractive index can also be tuned without using oxygen by adjusting the silicon-nitrogen ratio. The highest refractive index value in silicon-related material systems is 3.45, which is the value of silicon itself.

The next subsections explain the properties of waveguides with cores made from doped silica, silicon oxynitride and silicon in more detail. The use of silicon nitride as core material is discussed in section 3.3, because this material is used in the high-index project

3.2.1 Doped silica

The doped silica technology [26], which was introduced in the late 1980s, is the most mature silicon-related technology for integrated optics. As discussed in section 3.1, doped silica waveguides are characterized by a large minimum bending radius and a high fiber coupling efficiency. Besides, doped silica waveguides have a relatively low propagation loss, which can be attributed to the wide bandgap (~ 9 eV¹ [29]) and the good homogeneity of the material.

Table 3.2 shows an overview of the values of the waveguide properties that have been described in chapter 2 for three relative index differences that are representative for germanium-doped silica waveguides. The table displays the absolute refractive index step, which is an alternative parameter to quantify the refractive index difference between core and cladding, the typical core dimensions of single-mode waveguides, the full-width half-maximum of the optical mode, the minimum bending radius² and the fiber coupling loss. In addition, typical values for the propagation loss have been included. The displayed values have been obtained from the literature and from calculations performed with the mode solver *Selene* [30]. All information in table 3.2, as well as in all other tables in this chapter, applies to a wavelength of 1550 nm which is the standard for optical communications because the attenuation in silica fibers is minimal at this wavelength (~ 0.1 dB/km) [7].

¹ A wide bandgap is positive for the transparency because it implies that light used in optical communications ($\lambda = 1550$ nm $\Leftrightarrow E = 0.8$ eV) cannot induce energy absorbing band-to-band electron transitions.

² The minimum bending radius of a waveguide is a somewhat arbitrary quantity since it depends on the bend loss that is tolerated. Because the values in table 3.2 as well as in the other tables in this chapter are originating from several sources (see table captions), based on different and sometimes unspecified criteria, they can only be regarded as indications.

Relative index difference	Absolute refractive index step	Core dimensions ($\mu\text{m} \times \mu\text{m}$)	FWHM of mode (μm)	Minimum bending radius (mm)	Fiber coupling loss (dB)	Propagation loss (dB/cm)
0.0025	0.004	8 x 8	13	25	0.01	0.01
0.0075	0.011	6 x 6	9	5	0.4	0.01
0.012	0.017	4.5 x 4.5	7	2.2	1.2	0.03

Table 3.2: Overview of the properties of germanium-doped silica waveguides. Three values of the relative index difference are displayed to give an indication of the influence of this parameter. The overview is based on several sources [26], [31], [32].

An example that illustrates some of the pros and cons of doped silica is the optical amplifier technology developed by *Cisilias*¹ [33] which is a spin-off company of COM. Their optical amplifiers are so-called erbium-doped waveguide amplifiers (EDWA's) which consist of germanium-doped waveguides that are also doped with the rare-earth element erbium. Erbium enables to amplify signals around a wavelength of 1550 nm when it is pumped with light with a wavelength of 980 nm. EDWA's are related to erbium-doped fiber amplifiers (EDFA's) which are more established optical amplifiers [34]. Advantages of EDWA's in comparison with EDFA's are their compactness, the fact that they can be integrated in arrays and the fact that they can be combined with passive components (e.g., pump/signal multiplexers and gain equalizers) on a single substrate. Figure 3.3 shows an illustration of an EDWA. The figure illustrates the major disadvantage of rare-earth-based optical amplifiers: long (~ 1 m) erbium-doped waveguides are required to create practical devices due to the low gain per unit length. Besides, figure 3.3 shows how the minimum bending radius of waveguides limits the possibilities to reduce the size of integrated optical circuits.

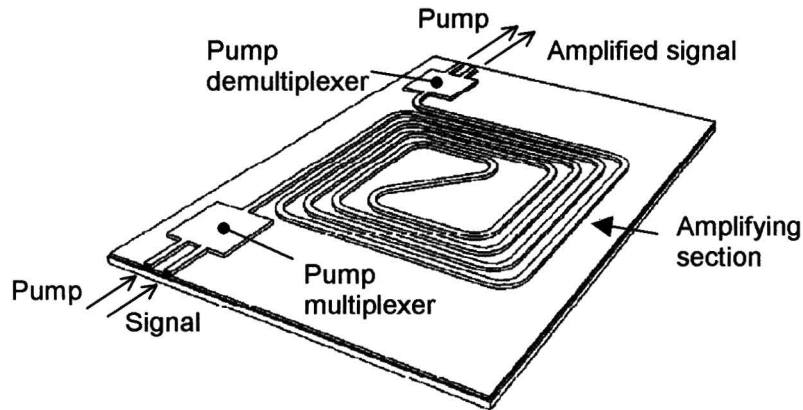


Figure 3.3: Layout of an erbium-doped waveguide amplifier (EDWA). Two disadvantages of doped silica are illustrated: long amplifier sections are required to obtain a significant gain per device and the density of waveguides in the center of the spiral is limited by the minimum bending radius.

3.2.2 Silicon oxynitride

Silicon oxynitride provides the possibility to produce integrated optical devices with a higher degree of integration than is possible with doped silica. In principle, the refractive index can be increased to about 2.0. However, in that case the decrease in fiber-to-chip coupling efficiency is significant². This could justify to increase the refractive index only slightly.

A silicon oxynitride technology that is based on such a trade-off between small minimum bending radius and high fiber-to-chip coupling efficiency has been developed by IBM [4]. In this technology, silicon oxynitride with a refractive index of 1.50 is used as core material. The corresponding waveguide characteristics are shown in table 3.3. The displayed core dimensions are not the exact values because the core of the waveguide is not rectangular, but has a ridge structure [35]. The displayed fiber coupling loss can be reduced to 1.7 dB by incorporating spot-size converters [36].

¹ Recently Cisilias merged with IONAS to form NKT Integration.

² For single-mode waveguides with a core index of 2, the coupling loss to standard single-mode fibers is about 10 dB.

Relative index difference	Absolute refractive index step	Core dimensions ($\mu\text{m} \times \mu\text{m}$)	FWHM of mode (μm)	Minimum bending radius (mm)	Fiber coupling loss (dB)	Propagation loss (dB/cm)
0.0033	0.05	3 x 2	4	1.5	3.8	0.1

Table 3.3: Overview of the properties of IBM's silicon oxynitride waveguides. The information is based on reference 35.

An example of a device that has been realized in IBM's SiON technology is the add-after-drop filter for wavelength division multiplexed communication systems that is shown in figure 3.4. The device is based on resonant couplers and can be tuned thermo-optically. Positive features of the displayed design are the good transmission characteristics (flat passband, low cross-talk, etc.) and the easy tunability [37]. The chip size is 75 mm x 5.6 mm. An equivalent component based on doped silica would be considerably bigger due to the large number of waveguide bends.

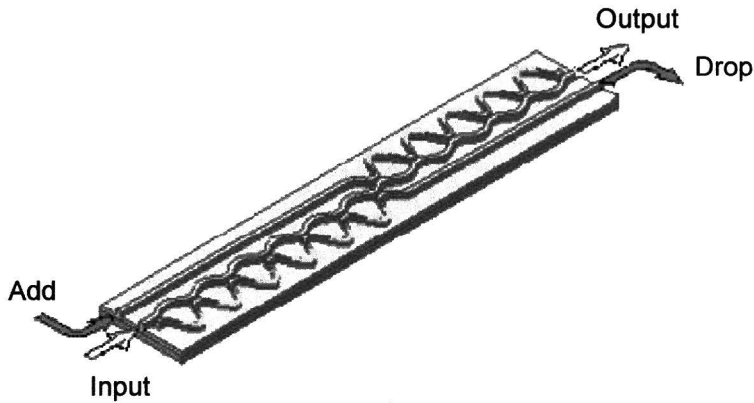


Figure 3.4: Illustration of an add-after-drop filter based on IBM's silicon oxynitride technology. The chip dimensions are 75 mm x 5.6 mm.

IBM's SiON technology is the first silicon-related technology other than doped silica that is on such a level that it can be regarded as a competitive optical technology for passive applications. However, the integration density is still low. This encourages investigating the feasibility of new technologies that could lead to further improvements.

3.2.3 Silicon

The utilization of silicon as core material is advantageous for optimal size reduction of optical circuits (considering silicon-related material systems). However, the associated technological requirements are high due to the small cross-sectional waveguide dimensions that are required to establish single-mode operation. Moreover, silicon has less good optical properties than both silica and silicon oxynitride. Nevertheless, promising results on silicon-based integrated optics have been obtained by MIT. One of their achievements is the reduction of propagation loss in silicon waveguides from over 30 dB/cm to 0.8 dB/cm [38], [39]. Information on their waveguides is shown in table 3.4.

The step size of the discontinuity in the electric field, which has been mentioned in chapter 2 (see formula 2.3), is significant for silicon waveguides. The ratio $E_{co,\perp} / E_{cl,\perp}$ is equal to 0.18. In doped silica and silicon oxynitride, this discontinuity can be largely neglected ($E_{co,\perp} / E_{cl,\perp} > 0.93$).

Potential applications of silicon waveguides do not only include the realization of all-optical devices, but also the replacement of electrical interconnects on electronic chips. This application is described briefly in section 4.4, because it could have a serious impact on the evolution of integrated optics.

Relative index difference	Absolute refractive index step	Core dimensions ($\mu\text{m} \times \mu\text{m}$)	FWHM of mode (μm)	Minimum bending radius (mm)	Fiber coupling loss (dB)	Propagation loss (dB/cm)
0.41	2	0.5 x 0.2	0.4	0.002	14	0.8

Table 3.4: Overview of the properties of MIT's silicon waveguides. The information is based on references 38 and 39.

3.3 Concept of the high-index project

The concept of the high-index project is related to aspects discussed in the previous sections. The essence of the concept is that waveguides with a low and waveguides with a high relative index difference are integrated on the same substrate (i.e. silicon) to benefit from the best properties of both: low fiber coupling loss and small minimum bending radii. Both aspects are discussed in this section. Subsection 3.3.1 introduces the material that has been chosen as core material for the waveguides with a high relative index difference: silicon rich nitride, and subsection 3.3.2 explains the opportunities and the associated challenges of integrating waveguides with a low relative index difference on the same substrate.

3.3.1 Silicon rich nitride

The material that has been chosen as core material for fabrication of the waveguides with a high relative index difference is silicon rich nitride deposited by low-pressure chemical vapor deposition (LPCVD). The precursors in this process are dichlorosilane (SiCl_2H_2) and ammonia (NH_3). The deposited material is characterized by a refractive index of about 2.1 which can be tuned by varying the gas flow ratio of the precursors [40].

Silicon rich nitride has an atomic silicon fraction that is larger than in stoichiometric¹ silicon nitride (Si_3N_4), which clarifies the term *silicon rich*. The reason why this particular type of silicon nitride was chosen is because the mechanical stress is significantly lower than in stoichiometric silicon nitride², which reduces material induced birefringence and facilitates device fabrication.

Properties of the silicon rich nitride waveguides are shown in table 3.5. The displayed propagation loss is applicable to multi-mode waveguides with cross-sectional dimensions of $8\ \mu\text{m} \times 1.3\ \mu\text{m}$ (width x height) because single-mode waveguides have not been fabricated yet due to technological problems (see section 5.5). The value for the minimum bending radius is a calculated value [41]. Because of all these complications, table 3.5 only serves as an indication that can be used to compare silicon rich nitride with the materials that have been mentioned in section 3.2. More detailed information on silicon rich nitride thin film and waveguide properties is presented in chapter 5. The ratio $E_{co,\perp} / E_{cl,\perp}$, which is a measure for the discontinuity at the interface between core and cladding (see formula 2.3), of silicon rich nitride waveguides is equal to 0.5.

Relative index difference	Absolute refractive index step	Core dimensions ($\mu\text{m} \times \mu\text{m}$)	FWHM of mode (μm)	Minimum bending radius (mm)	Fiber coupling loss (dB)	Propagation loss (dB/cm)
0.25	0.6	0.6 x 0.6	0.8	0.040	10	0.7

Table 3.5: Overview of indicative values of the properties of silicon rich nitride waveguides. The information is based on calculations performed with Selene and on the experiments discussed in chapter 5.

Because the refractive index of silicon rich nitride is not as high as the refractive index of silicon, the achievable integration density is not as high either. However, a positive consequence is the fact that the technological requirements to fabricate single-mode waveguides are not as tight.

The above-described considerations explain the choice of silicon rich nitride as core material. Chapter 5 presents a number of experiments that have been performed to investigate the suitability of silicon rich nitride for this application.

3.3.2 Fiber-to-chip coupling efficiency

<<confidential>>

¹ *Stoichiometric* refers to the state of an ionic compound wherein there are equal amounts of cations and anions [42]. The chemical formula of stoichiometric silicon nitride is given by Si_3N_4 because the electric charges of silicon and nitrogen are 4+ and 3- respectively.

² The mechanical stress in our films is below 100 MPa [43], and values below 10 MPa have been reported for silicon rich nitride [44]. In comparison, the mechanical stress in as-deposited stoichiometric silicon nitride is 1.2 GPa [45].

<<confidential>>

<<confidential>>

4 Applications of high-contrast material systems

This chapter lists a number of potential applications of high-contrast silicon-related material systems for integrated optics, where the term *high-contrast* refers to a high relative index difference. The purpose of this chapter is to provide an overview of possible future directions for the high-index project.

4.1 Optical filters

The most evident application of high-contrast silicon-related material systems is the realization of optical filters. Recently, the demand for optical filters has increased considerably because of the deployment of commercial wavelength division multiplexed (WDM) communication systems, and optical filters are essential components for these systems. In addition to traditional designs like bandpass filters, new applications have emerged such as gain equalization and dispersion compensation [17].

Optical filters can be realized in established technologies as doped silica and silicon oxynitride. However, the application of high-contrast waveguides offers the possibility to produce more compact filters with better performance. This is explained in the next subsections.

4.1.1 Working principle of optical filters

The optical filters under consideration are generalized interferometers which split incoming signals into a number of paths, delay the various signal parts and recombine them. Basically, there are two fundamental types of filter elements: finite impulse response (FIR) and infinite impulse response (IIR) elements. Two representations of these types are shown in figure 4.1. The essential difference between the two types is that their transfer functions are fundamentally different, with as most pronounced feature the finite versus infinite duration of the impulse responses [17]. The displayed IIR element is also referred to as ring resonator.

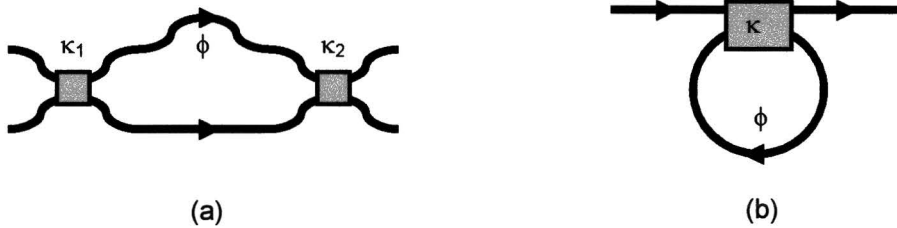


Figure 4.1: Illustration of (a) a finite impulse response (FIR) filter element and (b) an infinite impulse response (IIR) filter element. This particular IIR element is also referred to as ring resonator.

In practice, filter elements are characterized by a magnitude and a phase response which both depend on coupling coefficient κ and phase shift ϕ . The filter response can be tailored by varying these parameters. This is usually done thermo-optically. Cascading and combining filter elements gives more design freedom, and can be used to realize an arbitrary filter response. The advantage of incorporating both FIR and IIR elements in a single device is that a desired response can in general be achieved with fewer stages [17]. This is illustrated in subsection 4.1.2.

In addition to the above-described difference in size, there is another relevant issue which concerns the *free spectral range (FSR)* of ring resonators. The free spectral range is the length of a period in the spectral response¹ and, for a ring resonator, the free spectral range increases with decreasing length of the feedback path:

$$FSR = \frac{c}{n_g L_u}, \quad (4.1)$$

where c is the velocity of light in vacuum, L_u is the length of the feedback path or *unit length*, and n_g is the effective group index which is given by:

$$n_g = n - \lambda \frac{dn}{d\lambda}, \quad (4.2)$$

¹ The spectral response of a ring resonator is intrinsically periodic because of the discrete set of delays that is generated by the feedback loop.

where n is the effective refractive index of the waveguide that forms the feedback loop. L_u is equal to $2\pi R$, when the feedback loop is a circle with radius R .

The consequence of the fact that the free spectral range increases with decreasing bending radius is that high-contrast material systems are more suitable to realize devices compatible with the current ITU grid for optical communications¹ than for example the intermediate-contrast silicon oxynitride technology. This is explained in subsection 4.1.3.

The relevance of the above-described filter theory for the high-index project is that the integration of ring resonators in devices can only be realized on the basis of material systems which waveguides have sufficiently small bending radii. In this context, high-contrast material systems are more suitable than either the low-contrast doped silica or the intermediate-contrast silicon oxynitride technology.

4.1.2 Bandpass filtering

Bandpass filters are basic building blocks for add/drop multiplexers and optical routers in wavelength division multiplexed (WDM) communication systems. Ideal bandpass filters have 100% transmission in the passband and 0% transmission outside the passband. This can be approximated by using a large number of filter elements. Because of practical reasons (area reduction, reduction of insertion loss and limitation of the influence of fabrication tolerances), it is advantageous to reduce the amount of filter stages as much as possible.

To illustrate the role that ring resonators can play in reducing the number of filter stages, figure 4.2 shows a schematic representation of a 4×4 optical router. The influence of the ring resonators which are indicated by the bold blocks with symbol Φ_x , is illustrated in figure 4.3 on page 21. Figure 4.3a displays the spectral magnitude response of the optical router without ring resonators, and figure 4.3b shows the spectral response with ring resonators. It can be seen that the ring resonators flatten the passband and lower the cross-talk. The latter has been indicated by the increase in useable bandwidth per frequency channel from 6 to 74 percent. The useable bandwidth per frequency channel is defined by the 30 dB cross-talk points.

The described performance improvements of optical routers cannot be achieved without ring resonators in a way equally effective as the one illustrated here [17], which demonstrates the added value of ring resonators for bandpass filter applications.

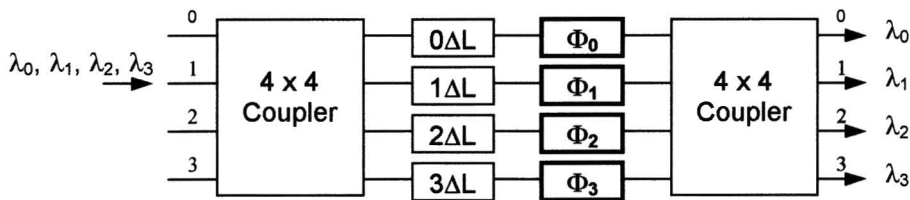


Figure 4.2: Schematic representation of a 4×4 optical router. The ΔL blocks represent different path lengths. The bold blocks with symbol Φ represent optional ring resonators. The influence of these elements is illustrated in figure 4.3.

¹ The International Telecommunications Union (ITU) has defined an allowed channel optical frequency grid based on 100 GHz spacing from a reference frequency of 193.1 THz = 1552.52 nm [46].

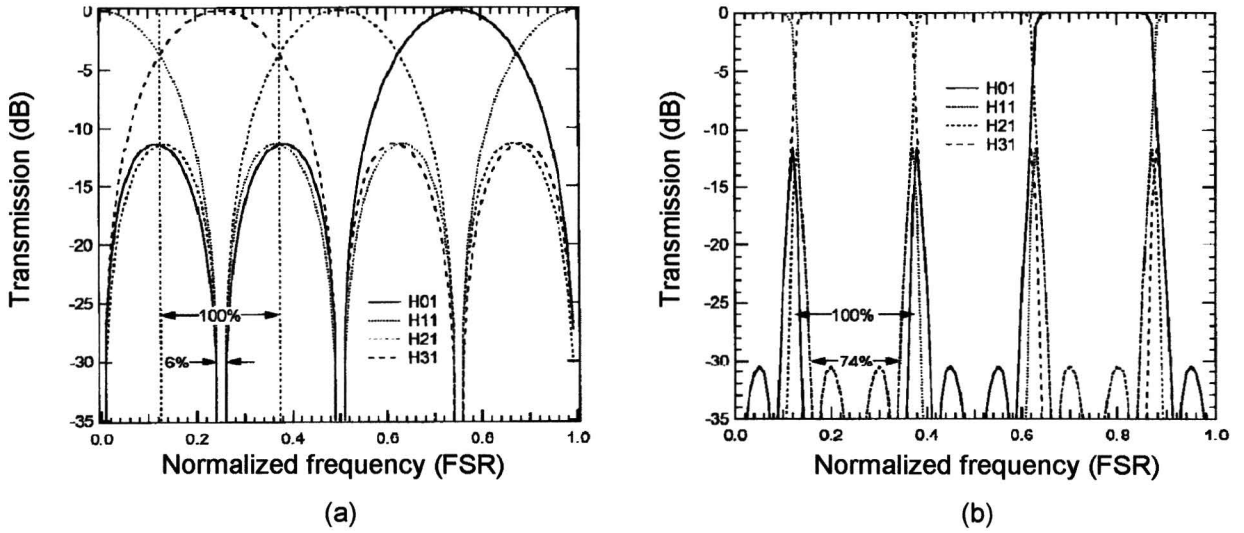


Figure 4.3: Spectral response of the 4 x 4 optical router that is displayed in figure 4.2 (a) without and (b) with ring resonators in the arms. H01, H11, H12 and H13 are the normalized outputs of channels 0, 1, 2 and 3 as function of input 1. The graphs were reprinted from reference 17.

4.1.3 Dispersion compensation

In standard single-mode fibers light pulses with a wavelength around 1550 nm are broadened in time and distance. This phenomenon is called *dispersion*. Compensation of dispersion becomes increasingly important with increasing bit rate in order to prevent pulses from overlapping each other. Dispersion compensation is another filter application that benefits from the properties of ring resonators.

The essence of dispersion compensation is that a frequency dependent group delay is induced to compensate the frequency dependent group delay caused by the fiber. Because the group delay in fibers is a linear function of frequency, a dispersion compensator should have a linear response as well, but with a negative slope compared to the dispersion in fibers. Ideally, the amplitude is unaffected, because the group delay τ_g is only dependent on the phase response Φ of the filter [17]:

$$\tau_g = -\frac{1}{2\pi} \frac{d\Phi}{df}, \quad (4.3)$$

where f is the frequency in Hz.

In principle, dispersion compensators can be realized by using only FIR filter elements. However, a number of arguments [47] suggest that ring resonators are the best choice for achieving low loss and extremely compact dispersion compensators. Figure 4.4 shows a design of a dispersion compensator that exists of four cascaded ring resonators. Figure 4.5 displays the spectral group delay of the individual ring resonators as well as the response of the total device. In the limit of low feedback path losses, the magnitude response is unity for all frequencies. Effects of a finite loss are discussed elsewhere [48].

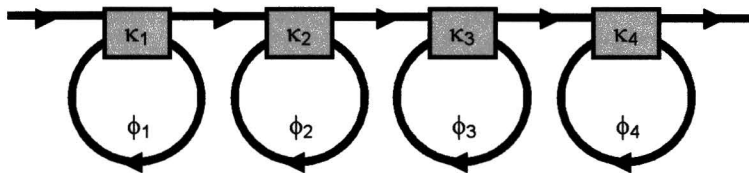


Figure 4.4: Layout of a dispersion compensator that is based on four cascaded ring resonators.

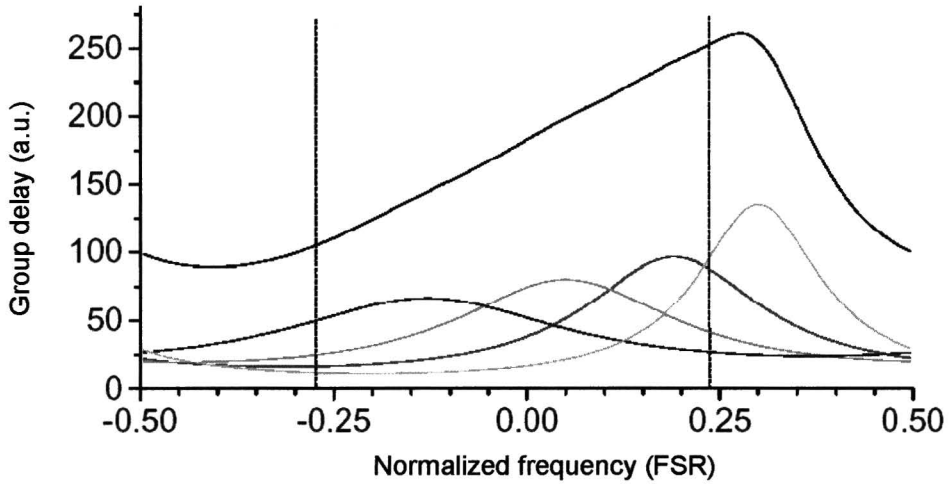


Figure 4.5: Spectral group delay of the individual ring resonators and a device consisted of four cascaded ring resonators (upper line). The useable bandwidth reaches over 50% of the free spectral range (graph was reprinted from reference 48).

The linear slope in figure 4.5, which is the useable part of the response for compensation of dispersion induced in fibers, reaches over half the free spectral range. Since the free spectral range of a ring resonator increases with decreasing length of the feedback path, as expressed in formula 4.1, the maximum achievable bandwidth of dispersion compensators increases with increasing relative index difference of the waveguide that forms the feedback path. Consequently, dispersion compensators as illustrated in figure 4.4 can have a wider usable bandwidth when they are fabricated in high-contrast material systems.

To show the practical relevance of the difference in useable bandwidth, table 4.1 compares the properties of a demonstrated dispersion compensator based on IBM's SiON technology [48] and a dispersion compensator that could be fabricated from silicon rich nitride waveguides. The table shows that the dispersion compensator based on silicon rich nitride can have a useable bandwidth of 100 GHz when the radius of the ring is reduced to 0.12 mm. Because of the low relative index difference of IBM's silicon oxynitride waveguides, the useable bandwidth of that dispersion compensator is limited to 25 GHz¹. This implies that these dispersion compensators limit the data capacity per channel of the ITU optical frequency grid which is based on 100 GHz spacing [46] (see formula 1.1). This proves that high-contrast material systems enable performance improvements of optical filters.

Technology	Relative index difference	Bending radius ring (mm)	Effective group index	Free spectral range (GHz)	Useable bandwidth (GHz)	Maximum ITU channel efficiency (%)
SiON (IBM)	0.033	0.55	1.5	50	25	25
SRN (COM)	0.25	0.12	2.0	200	100	100

Table 4.1: Comparison between the usable bandwidths of a dispersion compensator that has been realized in IBM's SiON technology and a similar device that could be realized in the material system that is under development in the high-index project.

Two remarks should be made regarding the above-described comparison. First of all, a negative effect of decreasing the radius of the rings is that the absolute dispersion slope (usually expressed in ps/nm) becomes less steep because of two effects: the delay per round trip decreases and the wavelength scale is stretched out. This implies that dispersion compensators have to be cascaded to achieve the same compensation effect. Second, the comparison between a realized and a non-realized device is not completely fair, though it illustrates the difference in physical limits of the application of both material systems.

¹ To achieve a useable bandwidth of 25 GHz the bend radius needs to be reduced to 0.55 mm, as is shown in table 4.1. This value is lower than the minimum bending radius described in section 3.4, which implies that more bend loss is tolerated, see reference 48.

4.2 Additional resonators applications

Optical resonators have a wide range of applications other than the ones described in section 4.1. A few of these applications are described in this section because high-contrast material systems are inevitable for the implementation of compact optical resonators. Notice that the description has been broadened from ring resonators to resonators in general because a wide variety of shapes are possible. The three applications that are discussed are: switching, lasing and device miniaturization.

4.2.1 Optical switching

Optical switching is based on the variation of the refractive index with applied light intensity by means of a nonlinear optical (NLO) material [7]. The primary limitation on optical switching is the weakness of nonlinear effects in currently available materials. To a certain extent, optical resonators are able to relax the requirements on the strength of these nonlinear effects. In the first place, high-finesse¹ resonators can have very high internal field intensities, which increases the phase shift induced by a nonlinear optical (NLO) material that is incorporated in the resonator. Second, the phase shift that is required to change the output levels of high-finesse resonators is relatively small due to the wavelength selectivity of resonators. This effect is illustrated in figure 4.6, where 4.6a shows a layout of a possible implementation of an optical switch, and figures 4.6b and 4.6c display the signal magnitudes of outputs 1 and 2 as function of the refractive index of the nonlinear optical material incorporated in the resonator. Because of the sharp peaks, which are associated with the high finesse, the two switching states are relatively closely spaced. The working principle of the illustrated switch, which is extensively discussed elsewhere [49], is based on the superposition of control beam $I_{control}$ and signal beam I_{signal} which together form input signal I_{in} . The variation in input intensity causes the variation in refractive index of the nonlinear optical material.

Another implementation of an optical switch is the incorporation of a resonator in one of the arms of a Mach-Zehnder interferometer. In addition to the above-described features, this implementation benefits from a third effect of resonators which enhances their ability to switch. This concerns a linear effect that is also employed in optical filters [50].

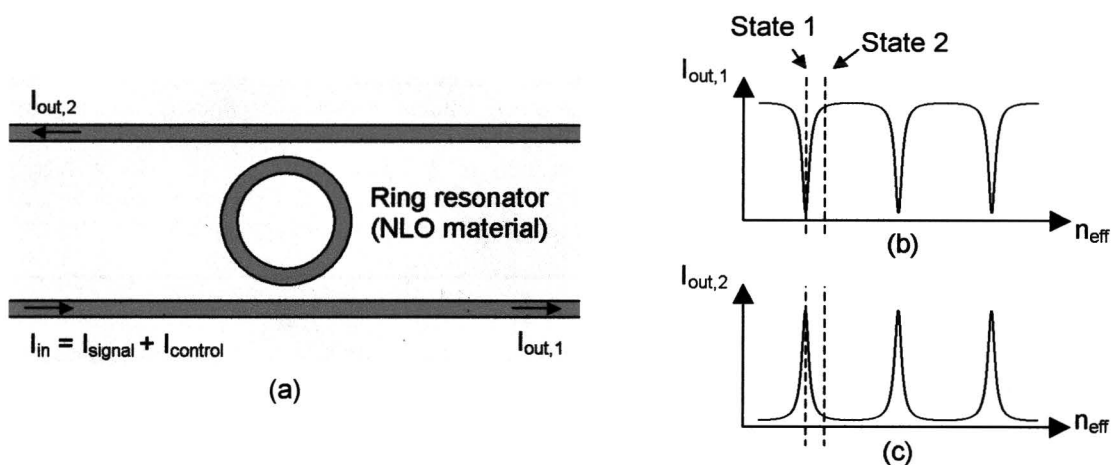


Figure 4.6: Illustration of an integrated optical switch based on a ring resonator with a nonlinear optical material. (a) Schematic top view of the device, and signal magnitudes of (b) output 1 and (c) output 2 as function of the effective refractive index of the nonlinear optical material (figure was reprinted from reference 49).

¹ The finesse F of a resonator is defined as the ratio of the distance between the peaks in the spectral transmission spectrum (free spectral range, FSR) to their full-width half-maximum ($F = FSR/FWHM$). The finesse is a normalized quantification for resonance.

A major concern related to the application of high-finesse resonators for optical device applications such as switching is that dynamical effects in high-finesse resonators are relatively slow, which limit the maximum modulation frequency¹. This is a relevant issue because the principle advantage of optics is data capacity. A restriction on data capacity could undermine the benefit of replacing electronic devices by optical devices.

An important design consideration that is related to this concern is originating from the relation between intensity magnification factor M , which is the ratio of circulating intensity to incident intensity, and maximum modulation frequency f_{max} . The maximum modulation frequency f_{max} of a ring resonator is roughly given by [50]:

$$f_{max} \cong \frac{c}{n_g F L_u}, \quad (4.4)$$

where c is the velocity of light in vacuum, L_u is the length of the feedback path or *unit length*, F is the finesse of the resonator and n_g is the effective group index which is given by formula 4.2.

The intensity magnification factor M scales quadratically with the finesse of the resonator [50]:

$$M \propto F^2 L_u. \quad (4.5)$$

From formulas 4.4 and 4.5 it can be concluded that any desired magnification factor M and maximum modulation frequency can be obtained, provided that the resonator can be made to small dimensions (lower L_u) and large enough finesse (higher F). It is beyond the scope of the thesis to present a quantitative analysis of required dimensions. However, compact resonators can only be realized in high-contrast material systems, which is another illustration of the fact that these particular material systems enable performance improvements of integrated optical devices. Nevertheless, it remains questionable whether switching frequencies on the order of terahertz² can be realized with switches based on high-finesse resonators.

4.2.2 Lasing

Two aspects in high-contrast material systems are advantageous for the fabrication of active devices such as lasers. The first aspect, which is not related to resonators, is the fact that light in high-contrast waveguides is more confined than light in low contrast waveguides (see chapter 3). This implies that for equal total power levels, light in the center of high-contrast waveguides is more intense than light in the center of low-contrast waveguides, which is an opportunity to increase pump efficiency [51]. Secondly, high-finesse resonators can have very high internal field intensities in a narrow wavelength range, as has already been mentioned in subsection 4.2.1, which enables them to increase pump efficiencies further as well as to act as wavelength selectors [52].

Therefore, resonators could be applied for the fabrication of compact arrays of light sources for WDM applications. In relation to this opportunity, it should be noticed however that both propagation and coupling losses are generally higher for high-contrast material systems. This limits the applicability of active devices at the present time.

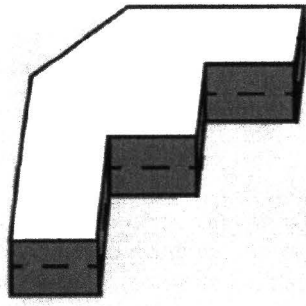
4.2.3 Device miniaturization

Optical resonators enable a higher degree of device miniaturization than what's possible with traditional waveguide bends. It has been reported [53] that low-finesse resonators can form right angle bends, T-junctions and crossings with excellent transmission characteristics. The waveguide intersection regions under consideration are resonant structures with symmetry, as is shown in figure 4.7.

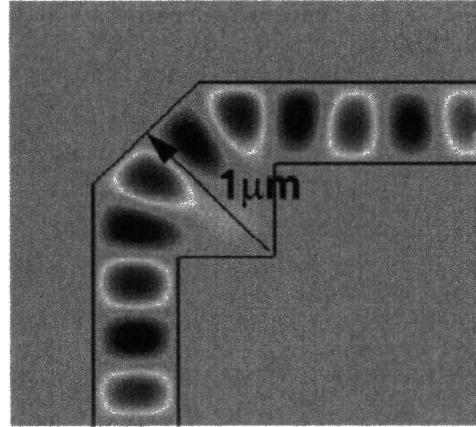
This example illustrates that also low-finesse resonators could be useful for applications in high-density integrated optics.

¹ The fact that operating frequencies of all-optical devices can be limited by effects such as cavity build-up time, cavity dynamical effects or non-linear response times is often overlooked. However, it is an important issue that proves that all-optical devices are not necessarily faster than electronic devices.

² In comparison, state-of-the art silicon-based (SiGe) transistors are capable of reaching operating frequencies of 210 GHz [54] and frequencies as high as 1.08 THz have been reported for so-called transferred-substrate heterojunction bipolar transistors [55].



(a)



(b)

Figure 4.7: (a) Schematic of a square resonator in a high-contrast material system with a 45°-cut at its outer corner and (b) corresponding electric field amplitude distribution.

4.3 Photonic bandgap structures

Photonic crystals are engineered structures with a periodic arrangement of dielectric materials in two or three dimensions. If the periodicity and symmetry of the crystal and the refractive indices of the materials are chosen well, then the band structure of such a crystal shows a photonic bandgap (PBG) for one or two polarizations, i.e. at particular frequencies light propagation is prohibited in any direction in the crystal. Photonic crystals that exhibit a photonic bandgap are referred to as photonic bandgap structures or photonic bandgap materials.

Photonic bandgap structures are considered to be promising structures for a number of applications, including inhibition and enhancement of spontaneous emission [56]. The promising aspect of photonic bandgap structures is the fact that they provide mechanisms to manipulate light and light-matter interaction that are incomparable to mechanisms in conventional optics. An illustrative example is the optical switch that is proposed in reference 57. The switching action in the described photonic bandgap structure is not associated with the operation of a resonator with an inevitable trade-off between modulation frequency and switching intensity (for given dimensions), which has been described in subsection 4.2.1, but it is associated with an abrupt discontinuity in the engineered broadband electromagnetic density of states of the photonic bandgap structure [57].

The relevance of high-contrast material systems for photonic bandgap structures is given by the fact that photonic bandgap effects are more pronounced in high-contrast than in low-contrast structures [15]. More information about prospects and practical limitations of photonic bandgap structures can be found elsewhere [56].

4.4 Optical interconnects for electronic devices

As bit rates of integrated electronic components increase, the metal interconnection lines that provide the communication paths between components become the bottleneck for device performances. This phenomenon is commonly referred to as *interconnection bottleneck* [58], and it is a result of the *aspect ratio limit* of electrical interconnects. The aspect ratio limit states that the data capacity C (bits/s) of electronic interconnects is proportional to aspect ratio ($=A/l^2$) of the electrical line [59]:

$$C \cong \gamma \frac{A}{l^2}, \quad (4.6)$$

where A is the effective cross-sectional area of the line, l is the length of the line and γ is a prefactor that depends on the type of line ($\gamma_{RC \text{ line}} = 10^{16}$ bits/s, $\gamma_{LC \text{ line}} = 10^{15}$ bits/s). The aspect ratio limit tells that the data capacity of an electrical line decreases with increasing length and decreasing cross-sectional dimensions. For so-called global on-chip interconnects this is already a problem, and the aspect ratio limit is expected to dominate

electronic device performances in the near future [58]. To give an indication, the bandwidth of an RC-line with a $1 \times 1 \mu\text{m}$ cross-section is $\sim 3.5 \text{ GHz}$ [59]. An opportunity to overcome the interconnection bottleneck is the application of optical interconnects. Optical interconnects do not suffer from the aspect ratio limit because the physics of loss and signal distortion is completely different [59].

The exciting aspect of optical interconnects is that it could be a first step in the monolithic integration of mainstream silicon-based electronics and integrated optics, which could be highly advantageous because it would combine the bandwidth capacity of optics with the processing capacity and the data storage capacity of electronics¹.

A relatively simple implementation of optical interconnects in electronic devices is illustrated in figure 4.8. The diagram shows an optical bus architecture for clock distribution. The architecture consists of a network of waveguides that distributes an optical signal of an external source to a number of photo detectors which transform the optical signals into electrical signals. The external source could be mode-locked laser, which raises possibilities not normally available in electrical systems because pulses are much shorter than pulses available from electrical circuits and the very fast rising edges imply that the clock phase could be very well defined [59].

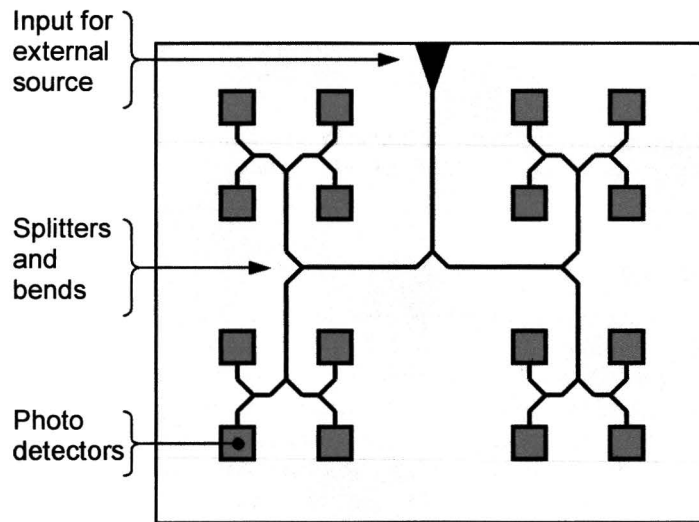


Figure 4.8: Illustration of an optical bus architecture for clock distribution in electronic devices.

Although there are several arguments for introducing optical interconnects to electronic devices, there are still a number of technological challenges that have to be overcome. A major challenge is the design of receiver amplifiers and transmitter drivers. The performance of CMOS-compatible photo detectors, which would be required for the application illustrated in figure 4.8, is still low [59]. Using silicon-based materials systems for light emission for optical interconnects still would require major breakthroughs.

An extensive analysis of opportunities and challenges of both off-chip and on-chip optical interconnects can be found elsewhere [59].

4.5 Summary

In this chapter a number of applications of high-contrast silicon-related material systems have been presented to give an impression of the opportunities offered by these material systems. The opportunities are related to size reduction and enhancement of functionality of devices based on conventional low-contrast silicon-related material systems.

Regarding optical filters, it has been shown that existing concepts can be implemented in a more compact way and to some extent with better performance in high-contrast material systems than can be done in low-contrast

¹ The processing capacity and data storage capacity of electronics is higher because its integration density is fundamentally better than the integration density of optics due to the relatively large wavelength of light: $\sim 1 \mu\text{m}$ (in waveguide materials and for telecommunications wavelengths). The wavelength is a relevant length scale in this context because most optical components rely on interference, and device dimensions are therefore necessarily restricted by wavelength [59].

material systems. Although there are a number of technological challenges to overcome, the surplus value of high-contrast material systems is obvious.

Other applications such as switching, lasing and enabling a monolithic merge between electronics and optics, which are examples of applications that would make integrated optics a more mature technology, seem to require substantial breakthroughs. However, all these applications can take advantage of several features of high-contrast material systems: small size of devices, ability to integrate high-finesse resonators and the possibility of obtaining a strong photonic bandgap effect.

Some of the technological challenges that prevent high-contrast silicon-related material systems from a fast introduction have been subject of the current project and are discussed in the next chapters.

5 Analysis of silicon rich nitride film and waveguide properties

This chapter presents an analysis of a number of silicon rich nitride (SRN) film and waveguide properties. The performance of this analysis is the main experimental work of the current master project. The objective was to investigate the suitability of silicon rich nitride for optical waveguide applications and to investigate whether process improvements could be implemented.

Before the experiments are described in section 5.2-5.4, section 5.1 presents an overview of the characteristics of silicon rich nitride as well as a summary of the status of the deposition process at the start of the master project. In this way, the motivation to perform the experiments is explained. The actual experiments comprehend the characterization of the uniformity of the refractive index and thickness of SRN films by prism coupling (section 5.2), the investigation of N-H related absorption in SRN films by Fourier transform infrared (FTIR) spectroscopy (section 5.3) and propagation loss measurements of SRN slab waveguides by dual prism coupling (section 5.4). After these experiments have been described, section 5.5 discusses some technological problems that are acting as a bottleneck for the development process at the moment and which are related to the deposition process. Section 5.6 emphasizes the recommendations for further research.

The content of sections 5.3 and 5.4 is the subject of poster presentation on ECOC 2002. The associated paper has been enclosed in appendix E.

5.1 Background

5.1.1 Arguments for the choice of silicon rich nitride

A number of arguments explain why silicon rich nitride deposited by low-pressure chemical vapor deposition (LPCVD) was chosen as potential core material for high-density integrated optics. Some of these arguments have already been mentioned in chapter 3, but for the sake of completeness they are included in the following overview as well (notice that the choice was made before the start of this master project):

- The refractive index of silicon rich nitride is relatively high, which enables the fabrication of waveguides with small bending radii. Because the refractive index is considerably lower than for silicon, the technological requirements for the fabrication of single-mode waveguides are not as tight. This enhances the possibility that optical lithography can still be used and that the less scalable electron beam lithography can be avoided. The relation between refractive index of the core and bending radius of the corresponding waveguide has been explained extensively in chapter 3.
- The propagation loss around the wavelength of 1550 nm is higher for silicon than what has been reported for stoichiometric silicon nitride (0.3 dB/cm [60]). Although promising results for the propagation loss of silicon have been achieved (0.8 dB/cm [38]), these values are difficult to realize. Values of several decibels per centimeter are more realistic. This difference in propagation loss is an additional reason for the choice of silicon rich nitride instead of silicon. However, it is not necessarily true that the propagation loss of stoichiometric nitride can be obtained in silicon rich nitride. This is a subject of research.
- The mechanical stress in SRN films is lower than in stoichiometric silicon nitride films, which is an argument that has been mentioned in chapter 3 as well. The mechanical stress in our films is below 100 MPa [43], which is much lower than the 1.2 GPa of as-deposited stoichiometric silicon nitride films [45].

The most important consequence of low mechanical stress is that it facilitates device fabrication. If the stress value of a deposited film is high, then the wafer has either a bowl shape, which is disadvantageous for the waveguide definition process, or the film cracks. Another advantage of low mechanical stress is the fact that stress-induced birefringence is low.

- Low-pressure chemical vapor deposition has been chosen as deposition method instead of plasma-enhanced chemical vapor deposition (PECVD) because the incorporation of hydrogen in LPCVD films has been reported to be less pronounced than in PECVD films [61]. Two possible explanations for this phenomenon are the fact that the hydrogen has more thermal energy in LPCVD than in PECVD processes due to the difference in temperature (LPCVD: 700-900 °C, PECVD: 200-400 °C) and the fact that the deposition rate in LPCVD processes (~ 5 nm/min) is lower than in PECVD processes (> 40 nm/min). Both elements could give hydrogen a better opportunity to desorb from the material during deposition.

The incorporation of hydrogen, or more specific N-H bonds, is a negative effect for optical waveguide applications because these bonds have an absorption peak near 1550 nm. This issue is further discussed in section 5.3.

- The recipe that has been used as a starting point for the project was an existing recipe that is normally used for etch masks. The availability of this recipe can be considered as a practical reason for the choice of silicon rich nitride. The parameters of the recipe are displayed in table 5.1. Varying the ratio of the precursors dichlorosilane (SiCl_2H_2) and ammonia (NH_3) enables to tune the refractive index in a range from about 2.06 to 2.16 at a wavelength of 1550 nm, while keeping uniformity and reproducibility at the same level [40].

The used LPCVD furnace, which deposits a boat of 30 wafers in one run, is a commercially available furnace system from *Tempress* [62]. The silicon wafers have a diameter of 10.0 cm.

Process parameter	Value
Pressure	< 200 mTorr
Temperature	> 800 °C
SiCl_2H_2 (DCS) / NH_3 flow ratio	3.2 : 1
Deposition time	4 hr
Process characteristic	Value
Deposition rate	5.1 nm/min
Film thickness	1.22 μm
Refractive index at 632.8 nm	2.09 ¹
Refractive index at 1550 nm	2.06

Table 5.1. Parameters and basic characteristics of the silicon rich nitride LPCVD process. More detailed information about the parameters cannot be given.

5.1.2 Motivation for the performance of the described experiments

At the start of the current master project some data concerning the silicon rich nitride deposition process was already available. Some information was related to the uniformity of the refractive index and thickness of SRN films. Because a few conclusions of that analysis relied on ellipsometry instead of prism coupling, and prism coupling is believed to be more accurate [22], [35], these measurements have been repeated partially. This experiment is presented in section 5.2.

Initially, not much information about the propagation loss in SRN waveguides was available. The only data about this issue was the outcome of a few cutback experiments (see section 5.4) which suggested that the propagation loss was about 1.6 dB/cm. However, the accuracy of these measurements was not very high. Therefore, attention has been paid to the measurement of propagation loss and the identification of loss mechanisms. The experiments that are related to this subject are presented in sections 5.3 and 5.4. The principle and additional results of the above-mentioned cutback method are described in section 5.4 as well.

The films used for these experiments were all deposited with the recipe that has been described in subsection 5.1.1. To get an impression of the influence of the deposition parameters, which could provide useful ideas for process improvements, it would be nice to vary gas flows, temperature and pressure. However, because of three practical limitations this has not been done during this project:

- The refractive index of the recipe that is described in subsection 5.1.1 is on the border of the range of what the prism coupler can measure. Refractive indices that are a little bit higher cannot be measured due to the type of prism used. The simple solution to overcome this problem would be to use a different type of prism. However, such a type was not available during the project.
- The resolution of some measurement methods, such as Fourier transform infrared spectroscopy, was not good enough to detect any difference between distinct SRN films within the refractive index range mentioned in subsection 5.1.1 (see section 5.3).
- For the dual prism coupling measurement it was not possible to produce particle-free films due to technological problems (see section 5.5). Only old films were available for these experiments. All these films had been deposited with the recipe described in subsection 5.1.1.

¹ See section 5.2 for more accurate information about the refractive index.

5.2 Refractive index and thickness uniformity of silicon rich nitride films

5.2.1 Introduction

In chapters 2 and 3 it has been illustrated that the cross-sectional dimensions and the refractive index of the core are important parameters for the optical properties of a waveguide. One of the consequences of this fact is that SRN films need to be deposited with a good uniformity to enable the design and the fabrication of devices. Especially the performance of components such as couplers (e.g., directional couplers or MMI couplers [11]) are sensitive for variations in the mentioned parameters.

To investigate whether the uniformity of the deposited SRN films is good enough, both the refractive index uniformity and the thickness uniformity have been analyzed by prism coupling using the attenuated total reflection (ATR) method.

5.2.2 Measurement principle

The basic principle of prism coupling is that light is coupled into a dielectric film by means of a prism. Only for certain angles θ of the incident beam, optical modes are excited and light is coupled into the dielectric film. The angle selectivity is a result of the phase matching condition between the light in the prism and the mode of the dielectric film that needs to be fulfilled to establish a significant energy transfer [11]. The refractive index and the thickness of the film are related to these particular angles.

The ATR method implies that light reflected by the waveguide is measured to determine whether an optical mode is excited, as has been illustrated in figure 5.1. An advantage of the attenuated reflection method is that substrate leakage is not relevant, which means that it is not necessary to have a buffer layer underneath the dielectric film. Further advantages of the prism coupling technique are the simplicity of both the setup and the calculation method [63], and the accuracy that is associated with this technique (see subsection 5.2.3). More information on prism coupling and the ATR method can be found in reference 82 as well as on the website of Metricon [64], which is a supplier of prism couplers.

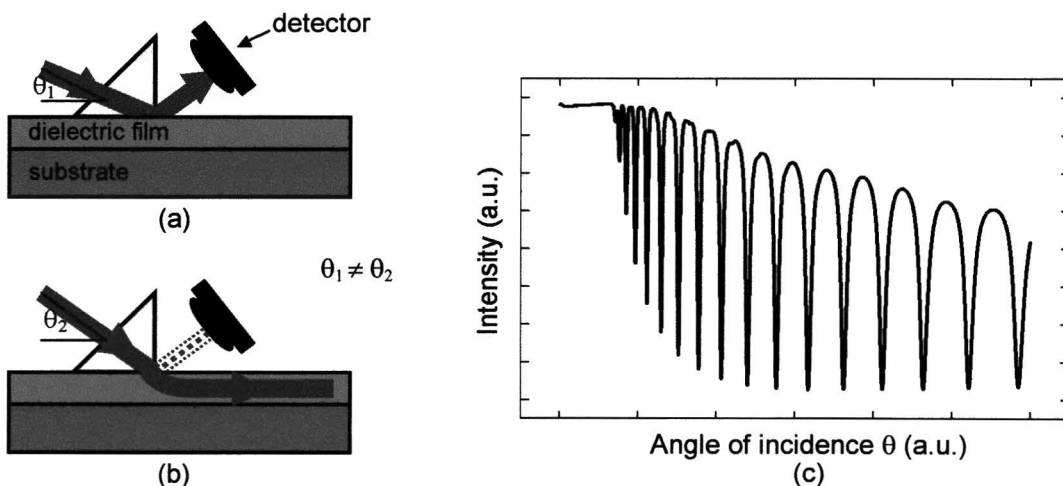


Figure 5.1: Illustration of the principle of prism coupling. (a) For angle θ_1 , light is reflected from the surface. (b) For angle θ_2 , light is coupled into a guiding mode of the dielectric film. (c) Typical detected intensity versus angle of incidence plot. The positions of the peaks are related to both the refractive index and the thickness of the film.

5.2.3 Experimental setup

The type of prism coupler that was used for the experiment is the commercial available *Model 2010* from *Metricon* [64] which is based on the above-described ATR method. The wavelengths that can be used are 632.8 nm (He-Ne laser) and 1550 nm (diode-laser). In this project, the measurements have been performed at a wavelength of 632.8 nm because the prism coupler is more accurate at this wavelength [65]. The refractive index is slightly different at 1550 nm as is shown in table 5.1. However, accuracy is the most important quantity for uniformity measurements, and the uniformity is not expected to be different at 1550 nm compared to 632.8 nm. The accuracy of the refractive index measurements is ‘a few times 10^{-4} ’ [63] and the accuracy of the thickness measurements is specified as 0.5 % + 50 Å. Due to limitations of the setup, only TE polarized light could be used to perform the measurements.

5.2.4 Experiment

The performed experiment comprehends of three parts:

- Both refractive index and thickness were measured at 5 positions on 5 wafers. Because it is hard to position the prism in an accurate way on a specific spot due to the design of the setup, the measurements have been performed at the positions that have been indicated in figure 5.2a. The reason for choosing these positions is the easy identification and the fact that these positions are not close to the edge. The wafers that were used for this analysis are wafers 11 to 15 inclusive. See figure 5.2b for the positions of these wafers during deposition.
- Refractive index and the thickness were measured in the center of all 25 SRN films that had been deposited in the LPCVD process.
- All measurements were repeated after an 1100 °C annealing process of 4 hours that was performed in a nitrogen atmosphere which is the standard anneal recipe.

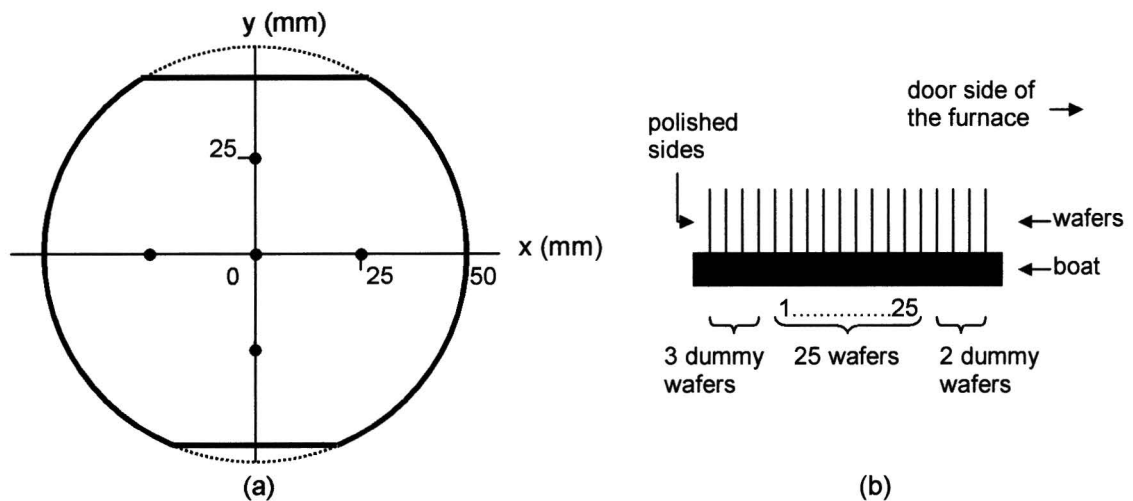


Figure 5.2: (a) Illustration of the five measurement positions (dots) that were used for the investigation of the uniformity of the refractive index and the uniformity of the thickness of SRN films. (b) Schematic overview of the positions of the 25 wafers on the boat during deposition.

5.2.5 Results

For all measurements, 4 or 5 intensity dips were observed in the angular intensity plot. This is enough for an accurate determination of both refractive index and thickness. The main results are presented in the following overview:

- For all 5 wafers examined, the measured refractive indices at 5 positions on a single wafer were within a spread of $7 \cdot 10^{-4}$ which corresponds to 0.03 % of the refractive index value. No spatial tendencies could be observed.
The film thickness in center of the wafer was measured to be smaller than at the outer 4 points. This tendency was observable for all 5 examined wafers, but the difference was very small (~ 10 nm, 0.8 % of the total thickness).
- For the measurements in the center of all 25 wafers of the LPCVD process, a systematic variation could be observed. Both refractive index and film thickness increase as function of position of the wafer on the boat. The results are shown in table 5.2, where the term *spread* refers to the interval between the lowest and highest value measured on the indicated wafers. So, the above-mentioned systematic variation is included in this number.

Wafer numbers	Spread in refractive index	Spread in refractive index (%)	Spread in thickness (nm)	Spread in thickness (%)
11-15	0.0014	0.07	44	4
6-20	0.0023	0.11	120	10
1-25	0.0054	0.26	210	17

Table 5.2. Spread in refractive index and film thickness in the center of a number of wafers from the boat of a LPCVD process. The wafer numbers indicate the positions of the wafers on the boat (see figure 5.2b). See the text above the table for an explanation of the displayed quantities.

- The anneal process appears to have a detectable influence on the refractive index and the thickness of the SRN films. The refractive index increases with 0.004 which corresponds with 0.2 %, while the film thickness decreases with 12 nm or 1 %. No change in uniformity could be detected after the anneal process.

5.2.6 Discussion

A few remarks can be made related to the results that have been presented in subsection 5.2.5. First of all, since the spreading in thickness and refractive index per wafer is close to the resolution of the prism coupler, the actual spread might be smaller than the spread in the detected values due to the limited accuracy of the measurements. Therefore, it is hard to get more detailed information than what is presented in subsection 5.2.5 on the basis of the Metricon prim coupler.

Second, it is important to apply a criterion to find whether the uniformity is good enough or whether it should be improved. In principle, the best way to analyze this is to investigate how variations in the refractive index and height of the core affect the optical properties of waveguides that are based on this LPCVD process. This could be done either theoretically or experimentally. A waveguide-theoretical investigation of fabrication tolerances is a difficult and time-consuming process, which was beyond the scope of this project. An experimental investigation could be to fabricate some simple components such as directional couplers, based on a number of SRN films of a single deposition process, and measure the difference in performance as function of the position of the wafers in the LPCVD furnace. This experimental analysis could not be performed because components such as directional couplers are still under development in the high-index project.

As an alternative, the characteristics have been compared with a publication of IBM's SiON technology [35], because this is a well-developed relatively high-contrast technology on the basis of which several working devices have been demonstrated (see subsections 3.2.2 and 4.1.3). Table 5.3 displays a comparison between both technologies. The specifications about the uniformity per wafer of both technologies are comparable because they were obtained by the same method on a similar wafer area. The table shows that the uniformity per wafer is better for SRN. However, especially the thickness uniformity over a number of wafers is not particularly good.

Technology	Spread in refractive index (%)			Spread in thickness (%)		
	Per wafer	5 wafers	15 wafers	Per wafer	5 wafers	15 wafers
SiON (IBM)	0.07	0.07	0.07	1	1	1
SRN (COM)	0.03	0.10	0.14	0.8	5	11

Table 5.3: Comparison between the characteristics of deposited films of IBM's SiON technology [35] and the SRN technology that is under development in the high-index project. Because no information was available about the reproducibility of IBM's single-wafer PECVD process, a reproducibility of 100 % has been assumed.

A third remark is related to the influence of annealing. The determination of this influence showed that there is no detectable change in uniformity, but that a densification of the films is observable. In the case of PECVD-grown SiON it is known that this densification is accompanied by the removal of hydrogen [35]. Because it is expected to be very disadvantageous for optical waveguide applications to have hydrogen in the SRN films, the influence of annealing needs a further investigation. Important questions are: is hydrogen present in as-deposited SRN films? And if that is the case, to what extent does annealing reduce the hydrogen concentration? These questions are addressed in sections 5.3 and 5.4.

Finally, in addition to these conclusions about the SRN films, it has been demonstrated that prism coupling is indeed more accurate than ellipsometry for the determination of the refractive index and the thickness of the SRN films under investigation. This can be deduced from the fact that it was impossible to detect any difference between the SRN films before and after annealing by ellipsometry [43], but that a clear densification of all 25 deposited films could be observed by prism coupling. Based on this experiment it is expected that the accuracy in refractive index measurements of the ellipsometer at COM is > 0.002 .

5.2.7 Conclusions

In summary, the investigation of the refractive index and thickness uniformity of SRN films by prism coupling resulted in four conclusions:

- The uniformity per wafer of both refractive index and thickness of the LPCVD-grown SRN films is good enough (0.03 %) for device applications, as has been deduced based on a comparison with IBM's SiON technology. This comparison was the best thinkable criterion when taking the arguments described in subsection 5.2.5 under consideration.
- It seems that the uniformity over a boat of 25 wafers needs to be improved before all wafers can be used to fabricate components with the same specifications, although it should be noticed that this conclusion is not based on a quantitative analysis (see section 5.2.6). Because the uniformity over 25 wafers is only important for a production process and not for the high-index project in its current state, it has no priority to improve it.
- The observed densification of the films by annealing, which could be accompanied by the removal hydrogen, poses questions related to the hydrogen concentration in SRN films. These questions ask for a further investigation.
- It has been demonstrated that the at COM available prism coupler is a more accurate instrument for the measurement of the refractive index and thickness of SRN films than the available ellipsometer (refractive index accuracy: a few times 10^4 vs. $>2 \cdot 10^3$, see subsections 5.2.3 and 5.2.7).

5.3 N-H related absorption in silicon rich nitride films

5.3.1 Introduction

Films that are deposited by means of precursors that incorporate both hydrogen and nitrogen may contain significant amounts of N-H bonds. This has been reported for plasma-enhanced as well as for low-pressure chemical vapor deposition [27]. N-H bonds have their intrinsic infrared absorption around a wavenumber of 3300 cm^{-1} which corresponds to a wavelength of 3000 nm^1 . The first overtone of this frequency can be found around a wavelength of 1500 nm , and its low-energy tail leads to unwanted absorption losses in the wavelength region of interest. The exact positions of the resonance peak and its overtones depend on the material structure. Particularly the electronegativity of the groups that surround the N-H bonds is expected to be important [66].

In principle, N-H bonds can be largely removed by annealing, but there are a few additional effects, which are discussed in section 5.6, that imply that the removal of hydrogen by annealing is not straightforward. These complications give reasons for investigating the incorporation of N-H bonds in SRN films and the influence of annealing on their concentration. The method that was used to perform this analysis is Fourier transformed infrared (FTIR) spectroscopy [67].

5.3.2 Measurement principle

Infrared spectroscopy is a characterization method that records the interaction of infrared radiation with samples, measuring the frequencies at which the sample absorbs the radiation. Determining these frequencies allows the identification of the sample's chemical composition, since chemical functional groups are known to absorb light at specific frequencies [67].

The frequencies of light that are absorbed are associated with transitions in the rotational and vibrational states of a compound. In order for a particular rotational or vibrational mode to directly absorb infrared radiation, the motion associated with that mode must produce a change in the dipole moment of the compound. This requirement implies that bonds such as N-N and Si-Si bonds cannot be detected by infrared spectroscopy, and that the influence of electronegativity on the position of the resonance peak, which has been mentioned in 5.3.1, sounds reasonable. For solids, internal rotations are often limited, so the major type of interaction is vibrational.

Fourier transform infrared (FTIR) spectroscopy is an implementation of infrared spectroscopy in which the spectrum is obtained on the basis of a Fourier analysis. The essential difference between FTIR spectroscopy and conventional, so-called *dispersive* infrared spectroscopy is that FTIR spectroscopy uses all wavelengths at the

¹ In FTIR spectroscopy, the entity that is commonly used to quantify the wave character of light is the wavenumber k , expressed in cm^{-1} . The relation between wavenumber k and wavelength λ is: $k = 1/\lambda$.

same time, while dispersive infrared spectroscopy makes a spectral scan. The consequence of this bandwidth difference is that FTIR spectroscopy benefits from a signal-to-noise ratio enhancement, described by *Fellgett's advantage* [67], also known as the multiplex advantage. Another advantage of FTIR is the fact that the radiative throughput is larger. This beneficial effect is known as *Jacquinot's advantage* [67].

More information about the differences between FTIR spectroscopy and dispersive infrared spectroscopy as well as about the realization of an FTIR spectrometer, which is based on a Michelson interferometer, can be found elsewhere [67].

5.3.3 Experimental setup

The FTIR spectrometer that was used for the performance of the experiment is the *MIR 8000* of *Oriel Instruments* [68] with a deuterated tri-glycine sulfate (DTGS) pyroelectric detector. This type is the most common detector used in FTIR instruments. It is chosen for its ease of use, good sensitivity, and excellent linearity. The spectral range of this detector is $6000\text{-}300\text{ cm}^{-1}$ ($1.7\text{-}28\text{ }\mu\text{m}$), which implies that fundamental N-H related absorption around 3300 cm^{-1} can be detected, but not the first overtone around 6600 cm^{-1} .

The *MIR 8000* is a fully automatic setup which is equipped with Matlab-based software that performs the FTIR analysis. The software provides absorbance graphs as are shown in subsection 5.3.5. More information about the experimental setup can be found elsewhere [69].

5.3.4 Experiment

The actual experiment comprehends the measurement of the absorption spectra of a number of SRN films as well as some PECVD-grown silicon oxynitride (SiON) films. The motivation to measure the absorption spectra of PECVD-grown SiON films was that they could serve as a reference (see section 5.3.6).

The SRN films were deposited with the recipe described in section 5.1.1 (thickness: $1.2\text{ }\mu\text{m}$). The PECVD-grown SiON films, which had a thickness of $2\text{ }\mu\text{m}$, were deposited with a recipe that was extracted from the literature [35]. All films were deposited on double-polished wafers because it has been reported that this improves the signal-to-noise ratio [35]. To investigate the influence of annealing, both as-deposited and annealed films have been measured. The anneal process was a 4 hours process at a temperature of $1100\text{ }^{\circ}\text{C}$ in a nitrogen atmosphere. Other anneal temperatures ($900\text{ }^{\circ}\text{C}$, $1000\text{ }^{\circ}\text{C}$, $1050\text{ }^{\circ}\text{C}$) have been used as well, but these experiments don't provide extra information.

5.3.5 Results

The results of the experiment are shown in figures 5.3 and 5.4. Figure 5.3 shows the measured spectral absorbance of the as-deposited and annealed SiON films. In both graphs, the two lines are shifted vertically for clarity. Both spectra were obtained by averaging 250 individual spectra which were all measured with a resolution of $4\text{ cm}^{-1}/\text{div}$. A measurement of a bare silicon wafer has been subtracted to eliminate background absorption.

It can be seen that the as-deposited material exhibits a peak at a wavenumber of 3370 cm^{-1} which can be attributed to N-H bonds. The peak has disappeared after annealing at $1100\text{ }^{\circ}\text{C}$. The origin of the other peaks has been obtained from the literature and is displayed in the graph. The fluctuations that can be attributed to H_2O and CO_2 could be avoided by performing the experiment in a chamber that is purged with nitrogen. Because of practical reasons, this was not possible during this project. The periodic variation that is visible from 6000 to 1500 cm^{-1} is probably due to etalon effects in the measurement setup. It appeared to be impossible to reduce the influence of these effects further then is shown in the graph.

Figure 5.4 shows the measured spectral absorbance of the as-deposited SRN and annealed SRN films. It can be seen that no absorption peak is visible near a wavenumber of 3300 cm^{-1} . For the rest, the same remarks are applicable as for figure 5.3.

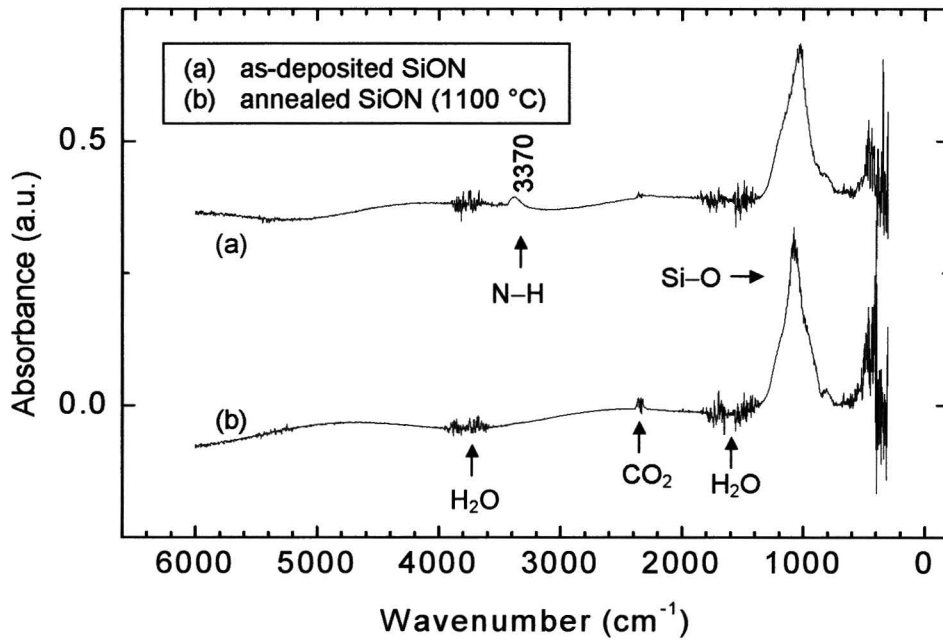


Figure 5.3: Spectral absorbance of as-deposited and annealed SiON. One line (a) has been shifted upward for clarity. N-H absorption is visible for as-deposited SiON.

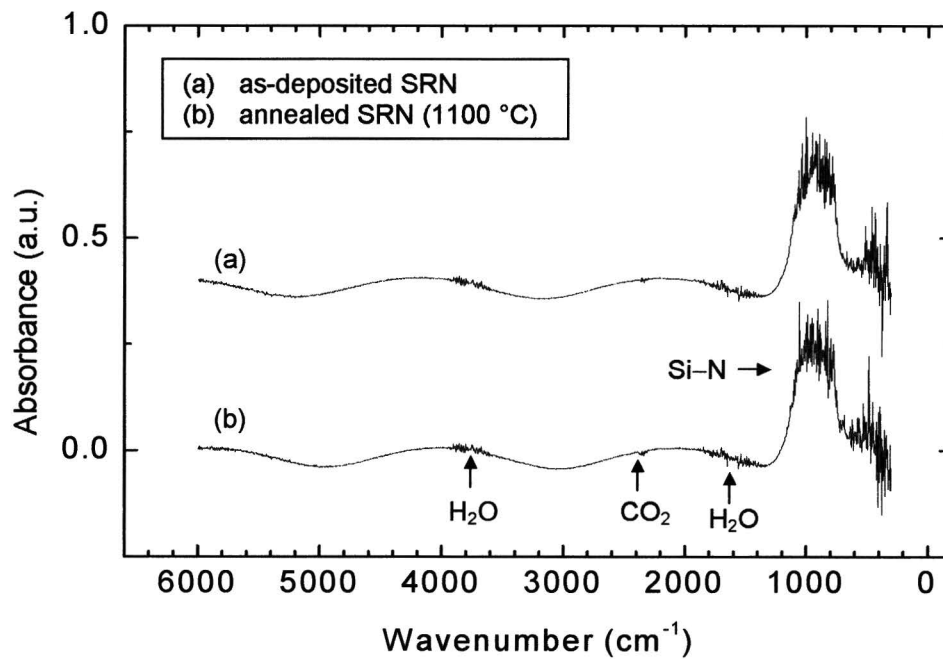


Figure 5.4: Spectral absorbance of as-deposited and annealed SRN. One line (a) has been shifted upward for clarity. No N-H absorption is visible for both as-deposited and annealed SRN.

5.3.6 Discussion

The measurements of the SiON films are in agreement with the results presented in reference 35. This confirms that the used FTIR setup is capable of detecting sufficiently strong N-H related absorption peaks. However, it is known that an anneal temperature of 1100 °C is not high enough to remove all hydrogen out of SiON films [22], [35], which implies that relatively small concentrations of N-H bonds are beyond the detecting limit of the equipment used. Small concentrations of N-H bonds could still pose a limit to the optical properties of a material as is shown in section 5.4.

The FTIR measurements of the SRN films show that the concentration of N-H bonds in both the as-deposited and the annealed SRN films is lower than what can be detected by the FTIR setup. This implies that the concentration of N-H bonds in LPCVD-grown silicon rich nitride is significantly lower than in as-deposited PECVD-grown SiON. This is not surprising due to the different process characteristics, as has been described in subsection 5.1.1. Based on the absence of N-H peaks in the FTIR spectrum of SRN films it was estimated, by a comparison with annealed PECVD-grown SiON data [22], that the N-H related propagation loss around 1550 nm is below 2 dB/cm.

The detection limit of Fourier transform infrared spectroscopy was found to be too low to investigate the influence of the anneal temperature on the concentration of N-H bonds. Therefore, other characterization methods need to be considered.

Finally, a difference between the SiON and the SRN spectra (figures 5.3 and 5.4) is the fact that the Si-O absorption peak for SiON is sharper than Si-N absorption peak for SRN. Besides, there is more noise visible on the Si-N peak than on the Si-O peak. It might be that this spectral broadening in SRN indicates that the investigated SiON is more homogeneous than the investigated SRN. However, the bad quality of the SRN films (see section 5.5) could also be responsible for the difference. More research is required to give an explanation.

5.3.7 Conclusions

The main conclusion of this experiment is that the N-H related propagation loss in SRN films around 1550 nm is below 2 dB/cm (see subsection 5.3.6). The detection limit of Fourier transform infrared spectroscopy is too low to give a better estimation. This implies that the application of another measurement method is required to perform a more thorough analysis.

5.4 Propagation loss of silicon rich nitride slab waveguides

5.4.1 Introduction

To continue the investigation of the loss mechanisms in SRN waveguides that had been started with Fourier transform infrared spectroscopy, the propagation loss in SRN slab waveguides was measured by dual prism coupling. The objective of these measurements was to obtain more detailed information about possible N-H related absorption and to determine an absolute value for the propagation loss in slab waveguides.

Since dual prism coupling is a characterization method that is not commercially available, the measurements described in this section were performed with a home-built setup of the *Lightwave Devices Group* of the *University of Twente* in Enschede, The Netherlands.

5.4.2 Measurement principle

In a dual prism coupling setup, light is coupled into and out of a slab waveguide by means of two prisms. The intensity of the outcoupled light is measured by a photo detector. The separation between the prisms d_{prism} is flexible so the intensity can be measured as function of the prism separation. The propagation loss is proportional to the decay rate of the detected intensity as function of prism separation. The principle is illustrated in figure 5.5. More information about dual prism coupling can be found elsewhere [70].

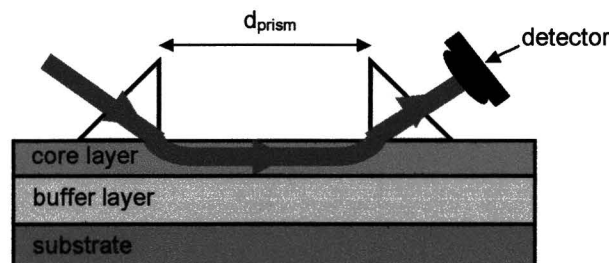


Figure 5.5: Illustration of the principle of dual prism coupling.

Compared to the prism coupling method for the determination of the refractive index and thickness of a dielectric film, which has been described in section 5.2, there are a few principal differences. First, since substrate leakage influences the propagation loss measurements, a buffer layer is required. Second, because it is required to measure the absolute intensity, it is necessary to take the responsivity of the photo detector into account.

5.4.3 Experimental setup

The home-built dual prism coupling setup of the University of Twente that was used for the performance of the experiment is illustrated in figure 5.6. The setup can be used to perform refractive index and thickness measurements as well as propagation loss measurements.

The central part of the setup is a stepper-motor-driven rotation table that provides the possibility to adjust the angle of incidence of an incoming laser beam. The setup has multiple inputs so several lasers can be connected simultaneously. Moveable mirrors serve as switches. In this experiment two inputs were used: one for a He-Ne laser ($\lambda = 632.8$ nm) and one for a tunable infrared laser ($\lambda = 1480$ – 1580 nm). Both inputs are equipped with polarizers.

Both prisms are attached to the sample by spring-loaded fixtures that provide the possibility to apply an adjustable downward pressure. The fixtures have not been indicated in figure 5.6. The downward pressure is an important parameter for obtaining an optimal coupling efficiency. The photo detector that measures the light coupled out of the slab waveguide by the second prism is attached to the fixture of this particular prism. The fixture, including prism and detector, can be moved parallel to laser beam propagating in the waveguide. In that way, the transmission can be measured as function of the prism separation without fluctuations originating from variations in the prism-to-detector transmission. Because the incoupling prism is fixed as well, the only parameter that has to be adjusted between individual transmission measurements is the waveguide-to-outcoupling-prism coupling efficiency, which can be done by regulating the downward pressure. The dependence on only one parameter is a major advantage of the dual prism coupling method as implemented in this setup (see subsection 5.4.6 for more information about this issue).

The displayed trans-impedance amplifiers convert the detected light intensity in a linear way to voltage, which is crucial for an accurate determination of the propagation loss. To improve the signal-to-noise ratio the setup is equipped with a chopper and a lockin amplifier. Furthermore, a normal angle calibrator has been integrated to enable the determination of the angle for which the beam is perpendicular to the prism surface.

A complication related to the measurement of SRN waveguides is the fact that the alignment of the laser beam, the prisms and the detector and the adjustment of the downward pressure on the prisms are based on the application of red light. Because silicon rich nitride absorbs red light [72], these operations have to be done with invisible infrared light, which complicates the procedure considerably.

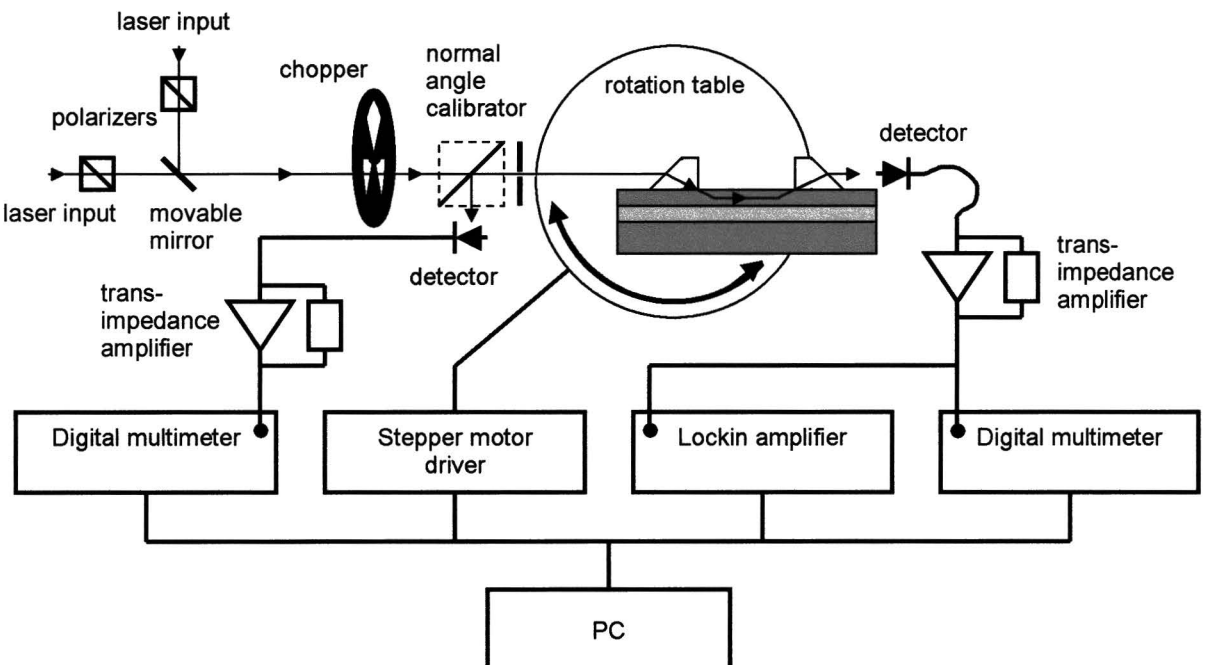


Figure 5.6: Schematic overview of the dual prism coupling setup of the University of Twente.

5.4.4 Experiment

The dual prism coupling setup was used for propagation loss measurements of three samples: an as-deposited and an annealed SRN waveguide, and an as-deposited PECVD-grown SiON waveguide. The recipes are exactly the same as the recipes described in the section about the FTIR spectroscopy (see 5.3.4). The only difference is that all films were deposited on thermally oxidized wafers. The SiON waveguides have been analyzed to continue the comparison that has been initiated in section 5.2.

Prisms made from the material LaSF N31 with a refractive index of 1.85 around a wavelength of 1550 nm were used for SiON and prisms made from the material rutile (TiO_2) with a refractive index 2.7 around a wavelength of 1550 nm were used for SRN. Oil with a refractive index of 1.64 was used to facilitate the outcoupling for the SRN samples.

The propagation loss as function of wavelength (1480-1580 nm) was determined by making wavelength scans for various prism separations. For every wavelength, the transmission (in dB) was plotted versus prism separation. Subsequently, a straight line was fitted using the least square method. The slope of the line is the negative propagation loss. Finally, the propagation loss was plotted as function of wavelength.

Only TE polarized light was used because of the alignment and pressure adjustment complications related to SRN films (see subsection 5.4.3). These complications were made worse by the fact that the exact refractive indices (n_{TE} and n_{TM}) of the rutile prism, which is highly birefringent, were unknown. This implies that the angles of incidence could not be calculated, but had to be found experimentally. The limited amount of time available for the performance of the measurements made it impossible to perform measurements with TM polarized light.

5.4.5 Results

The results of the dual prism coupling experiment are illustrated in figures 5.7 - 5.9. Figure 5.7 shows the transmission vs. prism separation of an as-deposited SRN film for five different wavelengths on a dB-scale. It can be seen that there is a clear linear tendency (on a dB-scale) for every wavelength with a difference in slopes for the various wavelengths, which implies that the propagation is not constant as function of wavelength.

The propagation loss versus wavelength is shown in figure 5.8 for both an as-deposited and an annealed SRN waveguide. It can be seen that there is a background loss of 0.5-0.6 dB/cm with on top of it an absorption peak centered around 1525 nm. For the as-deposited sample the absorption peak has a height of 0.8 dB/cm, while the peak has reduced to 0.5 dB/cm for the annealed sample. Based on the error in the linear fit of the data in figure 5.7, the accuracy of the dual prism measurements is estimated to be 0.05 dB/cm.

Figure 5.9 shows the propagation loss versus wavelength for as-deposited SiON and as-deposited SRN waveguides. The graph shows that the absorption peak in SiON is much stronger than in SRN. Besides, it is shown that the peak in SiON is centered around a smaller wavelength than in SRN.

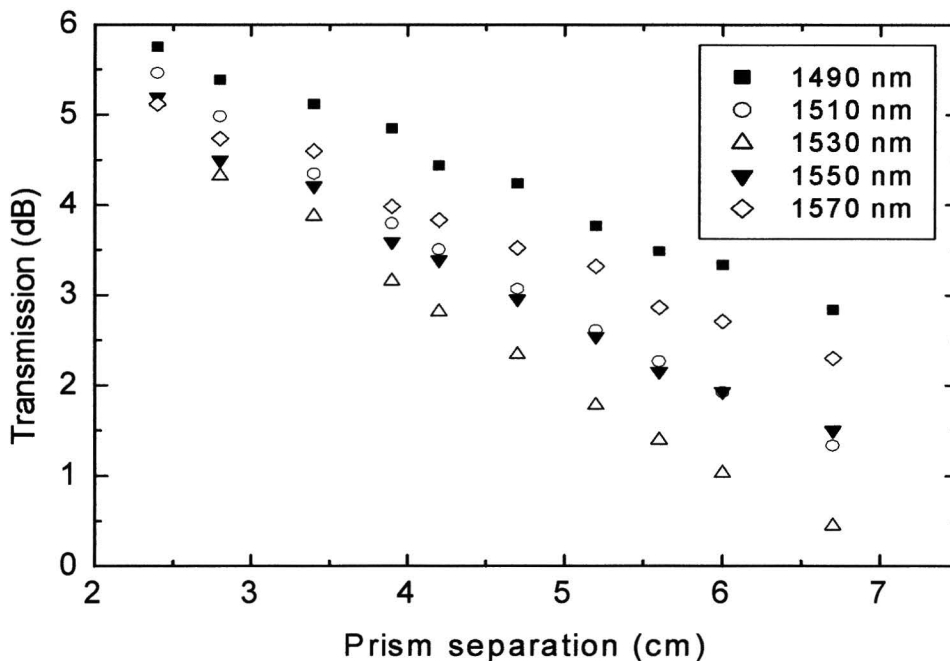


Figure 5.7: Transmission versus prism separation for an SRN waveguide that had been annealed at 1100 °C for 5 different wavelengths.

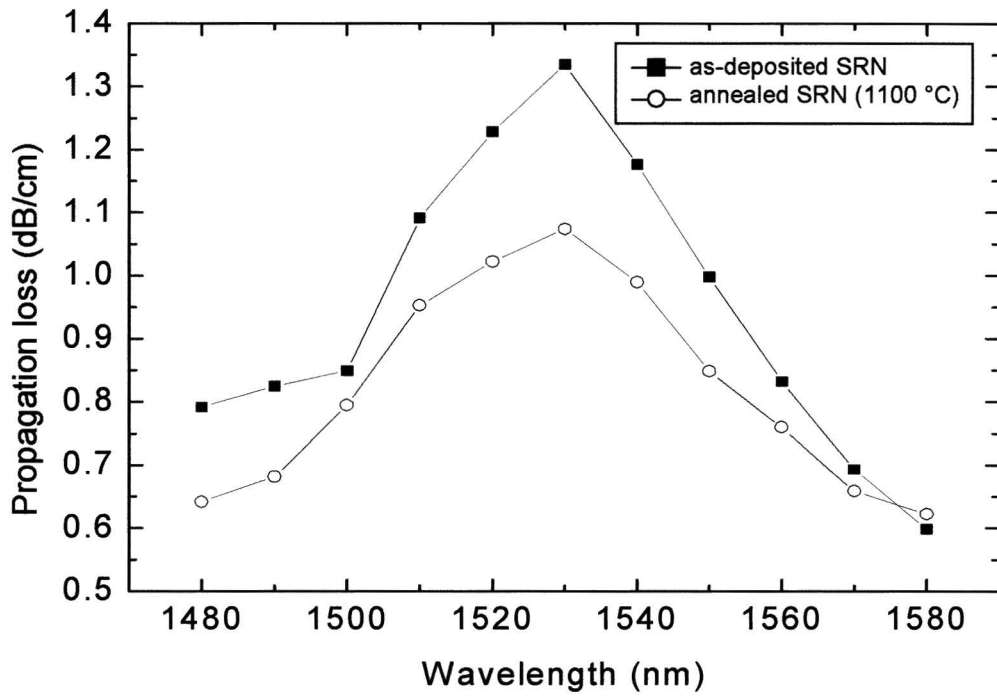


Figure 5.8: Propagation loss versus wavelength for an as-deposited SRN waveguide and an SRN waveguide that had been annealed at 1100 °C. The lines are meant to guide the eye.

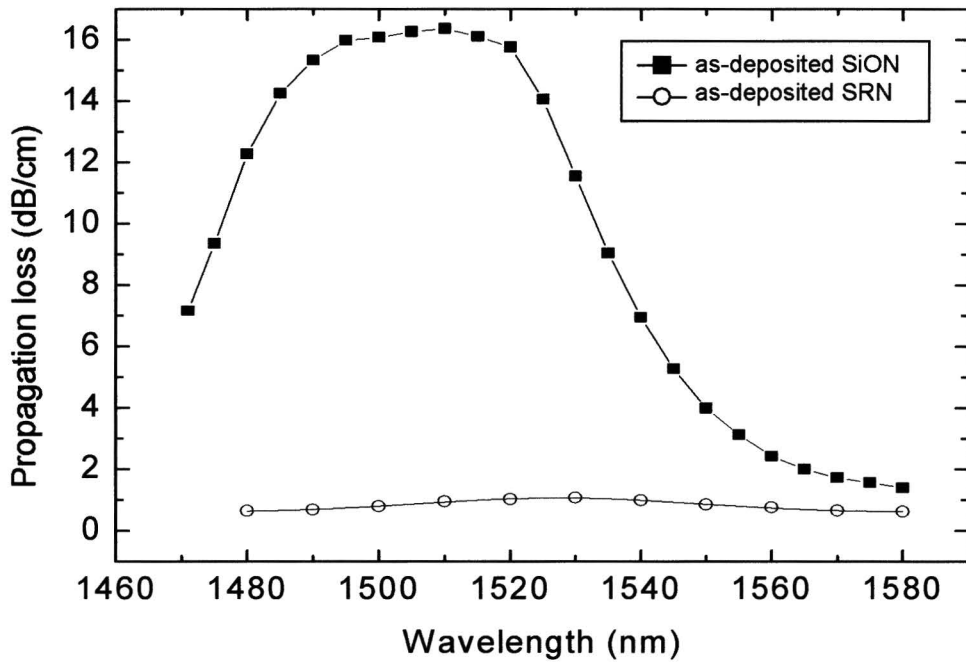


Figure 5.9: Propagation loss versus wavelength for an as-deposited SiON waveguide and an as-deposited SRN waveguide. The lines are meant to guide the eye

5.4.6 Discussion

The results of the dual prism coupling experiment allow a number of conclusions about the abilities of the dual prism coupling method as well as about the optical quality of the silicon rich nitride under investigation.

First of all, the dual prism coupling method proved to be a very useful tool for the accurate determination of propagation loss in slab waveguides. This is expressed by the clearness of the linear relationship between transmission (on a dB-scale) and prism separation (see figure 5.7). The small error (0.05 dB/cm) can be attributed to the fact that only one parameter, the downward pressure of the outcoupling prism, needs to be adjusted between individual transmission measurements. In comparison, the material losses in a waveguide can also be measured by a cutback experiment of a wide waveguide because sidewall roughness can be neglected for this type of waveguides [38]. However, because a cutback experiment is based on a stepwise reduction of the length of a waveguide, both the in- and outcoupling fibers have to be adjusted between every transmission measurement. Particularly for high-contrast waveguides with a small mode-size, this is a laborious activity. Variations in the in- and outcoupling efficiency are a source of errors in the cutback experiments. As a consequence, the dual prism coupling measurements have provided more accurate data on propagation loss than has been obtained cutback experiments. To illustrate this, figure 5.10 shows a graph of a cutback experiment that was performed in the high-index project¹. The graph shows that the scattering in the measurements is much worse than for the dual prism coupling measurements shown in figure 5.7 (0.2-0.3 dB/cm vs. 0.05 dB/cm). The propagation loss was determined to be 0.7 ± 0.3 dB/cm at a wavelength of 1543 nm (see figure 5.10).

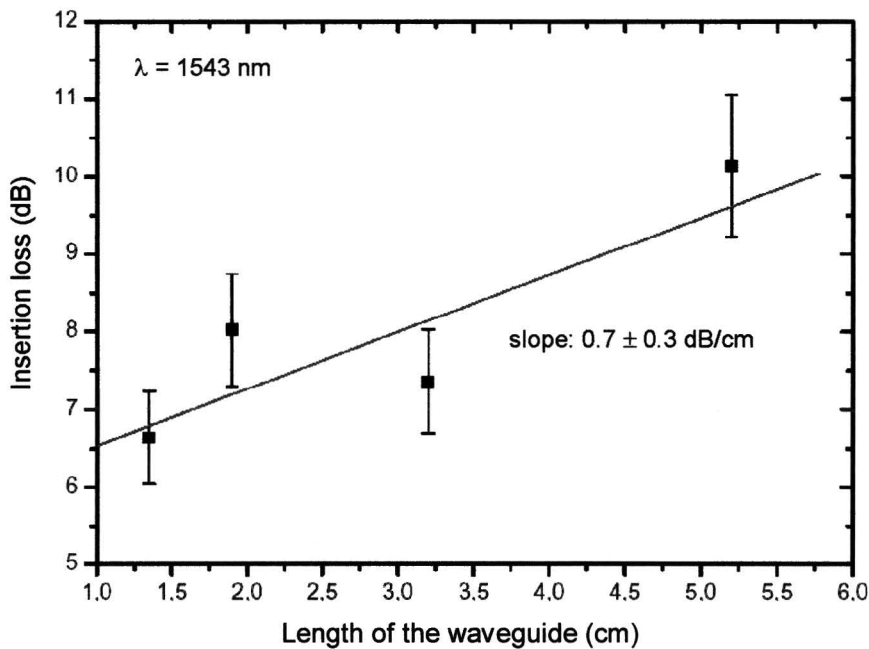


Figure 5.10: Insertion loss versus waveguide length of a cutback experiment of an SRN waveguide (reprinted from reference 40).

Regarding the SRN films it can be concluded that N-H related absorption is observable in both the as-deposited and annealed films. The anneal temperature of 1100 °C is too low to remove all hydrogen. This suggests that a reduction of N-H related absorption is possible by annealing at higher temperatures. This possibility, including some considerations, is discussed in section 5.6. The measured propagation loss of 0.6-1.3 dB/cm can be regarded as a promising value for a material with a refractive index as high as 2 (see chapter 3 for a comparison with alternative materials), especially because no optimization procedure has been started yet.

Furthermore, from figure 5.9 it can be concluded that the absorption peak in as-deposited SiON is very strong, which confirms the conclusion of section 5.3 that FTIR is a characterization technique with a very low detection limit for characterization purposes related to optical waveguide applications. Therefore, the investigation of N-H related absorption by FTIR could only be useful in the start of a development process.

¹ Cutback experiments haven't been part of this master project.

5.4.7 Conclusions

The main conclusions of the dual prism coupling setup are:

- The dual prism coupling method is a characterization method capable of measuring the propagation loss in material films in a more accurate way than what has been demonstrated with the cutback method (accuracies: 0.05 dB/cm vs. 0.2-0.3 dB/cm). This offers the possibility to obtain unique information with this characterization method (for example figure 5.8).
- The propagation loss of SRN films is within a range from 0.6 to 1.3 dB/cm around a wavelength of 1550 nm, which is promising for a material with a refractive index as high as 2 (see subsection 5.4.6).
- The propagation loss can partly be attributed to N-H related absorption (see subsection 5.4.6). This implies that it could be improved by avoiding the formation of N-H bonds or by removing them. Possibilities to realize this are discussed in section 5.6.

5.5 Particles in silicon rich nitride films

Before the analysis of SRN film and waveguide properties is completed with a discussion of ideas for future work in section 5.6, this section pays attention to an important technological problem that has limited the progression in the high-index project considerably the last half year and which was still a bottleneck during the writing of this thesis.

The problem is the incorporation of large amounts of particles in the SRN films during the LPCVD deposition process, which is illustrated in figure 5.11. The problem was detected in February 2002, but further investigations made clear that it has been present since October/November 2001. In July 2002, the problem has not been solved, despite a number of attempts to trace the problem. Since particle-free SRN films have been deposited in the past, it is expected that the cause of the problem is a technological issue (related to the LPCVD furnace or gas supply). However, there is no clear evidence for this. Cutback experiments, which weren't done within the framework of this master project, show that the propagation loss in waveguides fabricated from contaminated SRN films is on the order 8 dB/cm [83].

The implication of this problem is that SRN films as described in this chapter cannot be reproduced at the moment. Consequently, further research to realize improvements is practically impossible. Therefore, solving the particle problem has a very high priority.

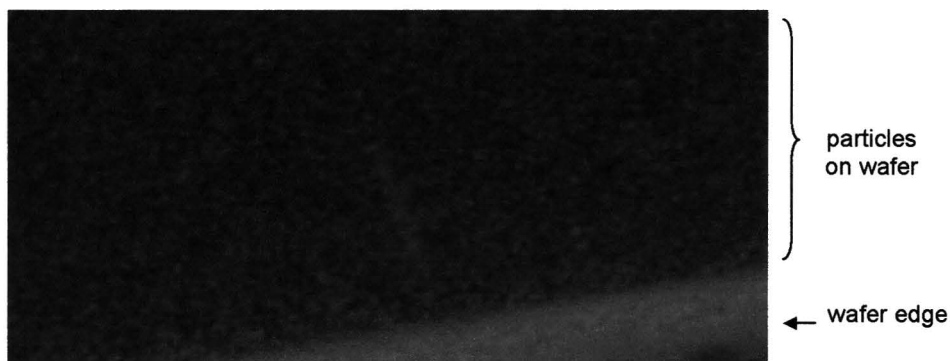


Figure 5.11: Particles in SRN films seen through an optical microscope (magnification: 10 x).

5.6 Future research

5.6.1 Opportunity

Provided that the problems described in section 5.5 will be resolved, the research presented in this chapter provides several ideas for process improvements. These improvements are mainly related to the spectral propagation loss of SRN waveguides shown in figure 5.8. The clear visibility of the absorption peak around a wavelength of 1525 nm confirms that a substantial part of the propagation loss is caused by N-H related absorption as was discussed in section 5.4 (for information about the origin of the remainder of the propagation loss see subsection 5.6.4). For PECVD-grown SiON, it has been reported that annealing at 1140 °C is an effective method to remove N-H bonds [35]. However, annealing SRN films at this temperature with the standard recipe (=standard temperature ramps) results in the creation of a sort of clustered structure which is observable by optical microscopy [43]. It is under investigation by X-ray spectroscopy whether this is a crystallization effect.

An opportunity to avoid this cracking or crystallization effect is to change the temperature ramps of the standard anneal recipe. This is motivated by the fact that it is known that avoiding thermal stresses can be accomplished by cooling the wafers at a sufficiently slow rate [42]. To illustrate how the anneal process could be improved, figure 5.12 compares the current anneal process in the high-index project with the anneal process developed by IBM to get rid of the very strong N-H related absorption in PECVD-grown SiON. It is shown that the ramps are less steep and the (un)load temperature is lower for the IBM recipe.

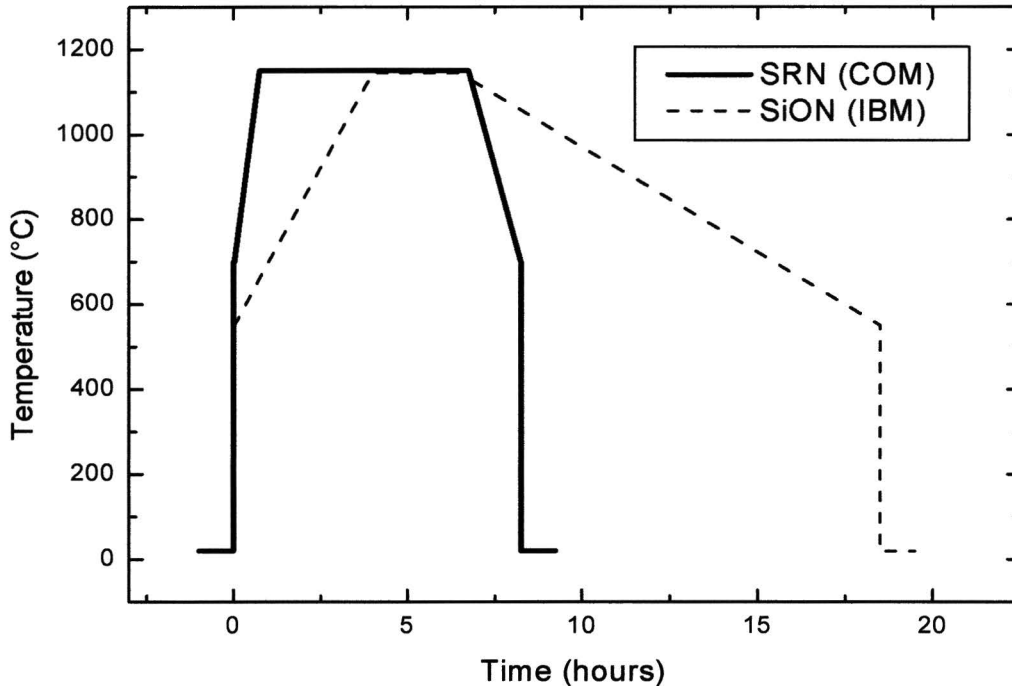


Figure 5.12: Temperature profiles of the current anneal process for SRN films in the high-index project and IBM's anneal process for PECVD-grown SiON.

5.6.2 Recommendations

Based on the above-described opportunity, the main recommendation of this analysis is to examine the influence of both the height of the maximum temperature and the steepness of the ramps on N-H related absorption loss as well as mechanical stress. The difficulty of such an investigation is the lack of sufficiently accurate measurement methods available at COM. Considerations presented in section 5.4 show that the cutback method is not accurate enough (0.02-0.03 dB/cm) at the moment to measure spectral tendencies in the propagation loss in detail. Unless the accuracy can be improved, an investigation as proposed above could only rely on the dual prism coupling method, which is unfortunately not available at COM. In addition, the stress measurements are complicated by the fact that the LPCVD process deposits silicon rich nitride on both sides of the wafer, which implies that the mechanical stress cannot be deduced from the wafer bending, as can be done for PECVD processes. Stripping the backside by reactive ion etching or using bonded wafers during deposition could solve this problem. Experiments have to show whether this is realistic. During this master project, there was not enough time to perform these measurements.

So, the main objective is to investigate whether anneal treatments can be as effective for LPCVD-grown SRN films as they are for PECVD-grown SiON films. There are two considerations that question the effectiveness of this approach:

- It has been observed that a 1-hour anneal treatment of stoichiometric silicon nitride at 1200 °C doesn't remove the absorption peak completely [60]. However, this could be explained by the short duration of the anneal treatment.
- Hydrogen could be inevitable in (non-stoichiometric) silicon rich nitride to passivate bonds that are not part of the silicon-nitrogen material matrix. Removing this hydrogen could induce destructive localized charge effects, which would imply that it is impossible to eliminate N-H related absorption in SRN films completely by annealing, without increasing the background loss (loss that cannot be attributed to N-H related absorption).

If the above-mentioned hypothesis of the importance of hydrogen for the stability of silicon rich nitride is correct, then an alternative method is required to get rid of N-H related absorption. An in principle very simple

solution would be to replace hydrogen by deuterium (D), which moves the first overtone from a wavelength of ~1500 nm to ~2000 nm far from the wavelength region of interest because the rare isotope deuterium is heavier than hydrogen H.

Because deuterated precursors SiCl_2D_2 and ND_3 with a high purity are probably too expensive to use them in an LPCVD process, the recommendation is to load SRN samples deposited with SiCl_2H_2 and NH_3 in a chamber with deuterium to replace the hydrogen largely with deuterium by means of diffusion. The influence of the duration of the deuterium treatment on the spectral propagation loss could be investigated to get an impression of how far the propagation loss can be reduced by the removal of N-H related absorption.

5.6.3 Remaining questions

If anneal or deuterium treatments are to be effective, then figure 5.8 suggests the propagation loss can at least be reduced to ~ 0.6 dB/cm. This leads to questions about the cause of the remainder of the loss. Possibilities are:

- The homogeneity of the silicon rich nitride could be relatively bad, which might induce scattering losses. The difference in sharpness of the Si-N and Si-O absorption peaks in SRN and SiON in the FTIR spectra could be an indication of the lack of homogeneity in SRN. Further research is necessary to establish whether this is true. Maybe the investigation with X-ray spectroscopy, which is in progress (see subsection 5.6.1), will provide information about this subject.
- For polycrystalline silicon waveguides it has been reported that dangling bond defect sites present at the grain boundaries cause absorption loss and scatter light [71]. The dangling bonds can be largely removed by hydrogen passivation. It is not clear whether dangling bonds have similar effects in silicon rich nitride. Literature research could provide information about this issue. There was not enough time available to pay attention to this issue during this master project.
- Silicon rich nitride has a complex refractive index for small wavelengths, which is probably due to electron-transition absorption loss. The imaginary part decreases as function of wavelength and gets below 0.05 around a wavelength of 600 nm [72]. However, because the relationship between propagation loss α and the imaginary part of the refractive index n_i is given by:

$$\alpha_{\lambda=1550 \text{ nm}} \text{ (dB/cm)} = 3.521 \cdot 10^5 n_i, \quad (5.1)$$

as is derived in appendix B, the imaginary part of the refractive index has to be below $3 \cdot 10^{-8}$ to establish a propagation loss below 0.01 dB/cm. It is not clear whether the imaginary part of the refractive is so low around 1550 nm.

- The presence of large amounts of particles in deposited films has been proven to be very disadvantageous for the optical quality of SRN waveguides. A limited amount of particles could be responsible for a propagation loss of ~ 0.6 dB/cm.

In this project, there was not enough time available to address the above-mentioned issues, but they could be relevant for a continuation. Next to literature research, an interesting experiment could be to obtain a spectral plot of the real and imaginary part of the refractive index. Such a measurement could be done with a spectroscopic ellipsometer over a broad wavelength range (e.g., 300-1700 nm, depending on the available equipment). If accurate enough, such a plot could give information on the influence of the tails of absorption peaks on the propagation loss around 1550 nm.

5.6.4 Conclusions

The main conclusion of the brief analysis of opportunities to improve the propagations loss is that a reduction of the propagation loss could be possible by the removal of N-H bonds through improved anneal treatments. Therefore, the main recommendation is to perform experiments to find out whether this is true. In addition, the influence of deuterium treatments on the strength of N-H related absorption loss could be investigated to establish an accurate distinction between N-H related propagation loss and propagation loss due to other sources, while avoiding possible complications with annealing (see subsection 5.6.2).

Besides, a number of other loss mechanisms could contribute to the propagation loss. Both literature research and experiments (for example spectroscopic ellipsometer measurements) are required to draw conclusions on their importance (subsection 5.6.3).

5.7 Summary

In this chapter, an analysis of a number of silicon rich nitride (SRN) film and waveguide properties has been presented. The objective of the analysis was to investigate the suitability of silicon rich nitride for optical waveguide applications and to investigate whether process improvements could be implemented.

The investigation of the refractive index and thickness uniformity of SRN films by prism coupling resulted in the conclusion that the spread in both refractive index (< 0.03 %) and thickness (0.8 %) of the LPCVD-grown SRN

films per wafer is good enough for device applications. This conclusion is based on a comparison with IBM's SiON technology, which was the best thinkable criterion in the current situation. The uniformity over a boat of 25 wafers needs to be improved before all wafers can be used to fabricate components with the same specifications, but because the uniformity over a boat of 25 wafers is only important for a production process and not for the high-index project in its current state, this has no priority at the moment (see section 5.2).

The conclusion of the investigation of N-H related absorption by Fourier transform infrared spectroscopy is that the N-H related absorption loss in the SRN films is below 2 dB/cm and that the detection limit of this characterization method is too low to obtain more accurate information (see section 5.3).

The measurement of propagation loss in SRN slab waveguides by dual prism coupling shows that the propagation loss of SRN films is within a range from 0.6 to 1.2 dB/cm in the wavelength region around 1550 nm, which is promising for a material with a refractive index as high as 2. Besides, the measurement shows that the propagation loss can partly be attributed to N-H related absorption (see subsection 5.4.6). This implies that the propagation loss could be improved by avoiding the formation of N-H bonds or by removing them. A method that is proposed to realize this reduction in propagation loss is the application of an anneal treatment with a higher temperature to remove more hydrogen and with less steep temperature slopes to avoid thermal stresses. This modification is the main recommendation of the performed analysis. Another recommendation is to investigate the influence of deuterium treatments on the propagation of SRN waveguides (see subsection 5.6.3). The outcome of such experiments could be investigated when the LPCVD particle problems have been solved (see section 5.5).

6 SRN ring resonator coupled to UV written waveguide

<<confidential>>

<<confidential>>

<<confidential>>

<<confidential>>

<<confidential>>

<<confidential>>

7 Conclusions and recommendations

This chapter summarizes the conclusions and recommendations presented in the preceding chapters.

7.1 Concept of the high-index project

An extensive explanation of the concept of the high-index project has been presented in chapters 2, 3 and 4. Apart from the fact that this part of the thesis serves as background information for the experimental work described in chapters 5 and 6, it is a detailed analysis of opportunities and challenges related to the high-index project, and therefore it forms a substantial part of the master project.

The comparison of material systems (section 3.1) shows that there are several candidates (e.g., silicon-related material systems, III-V semiconductors and polymers) for becoming the dominant enabling technology for integrated optics. An important conclusion of the comparison is that two features of silicon-related material systems are very advantageous:

- Silicon-related material systems are compatible with mainstream semiconductor processing industry, which is an advantage because of the scalability and the associated low-cost perspective (section 3.1).
- Integrated optics based on silicon-related material systems could be combined with mainstream microelectronics in a monolithic way. This would combine the computation and data storage capacity of electronics and the transmission capacity of optics (section 4.4).

Within the category of silicon-related material systems, a distinction can be drawn between material systems that rely on low-contrast waveguides and material systems that rely on high-contrast waveguides. Optical components based on low-contrast waveguides are characterized by high fiber-to-chip coupling efficiency and low integration density. The opposite is true for optical components based on high-contrast waveguides. The conclusion of the analysis of this issue (section 3.2) is that it limits the possibility of fabricating low-loss high-density integrated optical devices based on either low- or high-contrast waveguides. The concept that is under investigation in the high-index project avoids this problem, as both low- and high-contrast waveguides are integrated on the same substrate. This enables to realize devices with both high fiber-to-chip coupling efficiency and high integration density. The conclusion of the analysis presented in section 3.3 is that this concept enhances the design freedom to improve the coupling efficiency between fibers and high-density integrated optical devices considerably, but that it is required to develop components that enable a sufficiently large light transfer between low- and high-contrast waveguides on chip. It depends on the application how large this coupling efficiency between low- and high-contrast waveguides on chip needs to be (see for example subsection 6.4.2).

An analysis of potential applications of high-contrast silicon-related material systems (chapter 4) shows that these material systems don't only provide the possibility of increasing the integration density, but that they enable to increase the functionality and to realize performance improvements as well. Examples that illustrate this are:

- Particular filter components can be fabricated with broader useable bandwidths when they are based on high-contrast material systems (section 4.1.3).
- High-quality optical resonators can be made suitable for higher modulation frequencies when they are based on high-contrast material systems (section 4.2.1).
- The photonic bandgap effect is stronger in high-contrast material systems (section 4.3).

These opportunities could increase the functionality of components based on silicon-related material systems. This is a relevant aspect of increasing the index contrast because the limited functionality of optical devices based on silicon-related material systems (especially compared to III-V semiconductors, see section 3.1) is a major drawback of this category of material systems.

7.2 Analysis of SRN film and waveguide properties

The main conclusions of the analysis of silicon rich nitride thin film and waveguide properties are listed below. Recommendations are listed after these. The conclusions are explained in more detail in the specified subsections.

- The index and thickness uniformity per wafer of the LPCVD-grown SRN films is good enough for device applications as has been derived based on a comparison with IBM's SiON technology (subsection 5.2.7).
- The Fourier transform infrared (FTIR) spectroscopy equipment applied to investigate N-H related absorption is not capable of detecting N-H concentrations that are as low as in the as-deposited and annealed SRN films (subsection 5.3.7). Based on a comparison with reported results, it was concluded that this implies that N-H related absorption loss in the wavelength region around 1550 nm is below 2 dB/cm for SRN waveguides (subsection 5.3.6). More accurate information about N-H related absorption loss could not be obtained by FTIR spectroscopy.

- The dual prism coupling measurements show that N-H related absorption loss is present in SRN waveguides (0.8 dB/cm at a wavelength of 1525 nm) and that this contribution can be reduced by annealing (subsection 5.4.7). Annealing at 1100 °C reduces the N-H related absorption peak at a wavelength of 1525 nm to 0.5 dB/cm.
- The dual prism coupling measurements show that in addition to the N-H related absorption loss, a background loss of ~0.5 dB/cm exists. The origin of this loss is not clear from the performed experiments. Possibilities are the tail of an electron-transition absorption peak in the UV or visible region, Rayleigh scattering or scattering due to defects in the SRN films (section 5.6).
- The progress in the optimization of the SRN films (as well as in the fabrication of waveguides) is being delayed by the LPCVD particle problem (section 5.5).

Based on the above-mentioned conclusions, the following recommendations have been formulated:

- N-H related absorption loss could be reduced by annealing at higher temperatures combined with the application of less steep temperature slopes to avoid thermal stresses (section 5.6). If the clustering/crystallization effect in SRN films after annealing at 1150 °C as observed by Karin Nordström Andersen and Peter Carøe Nielsen (section 5.6) is a stress-induced effect then it can probably be avoided by reducing the steepness of the temperature slopes. On the other hand, if the clustering/crystallization effect is a result of the fact that SRN becomes unstable when too much hydrogen is removed, then this is not a solution. This latter explanation could be true as well, because SRN is a non-stoichiometric compound. Hydrogen could be inevitable in this material to passivate bonds that are not part of the silicon-nitrogen material matrix. Removing this hydrogen could induce destructive localized charge effects, which would imply that it is impossible to eliminate N-H related absorption in SRN films completely by annealing without negative consequences.
The recommendation related to the influence of annealing is to investigate the effect of the height of the anneal temperature and the steepness of the associated slopes on both the N-H related absorption peak and the background loss in the propagation loss spectrum of SRN waveguides around a wavelength of 1550 nm.
- N-H related absorption loss could be reduced by the application of deuterium instead of hydrogen. This avoids the annealing problems discussed above. Because the deuterated gasses SiCl_2D_2 and ND_3 are probably too expensive to perform LPCVD processes with, an alternative experiment would be to load the samples after cleanroom processing in a deuterium chamber. This might eliminate the N-H related absorption loss without that the background loss is increased. Therefore, a recommendation is to investigate the influence of deuterium treatments on the propagation loss in SRN waveguides.
- A measurement of the imaginary part of the refractive index as function of wavelength by spectroscopic ellipsometry could be performed to get an impression about the origin of the background loss. Such a measurement could provide enough information to draw conclusions about the influence of Rayleigh scattering and electron-transition absorption losses in the 1550-nm wavelength region. A concern regarding this experiment is the accuracy of spectroscopic ellipsometry. Therefore, the recommendation is to try to perform the described experiment and to draw conclusions about the capability of spectroscopic ellipsometry to provide useful information (section 5.6).

7.3 SRN ring resonator coupled to UV written waveguide

<<confidential>>

A Mathematical analogy between waveguide theory and quantum mechanics

Characteristics of optical mode profiles can be derived in a way similar to what is done in quantum mechanics as both electromagnetism and quantum mechanics deal with wave propagation¹. In this appendix, the mathematical analogy between waveguide theory and quantum mechanics is used to improve the understanding of optical waveguiding. First, a general comparison is made to explain the confinement of light in another way than by total internal reflection. Subsequently, the comparison is focused on a specific refractive index profile to derive a qualitative relation between relative index difference and single-mode criteria of waveguides.

A.1 Light confinement according to the variational theorem

Table A.1 lists and compares a number of properties of quantum mechanics and electromagnetism. The comparison is focused on the variational theorem for both these branches of physics. The variational theorem can be used to solve the master equations. The *heuristic* or *rule of thumb* that is associated with it helps to understand the shape of the resulting functions. The heuristic learns that eigenstates tend to concentrate in certain regions to minimize their energy, while remaining orthogonal to lower-order modes. For quantum mechanical wave functions these regions correspond to a low potential, while for the electric displacement \mathbf{D} in electromagnetism, these regions correspond to a high refractive index.

Property	Quantum mechanics	Electromagnetism
Main functions	Scalar wave function Ψ	Vector fields \mathbf{E} and \mathbf{H}
Master equations	Schrödinger equation	Maxwell equations
Variational theorem	$E_{\text{var}} = \frac{\langle \Psi H \Psi \rangle}{\langle \Psi \Psi \rangle}$ $= \left(\frac{1}{\langle \Psi \Psi \rangle} \right) \int d\vec{r} \Psi^* H \Psi$ <p>E_{var} is minimized when Ψ is an eigenstate of the Hamiltonian H which is under certain conditions [14] given by:</p> $H = \frac{\hbar^2}{2m} \vec{\nabla}^2 + V.$	$E_{\text{var}} = \frac{(\vec{H}, \vec{\Theta} \vec{H})}{(\vec{H}, \vec{H})}$ $= \left(\frac{1}{2(\vec{H}, \vec{H})} \right) \int d\vec{r} \frac{1}{\varepsilon} \left \frac{\omega}{c} \vec{D} \right ^2$ <p>E_{var} is minimized when \mathbf{H} is an eigenstate of Θ. The exact form of operator Θ is specified elsewhere [15].</p>
Heuristic related to variational theorem	The wave function concentrates in regions of low potential, while remaining orthogonal to lower-order states.	The \mathbf{D} field concentrates in high- ε regions, while remaining orthogonal to lower-order modes.

Table A.1: Comparison between quantum mechanics and electromagnetism that shows that the localization of light in the core of a waveguide can be understood on the basis of a variational method that is similar to the method that is used to understand the localization of a wave function in a quantum well². The comparison is based on a more extensive account that can be found elsewhere [15].

In short, the electromagnetic variational theorem provides an alternative way to understand the confinement of light in waveguides. In contrast to total internal reflection, the variational theorem is also able to explain optical leakage (see sections 2.4 and 2.5).

¹ Although significant similarities exist between quantum mechanics and electromagnetism, the interpretation of a quantum mechanical wave function is fundamentally different from the interpretation of an electromagnetic wave, which clarifies that the resemblance is merely an analogy.

² Due to typographic limitations the vectors in the formulas are indicated with an arrow above the character, instead of with a bold character, as is done in the rest of the text.

A.2 Single-mode criteria

The comparison is now focused on the similarity between the confinement of a wavelike particle in a one-dimensional quantum well and the confinement of a lightwave in a slab waveguide. These specific configurations have been chosen because of their striking resemblance and their relative simplicity. An analogy that would be more illustrative from an applications point of view is the description of an electromagnetic wave in a step-index fiber, which is from a mathematical point of view nearly equivalent to the electron wave function in the famous corral of 48 iron atoms observed by scanning tunneling microscopy [16]. However, because of the mathematical complexity that would be involved, it is more appropriate to stick to a one-dimensional example. The definitions of the quantum well and the slab waveguide are depicted in figure A.1.

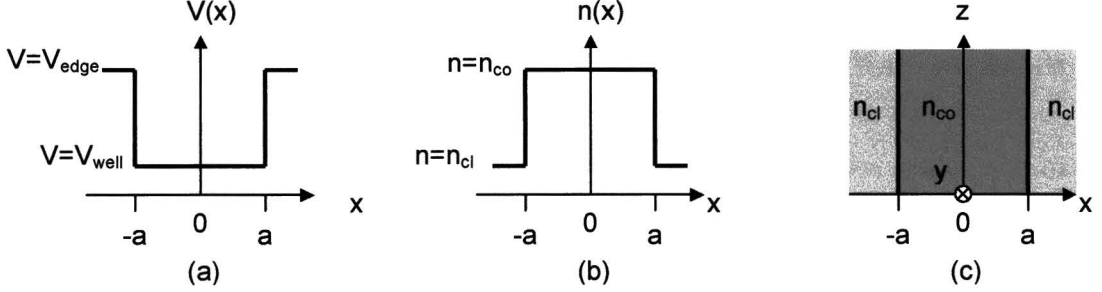


Figure A.1: (a) Potential of a one-dimensional quantum well. (b) Refractive index profile of a slab waveguide with the corresponding waveguide geometry (c).

The z direction (see figure A.1c) is chosen as the propagation direction of the electromagnetic wave. For simplicity, only the electric field of the TE mode E_{TE} , which is the mode with the electric field parallel to the y direction, is considered. Because of symmetry reasons E_{TE} is independent of y . Besides, it is known that the mode is a traveling wave along the z direction, which means that the z dependence of E_{TE} can be split off. This implies that the Maxwell equations can be reduced to the following scalar wave equation for E_{TE} :

$$\frac{d^2 E_{TE}(x)}{dx^2} + [k_0^2 n^2(x) - \beta^2] E_{TE}(x) = 0, \quad (\text{A.1})$$

where β is the propagation coefficient in the z direction, $n(x)$ is the refractive index profile and k_0 is the wave vector in vacuum.

This equation is analog to the equation that describes the wave function in a one-dimensional quantum well:

$$\frac{d^2 \varphi(x)}{dx^2} + \frac{2m}{\hbar^2} [E - V(x)] \varphi(x) = 0, \quad (\text{A.2})$$

where $\varphi(x)$ is the spatial wave function, m is the mass of the confined particle, \hbar is the Planck constant divided by 2π , E is the energy of the particle and $V(x)$ is the potential.

Both equations A.1 and A.2 are eigenvalue equations of exactly the same form. Also the boundary conditions are equivalent: requirement of continuity of the eigenfunctions and their first-order derivatives to x . This proves the resemblance between both cases. The relation between the depth of the quantum well and the height of the index profile for the specific configurations that have been indicated in figure A.1 is given by:

$$V_{\text{edge}} - V_{\text{well}} = \frac{k_0 \hbar}{2m} (n_{\text{co}}^2 - n_{\text{cl}}^2). \quad (\text{A.3})$$

In reference 14 can be seen how the eigenvalue equations for the profiles of figure A.1 can be solved based on a graphical determination of the eigenvalues. A typical result for the electromagnetic case is displayed in figure A.2. It is shown that a substantial part of the mode is located in the cladding, which is an example of a phenomenon that cannot be explained by ray optics. Figure A.2b shows that an increase in relative index difference leads to an increase in the number of modes. A way to enlarge the relative index difference without increasing the number of modes is illustrated in figure A.2c and comprehends the reduction of the size of the core. This behavior is similar to the influence of the depth and the width of a quantum well on the number of allowed modes.

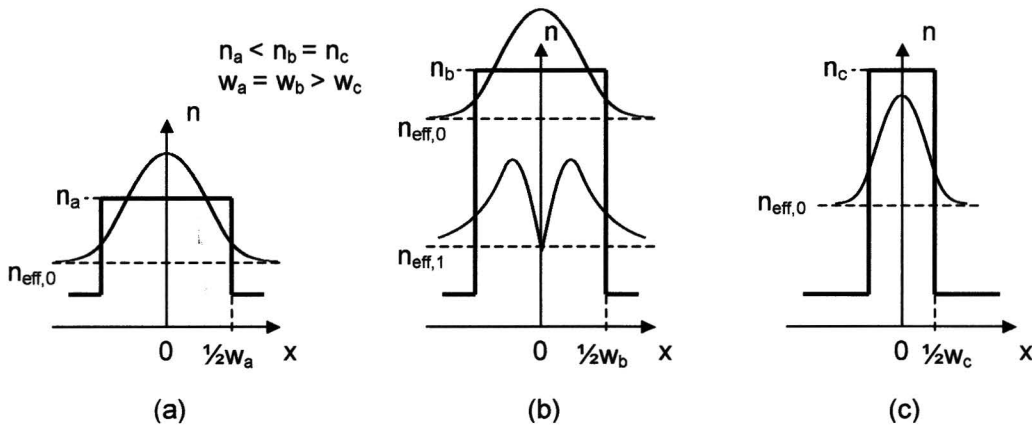


Figure A.2: (a) Mode profile of the TE mode of a single-mode slab waveguide. (b) Equivalent diagram for a slab waveguide of the same dimensions but with a larger relative index difference. (c) Diagram of a slab waveguide with a large relative index difference but with a reduced core width.

In integrated optics, increasing the relative index difference enables the reduction of bending radii of waveguides, as has been shown in sections 2.1 and section 2.5. However, because single-mode operation of waveguides is required to create useful devices due to the difference in propagation constant between different modes¹, a consequence is that the core size needs to be reduced.

Chapter 3 gives an overview of the required core dimensions to ensure single-mode operation for various material systems.

¹ The difference in propagation constant is problematic due to the interference-based working principle of many components.

B Numerical analysis of buffer thickness requirements

This appendix presents a numerical analysis of substrate leakage as function of buffer thickness for waveguides with various relative index differences.

A delay in the supply of oxidized wafers due to particle problems, which has been resolved by now, was the motivation for the performance of this analysis. The objective was to find out to what extent the oxidation time could be reduced for wafers that will be used for the realization of optical components based on silicon rich nitride compared to doped silica.

B.1 Introduction

COM's fabrication process of silica buffer layers is based on a so-called *wet oxidation* process [76]. The chemical reaction of this process is:



The reaction takes place around a temperature of 1100 °C and at atmospheric pressure (in case of the process at COM). For every micrometer of SiO₂, about 0.46 micrometer of Si is consumed [77]. Wet oxidation is a catalytic process that is ten times faster than dry oxidation (with O₂ instead of H₂O), which clarifies the choice of wet oxidation for the growth of buffer layers. Oxidized wafers are commonly referred to as APOX (atmospheric pressure oxidized) wafers.

The oxidation process is diffusion-limited, which implies that the buffer thickness d_{buffer} increases with the square root of time t [77]:

$$d_{buffer} \propto \sqrt{t}. \quad (B.2)$$

Consequently, a reduction of the required buffer thickness, which is possible if the size of an optical mode decreases, is very advantageous for a reduction of process time. The practical relevance is shown in table B.1 which displays the typical process times for a number of buffer thicknesses. More information about the oxidation of silicon can be found elsewhere [76].

Buffer thickness (μm)	Process time (days)
4	1.5
8	5
12	12
16	22

Table B.1. Typical thermal oxidation process times for a number of buffer thicknesses. Exact data about the process used at COM was not available.

B.2 Calculation method

The requirements of the buffer thickness were analyzed by calculating the propagation loss due to substrate leakage for waveguides with different relative index differences. The calculations were performed with the 2D mode solver *Selene*. *Selene* is a commercial software package that has the capability to calculate the optical modes (field distributions and propagation constants) of channel waveguides based on their refractive index profiles.

Selene can be used to calculate losses in waveguides due to geometrical effects (bending loss or substrate leakage) because of the fact that the program is capable of dealing with a complex refractive index, by means of the *Bend-2D* solver, and the imaginary part of the refractive index is (under certain conditions, see below) proportional to the propagation loss, as is derived below.

A refractive index profile that forms the input for a calculation is illustrated in figure B.1. The figure shows the core, the cladding and the substrate of a waveguide. The buffer thickness has been indicated with d_{buffer} . Besides, the border of the calculation window is shown. The calculation window is the area in which the optical modes are evaluated. As can be seen, the lower boundary of the calculation window has been positioned just below the top surface of the substrate. This has been done to simulate that the part of the optical mode that overlaps the

substrate radiates away. Selene takes this radiation effect into account by expressing the refractive index as a complex number. More detailed information about Selene can be found elsewhere [78].

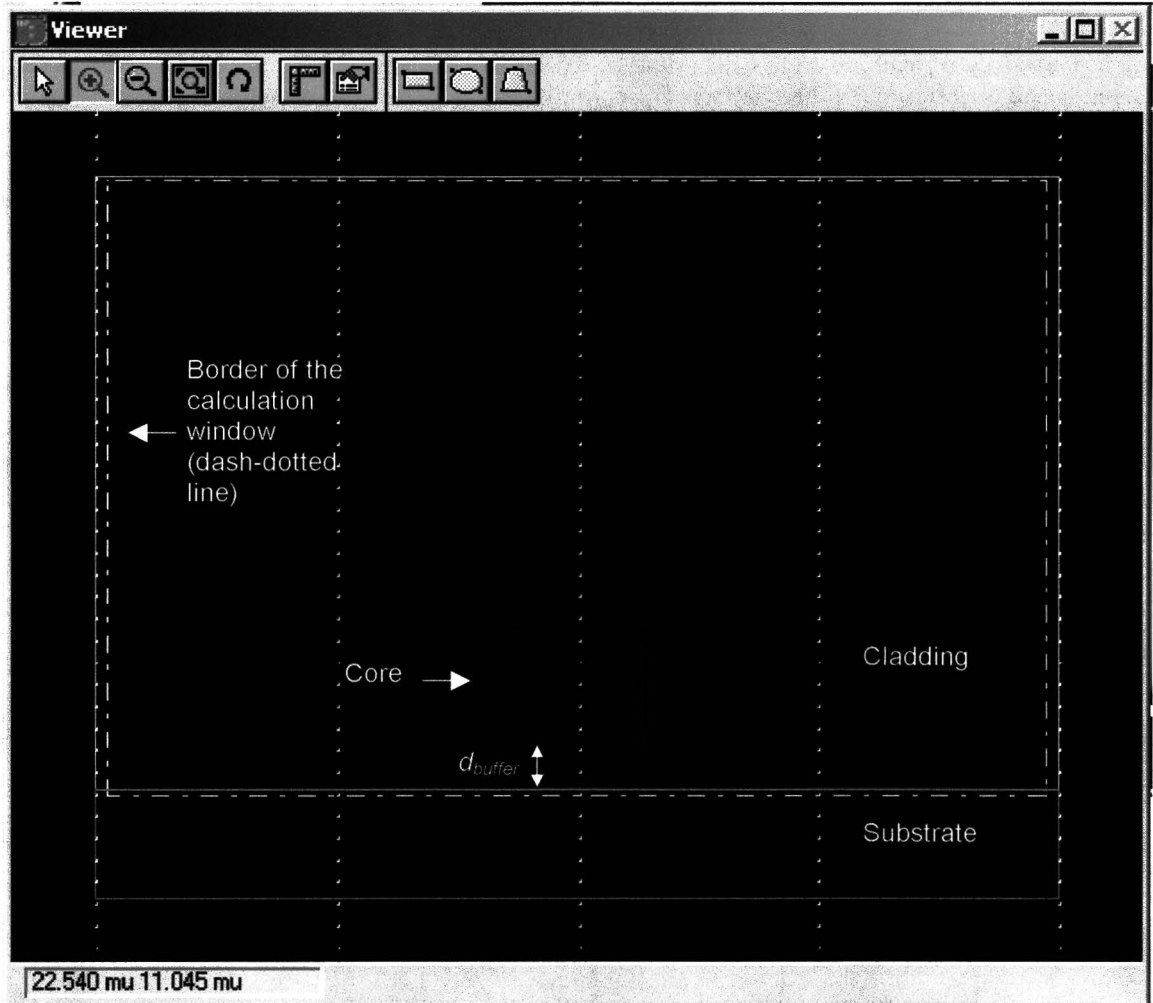


Figure B.1: Illustration of the waveguide structure and the calculation window as used by Selene to calculate losses related to substrate leakage.

As was mentioned above, the propagation loss in waveguides is proportional to the imaginary part of the effective refractive index. This can be understood on the basis of the description of a propagating wave E in one dimension representing the electric component of an electromagnetic wave:

$$E = E_A \cdot e^{2\pi i \left[\frac{nx}{\lambda} - \frac{t}{T} \right]} = E_A \cdot e^{2\pi i \left[\frac{(n_r + in_i)x}{\lambda} - \frac{t}{T} \right]}, \quad (\text{B.3})$$

where E_A is the amplitude, t is the time, T is the period, x is the traveled distance, λ is the wavelength in vacuum and n is the refractive index that consists of a real and an imaginary part (n_r and n_i). E can be written with an exponentially decaying factor:

$$E = \left\{ E_A \cdot e^{2\pi i \left[\frac{n_r x}{\lambda} - \frac{t}{T} \right]} \right\} \cdot e^{-\frac{2\pi n_i}{\lambda} x}. \quad (\text{B.4})$$

The power density P of an electromagnetic wave is given by the time-averaged Poynting vector. In the weak-guidance approximation P is proportional to the integral of $|E|^2$ over an adequately large cross-section A [11]. Because the integral of an exponential function is proportional to the function itself, P can be written as:

$$P \propto \int |E|^2 dA \propto e^{-\frac{4\pi n_i}{\lambda} x}. \quad (\text{B.5})$$

The exponentially decaying factor can be rewritten as a power of 10:

$$P \propto 10^{-\frac{1}{10}\alpha x}, \quad (\text{B.6})$$

where α is the propagation loss in dB per unit length. From formulas B.5 and B.6 it can be deduced that the relationship between propagation loss α and imaginary part of the refractive index n_i is given by:

$$\alpha = \frac{4\pi \cdot 10 \cdot \log_{10}(e)}{\lambda} n_i \quad (\text{B.7})$$

$$\alpha_{\lambda=1550 \text{ nm}} (\text{dB/cm}) = 3.521 \cdot 10^5 \cdot n_i$$

Formula B.7 implies that imaginary refractive index values on the order of 10^{-8} correspond to propagation loss values on the order of 0.01 dB/cm. Consequently, the imaginary part of the refractive index needs to be calculated very accurately to simulate substrate leakage. Because formula B.5 is only valid in the weak-guidance approximation according to reference 11, the numerical factor in formula B.7 might not be an accurate value for high-contrast waveguides. However, the essence that small values of the refractive index could imply substantial losses due to substrate leakage remains. In the analysis presented below, it is assumed that the factor of $3.521 \cdot 10^5$ is correct. This is also done by Selene, as can be deduced from the values that are displayed in the *numeric window* after a calculation has been performed.

B.3 Experiment

For the waveguide structures that are described in table B.2, the propagation loss due to substrate leakage has been calculated based on the method presented in section B.2. In figure B.2, the mode profiles are shown to illustrate the difference in confinement. This difference is expected to lead to a significant difference in substrate leakage.

Technology	Relative index difference Δ	n_{co}	n_{cl}	Core dimensions (μm^2)
Doped silica	0.007	1.455	1.445	5.5 x 5.5
Doped silica	0.014	1.465	1.445	4 x 4
SiON	0.033	1.50	1.445	ridge [35]
SRN	0.25	2.06	1.445	0.6 x 0.6

Table B.2. Waveguide structures for which the propagation loss due to substrate leakage has been analyzed.

All calculations were performed with the Bend-2D solver with the *Complex* and *FullVec* options selected based on a grid of 256 x 256 points. The target refractive index values were calculated by the finite difference method. For every waveguide structure the substrate leakage was calculated for a number of buffer thicknesses for both polarizations.

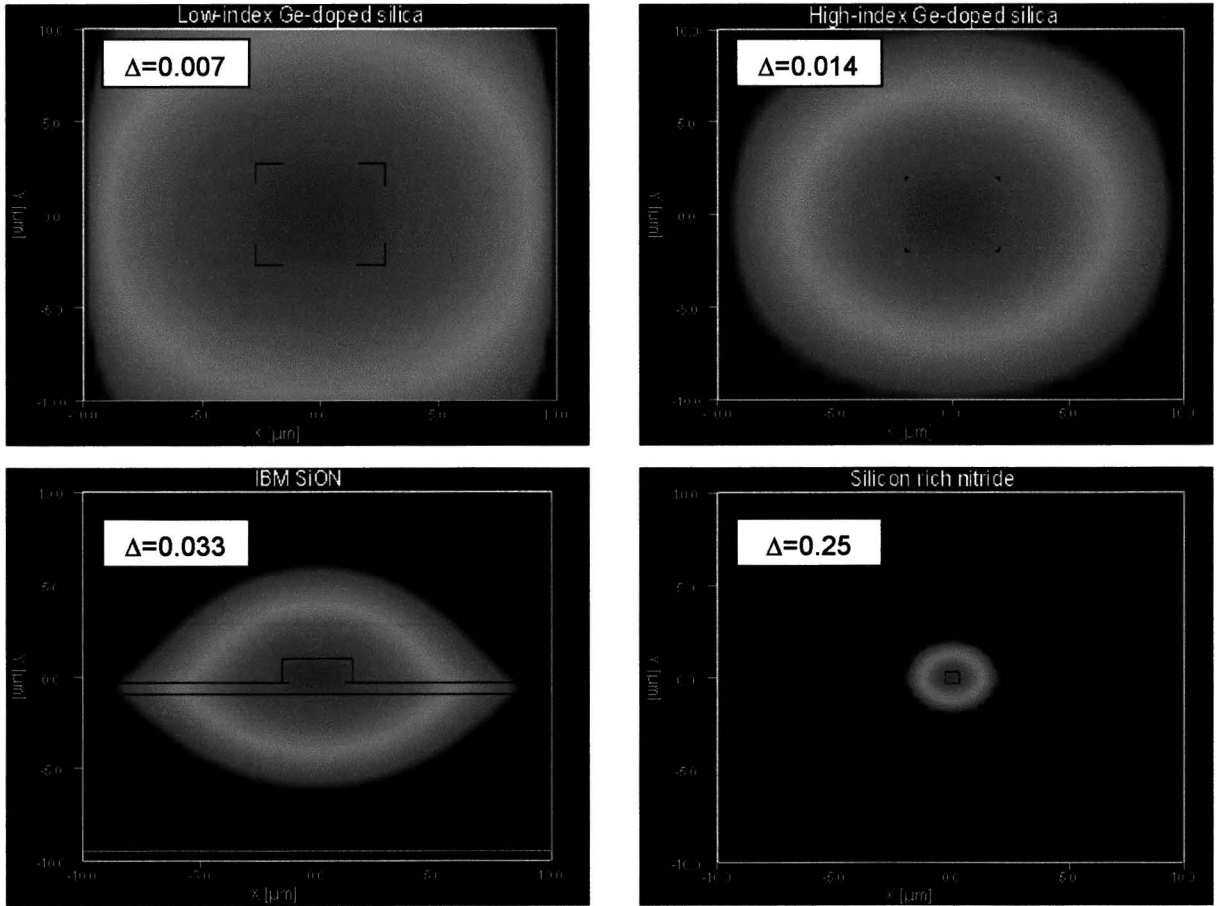


Figure B.2: Illustration of the mode profiles ($|E|^2$) of the four types of waveguides that are subject of the analysis of substrate leakage. The mode profiles were calculated with Selene.

B.4 Results

The results of the calculations of substrate leakage are shown in figure B.3. The graph displays the propagation loss due to substrate leakage as function of buffer thickness for the waveguide structures mentioned in section B.3. Figure B.3 only shows the calculations for one polarization, but the tendency and the order of magnitude of the values are the same for both polarizations.

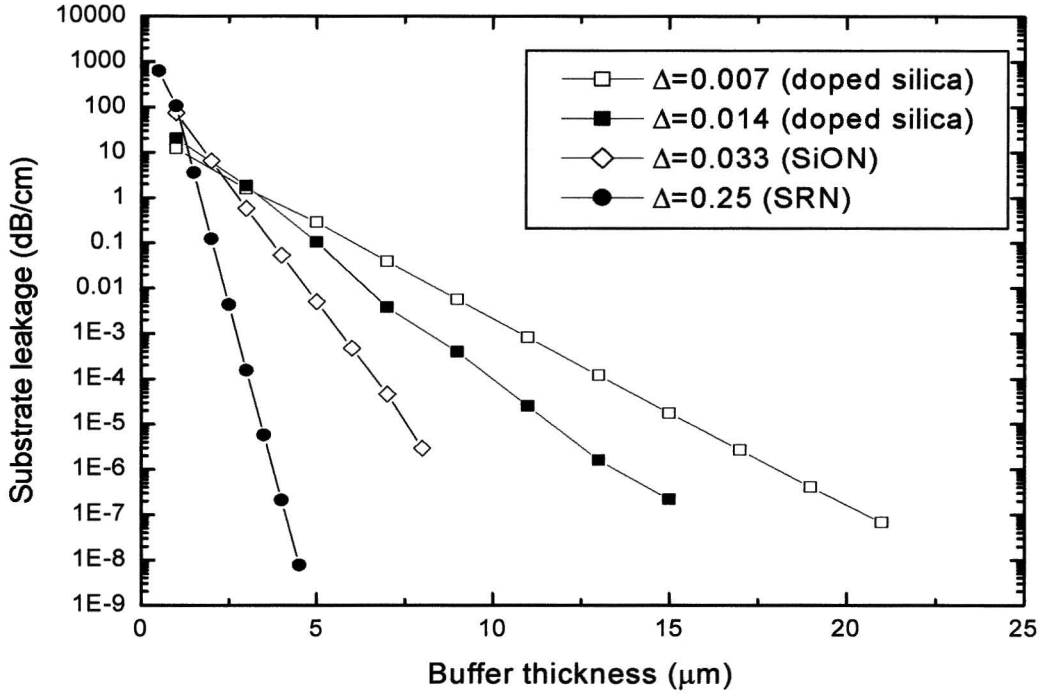


Figure B.3: Calculated propagation loss due to substrate leakage as function of buffer thickness for a number of relative index differences.

B.5 Discussion

Figure B.3 shows that there is a clear difference between the buffer thickness dependence of the propagation loss for the various types of waveguides. It is shown that in order to keep substrate leakage below a certain level (for example 0.01 dB/cm), a thicker buffer layer is required for waveguides with a lower relative index difference. This tendency was expected because of the difference in mode size.

Also the linear dependence of the logarithm of the substrate leakage (in dB/cm) as function of the buffer thickness was expected since the tail of an optical mode in the cladding has an exponentially decaying shape. So the overlap is increasing exponentially as function of decreasing buffer thickness. An analytical model of substrate leakage in the weak-guidance approximation, which can be found elsewhere [11], predicts this linear behavior as well.

Although the tendencies are as expected, it is impossible to conclude that the calculated values are reliable. An experimental investigation seems to be required to draw conclusions about this issue. However, because the importance of this experiment is relatively low, it was decided to use a comparison with IBM's SiON technology to draw conclusions about the required buffer thickness for SRN waveguides.

The buffer thickness of the SiON waveguides is 8.5 μm [35]. According to figure B.3, this corresponds to a substrate leakage of 10⁻⁶ dB/cm, which suggests that either the chosen thickness is relatively large or that the performed simulations are too optimistic. Applying the same criterion (10⁻⁶ dB/cm) on the SRN waveguides results in a required buffer thickness on the order of 4 μm. This implies that an oxidation time of about 1.5 days is enough, which is considerably less than the standard process of about 4 weeks which is used for doped silica waveguides [32]. When SRN waveguides are combined with doped silica waveguides it is obviously impossible to reduce the oxidation time.

Besides the conclusion about the required buffer thickness for SRN waveguides, the analysis shows that the performance of a numerical analysis is insufficient to draw conclusions about quantitative effects, which demonstrates that performing simulations is useful to investigate tendencies and to evaluate opportunities, but

that experiments are inevitable. This is believed to be a general characteristic concerning the performance of simulations for optical waveguide applications.

B.6 Conclusions

The main conclusion of the numerical analysis combined with a comparison with IBM's SiON technology is that an oxidation time of 1.5 days, leading to a buffer thickness of 3.5-4 μm , is sufficient for wafers that are used for the fabrication of optical devices based on SRN waveguides.

C COM's waveguide fabrication process

This appendix presents a brief overview of the waveguide fabrication process used at COM. The overview provides background information related to the work presented in this thesis. More detailed information on COM's waveguide fabrication process can be found elsewhere [32], [79].

The fabrication process starts with a substrate which is a circular slice of crystalline silicon with a diameter of 10.0 cm and a thickness of about 0.5 mm (figure C.1a). The supplied substrates have usually been polished on one side. The first step of the fabrication process is the creation of a silica buffer layer (figure C.1b) based on thermal oxidation of a part of the silicon wafer. Section B.1 presents a short overview of the characteristics of this process which creates silica layers on both sides of the wafer. Normally, about 200 wafers can be oxidized simultaneously, which is an important feature of this process because of the long oxidation time (see appendix B).

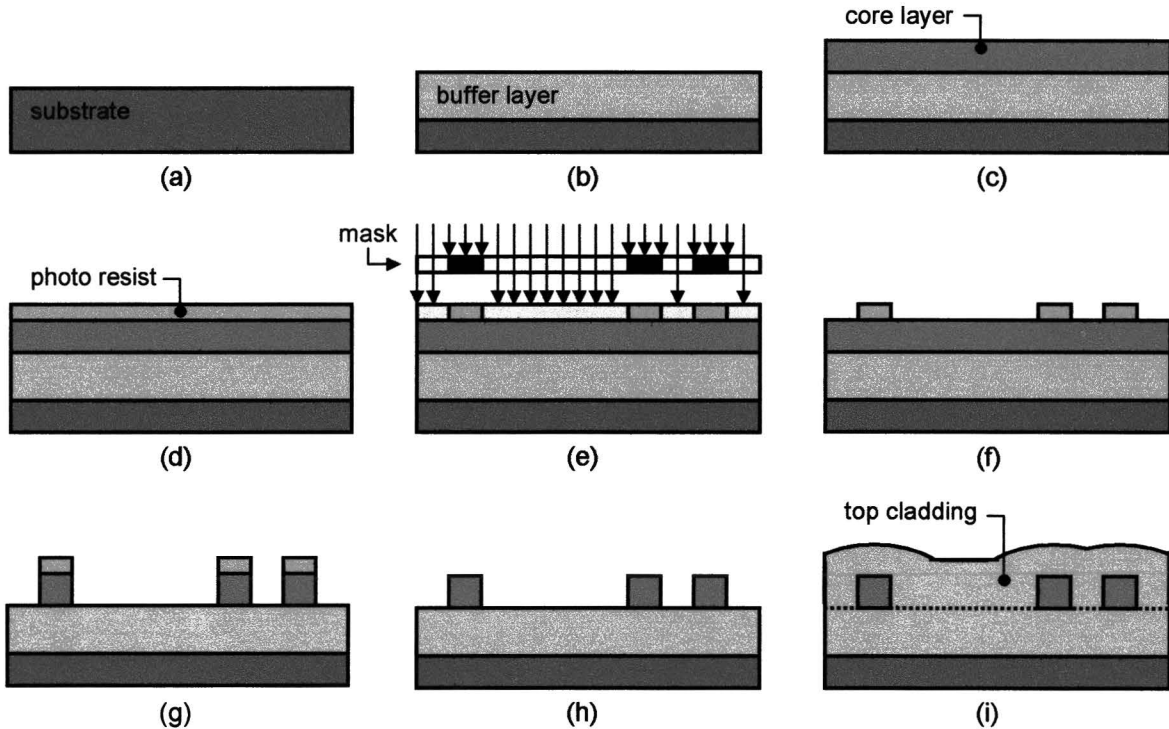


Figure C.1: Schematic representation of COM's waveguide fabrication process. The individual steps are clarified in the text.

Secondly, the core layer is deposited on top of the buffer layer (figure C.1c). The deposition methods that are available for this step are plasma-enhanced chemical vapor deposition (PECVD) and low-pressure chemical vapor deposition (LPCVD). Most types of core layers that have been developed at COM rely on PECVD because this method is more suitable to introduce dopants [32]. Examples of applied dopants, which have various applications, are boron, phosphorus, germanium, erbium, ytterbium and aluminium.

Subsequently, a layer of photo resist is spin-coated and baked on the wafer (figure C.1d). A pattern is transferred from a pre-fabricated proximity mask to the layer of photo resist by UV exposure (figure C.1e). The wavelength of the mercury UV lamp is 365 nm. The exposed photo resist is removed by developing (figure B.1f). After the photolithography has been finished by hard-baking the photo resist, the waveguide pattern is transferred from the photo resist to the core layer by reactive ion etching (figure C.1g). The remaining photo resist is removed by a plasma process (figure C.1h). Finally, a cladding layer of borophosphosilicate glass (BPSG) is deposited on top of the waveguides by PECVD (figure C.1i). By heat treatments the viscosity of the BPSG is made smaller, so voids between closely spaced waveguides are filled up and a uniform cladding is realized. After the cleanroom processing, the wafer can be diced or cleaved into chips.

Variations of the described process could include the realization of multiple levels of waveguides [80], the combination of different types of waveguides in one plane [80] or the addition of heaters to introduce the possibility of tuning components thermo-optically [35].

D Ring resonator modeling software

During the master project, a computer program has been created to model the transmission characteristics of an optical ring resonator. The main objective was to visualize the spectral response of a ring resonator in an orderly way. As a result, the program provides insight in how parameters as coupling coefficient and propagation loss affect the response. The second objective, which clarifies why Labview was chosen as a platform for the implementation of the software, was to combine the model with control software for an optical setup to enable the fitting of experimental spectra to determine the parameters of fabricated ring resonators. This objective has not been realized because of reasons discussed in section C.2. The model has been used to analyze the spectrum of the SRN ring coupled to a UV-written waveguide as is described in section 6.3.

D.1 Mathematical model

The computer program is based on a simple analytical model that is originating from signal processing theory. The model doesn't rely on waveguide theory, which means that it can only be used to evaluate transmission characteristics as function of an assumed coupling coefficient between straight waveguide and ring. So, the coupling ratio cannot be calculated from the coupler geometry. The model, which is based on a model that is described elsewhere [12], is only valid for continuous waves because steady-state behavior is assumed (see below).

Figure D.1 shows a ring resonator including the definitions of some symbols. The symbols E_1 , E_2 , E_3 and E_4 refer to field amplitudes ($|E|^2$ is equal to light intensity), x is the amplitude transmission per round trip, y is the amplitude reflection coefficient between ring and straight waveguide, and ϕ is the phase shift per round trip¹. Both x , y and ϕ are dimensionless parameters.

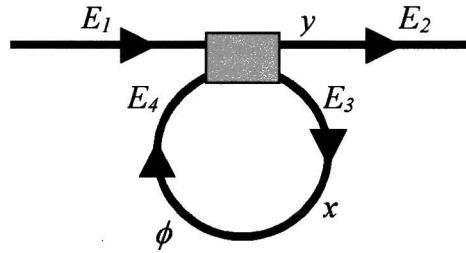


Figure D.1: Illustration of a ring resonator including the symbols that are used to describe the transmission characteristics.

Output E_2 is determined by an infinite sum of contributions because the ring acts as an infinite loop. The infinite sum can be reduced to a short expression by using the geometric series, which results in the following expression for the steady-state transfer function t :

$$t = \frac{E_2}{E_1} = \frac{y - xe^{-i\phi}}{1 - xye^{-i\phi}}. \quad (\text{D.1})$$

The ratio E_3/E_1 , which is referred to as transfer function m , is given by:

$$m = \frac{E_3}{E_1} = \frac{1 - y^2}{1 - xye^{-i\phi}}. \quad (\text{D.2})$$

Transfer functions t and m describe all relevant aspects of the optical behavior of the system in a rather abstract way. To obtain insight in the physical meaning of this behavior the intensity transmission and the phase response

¹ Due to practical reasons the coefficients used in the analysis of the properties of the fabricated ring resonator described in section 6.3.3 are optical power loss per round trip γ and power coupling ratio K instead of the coefficients x and y . The relationship between both sets of parameters is: $K = 1 - \gamma^2$ and $\gamma = 1 - x^2$.

of both transfer functions can be calculated. The most relevant expressions are the intensity transmission T , internal intensity magnification M , which is the ratio of circulating intensity to incident intensity, and the phase response Φ of transfer function t :

$$T = t \cdot t^* = \frac{x^2 + y^2 - 2xy \cos(\phi)}{1 + x^2 y^2 - 2xy \cos(\phi)} = 1 - \frac{(1 - x^2)(1 - y^2)}{(1 - xy)^2 + 4xy \sin^2(\phi/2)}, \quad (\text{D.3})$$

$$M = m \cdot m^* = \frac{1 - y^2}{1 + x^2 y^2 - 2xy \cos(\phi)}, \quad (\text{D.4})$$

$$\Phi = \tan^{-1} \left(\frac{\text{Im}(t)}{\text{Re}(t)} \right) = \tan^{-1} \left(\frac{x(1 - y^2) \sin(\phi)}{y(1 + x^2) - x(1 + y^2) \cos(\phi)} \right). \quad (\text{D.5})$$

The group delay τ_g of signals that pass the system in terms of unit delays is determined by phase response Φ :

$$\tau_g = -\frac{d\Phi}{d\phi} = -\frac{x(1 - y^2)[y(1 + x^2) \cos(\phi) - x(1 + y^2)]}{[y(1 + x^2) - x(1 + y^2) \cos(\phi)]^2 + [x(1 - y^2) \sin(\phi)]^2}, \quad (\text{D.6})$$

where a unit delay is defined as the time that it takes a signal to pass the ring once.

Although the total behavior of the system is relevant for every application one could say that that intensity transmission T is especially relevant for bandpass filter applications, like in wavelength division multiplexing, internal intensity magnification M is especially relevant in laser and switching applications, which need high internal power densities and group delay τ_g is especially relevant for dispersion compensation.

The computer program that is described in section D.2 uses formulas D.3, D.4, D.5 and D.6 to plot spectra of these four quantities for any specified combination of x and y .

Next to the spectra, the computer program calculates and displays a number of ring resonator characteristics based on the quantities x , y , the wavelength of light λ , the length of the racetrack L , which is equal to 2π times the radius if the racetrack is a ring, and the effective group index of the racetrack waveguide N_g [11].

The quantities that are calculated are the free spectral range (FSR) in terms of wavelength $\Delta\lambda$ and frequency Δf , the spectral width (FWHM of intensity transmission) in terms of both free spectral range δFSR , wavelength $\delta\lambda$ and frequency δf , the finesse F , the quality factor Q , the propagation loss α in terms of dB/cm and the intensity transmission into the ring K in terms of dB. The following formulas are used:

$$\Delta\lambda = \frac{\lambda^2}{N_g L}, \quad (\text{D.7})$$

$$\Delta f = \frac{c}{N_g L}, \quad (\text{D.8})$$

$$\delta FSR = \frac{1 - xy}{\pi \sqrt{xy}}, \quad (\text{D.9})$$

$$\delta\lambda = \frac{1 - xy}{\pi \sqrt{xy}} \cdot \frac{\lambda^2}{N_g L}, \quad (\text{D.10})$$

$$\delta f = \frac{1 - xy}{\pi \sqrt{xy}} \cdot \frac{c}{N_g L}, \quad (\text{D.11})$$

$$F = \frac{1}{\delta FSR} = \frac{\Delta\lambda}{\delta\lambda} = \frac{\Delta f}{\delta f} = \frac{\pi\sqrt{xy}}{1-xy}, \quad (\text{D.12})$$

$$Q = \frac{\lambda}{\delta\lambda} = \frac{f}{\delta f}, \quad (\text{D.13})$$

$$\alpha = -\frac{20 \log x}{L}, \quad (\text{D.14})$$

$$K = 10 \log(1-y^2), \quad (\text{D.15})$$

where c is the velocity of light in vacuum. Formulas D.9, D.10, D.11 and D.12 are only valid if $\Delta f \gg \delta f$. The quantity ϕ , which is used to plot the spectra, can be specified as function of the introduced parameters as well:

$$\phi = \frac{N_g L}{\lambda} \quad (\text{D.16})$$

D.2 Computer program

Figure D.2 shows the main window of the computer program. In the upper left corner parameters x and y can be specified. Below that, the values for λ , L and N_g can be defined. The section with the name *Computed resonator characteristics* displays the characteristics that are calculated with formulas D.7–D.15. The four graphs show the spectral responses according to formulas D.3–D.7. The section *Display options* provides the possibility to specify the number of free spectral ranges that are displayed in the graphs as well as the quantities that are put on the axes. For example the horizontal axes can be specified as normalized frequency f/FSR , frequency f (THz) or wavelength λ (nm). Furthermore it is possible to export the data of a graph to file `c:\exptable.txt` which could be imported in a spreadsheet program. The main advantage of the layout is that the influence of parameter variations on nearly all relevant characteristics can be watched simultaneously.

The program has been implemented in Labview 6 [81]. Labview is a graphical software system for developing scientific and engineering applications and provides the possibility of controlling a tunable laser and acquiring data from a power meter. COM's optical characterization setup is equipped with an EXFO [75] unit with both such a tunable laser and a power meter. To keep open the possibility of implementing the model in a characterization routine that can determine both the propagation loss in the ring and the coupling coefficient from the transmission spectrum, it was chosen to use Labview as a platform for the above-described computer program.

It is expected that ring resonators will become important components in the high-index project, which justifies to put some effort in realizing an efficient characterization routine. However, because of two reasons the model has not been integrated with software to control the optical characterization equipment:

- Ring resonators cannot be fabricated on a routine basis at the moment. This implies that developing an automatic characterization routine doesn't pay off at present.
- The spectral resolution of the EXFO unit is 0.01 nm. This is relatively low for the measurement of transmission spectra of optical resonators because of the sharpness of the peaks. A thorough analysis is necessary to investigate whether the EXFO unit is suitable for the characterization purposes in the high-index project. Such an analysis was beyond the scope of the master project because it concerns a long-term issue.

The computer program, including the *graphical* source code, is available from the *HighIndex* folder on the COM intranet.

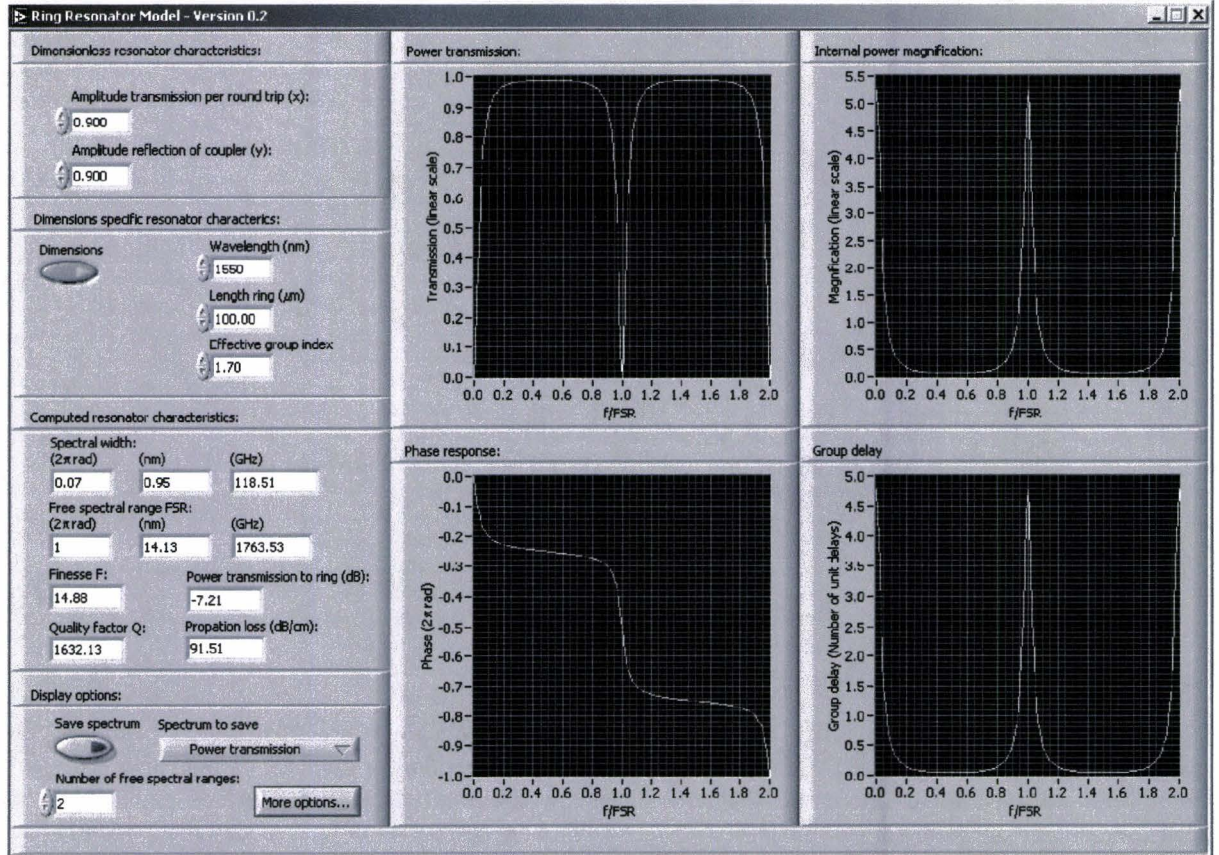


Figure D.2: Illustration of the computer program that calculates and displays the spectral responses and the values of a number of transmission characteristics of a ring resonator.

E Poster and conference papers

This appendix shows the poster that has been presented at the annual meeting of the Danish Physical Society (DFS) in Nyborg, Denmark on May 30-31, 2002. The size of the full-color poster was 91 x 106 cm² (width x height). Besides, on the next pages the conference papers that were submitted to the 28th European Conference on Optical Communication (ECOC) 2002 are shown. The paper *Optical loss analysis of silicon rich nitride waveguides* has been accepted as a poster presentation, while the paper *High-index ring resonator coupled to UV-written waveguide* has been accepted as an oral presentation. ECOC 2002 takes place in Copenhagen, Denmark on September 8-12, 2002.

Optical loss analysis of silicon rich nitride (SRN) waveguides and their applications

H. Mertens (1), W. E. Svendsen (2), K. A. Andersen (3), H. T. Philipp (4)
 COM[†], Technical University of Denmark (DTU), Building 345 West, DK-2800 Kgs. Lyngby
 1: hm@com.dtu.dk, 2: ws@com.dtu.dk, 3: ka@com.dtu.dk, 4: htp@com.dtu.dk

[†] COM is an unclassified information and research center in telecommunication and optical technologies. COM is located at COM 673
 Contact info: for more information see the COM high-index project contact leader W. E. Svendsen (ws@com.dtu.dk)

Fabrication

The SRN waveguides and components are fabricated in the state-of-the-art cleanroom at COM. The fabrication process consists of buffer growth, core layer deposition, photoresist, core layer etching and top cladding deposition. These steps are discussed below.

1. Silicon substrate

A silicon wafer with a diameter of 100 mm is used as the substrate.

2. Thermal oxidation of substrate

A SiO₂ buffer layer of several micrometers is grown by thermal oxidation of the substrate.

3. Low pressure chemical vapor deposition (LPCVD) of SRN

The SRN core layer is deposited by LPCVD. The refractive index can be tuned by varying deposition parameters. We use $n = 2.08$. The layer is annealed afterwards.

4. Spincoating of photo resist

A layer of photo resist is spun on top of the core layer.

5. Exposure of photo resist

The pattern of waveguides is transferred from a photomask to the photoresist by UV exposure. This is a critical process because the waveguides are of submicron dimensions.

6. Development of photo resist

The exposed photo resist is removed by chemical etching. This is a critical step as it defines the width of the waveguides.

7. Core layer etching

The waveguide pattern is transferred to the core layer by reactive ion etching (RIE). Obtaining small side wall roughness is important in this step.

8. Photo resist strip

The remaining photo resist is removed by a plasma process.

9. Top cladding deposition

A layer of borophosphosilicate glass (BPSG) is deposited on top of the waveguide. BPSG is used because it flows better than pure SiO₂.

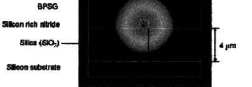
10. Packaging

After processing, the wafer is etched into chips. Optionally, the facets are polished and the wafers are glued to the waveguides.

Legend

- Silicon (Si), $n = 3.5$
- Silicon rich nitride (SRN), $n = 2.08$
- Buffer glass (SiO₂ and BPSG), $n = 1.45$
- Photo resist
- Exposed photo resist

Light in propagation
 The figure below illustrates why the waveguide structure has the shape as depicted in the fabrication scheme above. The figure, which shows the light intensity in the waveguide structure, clarifies that a significant part of the beam is located outside the waveguide core. To make sure that the light stays confined in the waveguide, the layers of borosilicate, low-loss glass (SiO₂ and BPSG) are integrated in the structure. These layers prevent leakage of light to the substrate and to the environment.



* The refractive index is high intensity, but represents a low intensity. The intensity profile is also calculated with a mode solver.

Objective

The COM high index project, of which the current work is part of, focuses on the development of a material system for high density integrated optics that is based on silicon rich nitride (SRN) waveguides. The primary goal is to enable the potential realization of low-loss passive integrated optical devices with a higher degree of integration than what can be achieved with current state-of-the-art technologies.

The motivation to use silicon rich nitride is based on the following opportunities:

- Silicon rich nitride has a high refractive index. This permits to create waveguides with a small bending radius (~40 μm).
- Silicon rich nitride has low mechanical stress. The low stress facilitates device fabrication and avoids material induced deformation of the waveguides.
- The silicon rich nitride technology is compatible with available semiconductor industry developed fabrication methods which have a broad cost base.

In contrast of these opportunities, the propagation loss in SRN waveguides has been analyzed by different characterization methods. The motivation is that it is essential to have a low propagation loss to be able to obtain a competitive optical technology.

Context

Optical telecommunications exploits the fundamental, physical properties of light to obtain high-capacity communication networks. Optical signals transport more information than conventional electronic signals because the carrier frequency of optical signals is much higher (~10¹⁵ THz) versus ~10 GHz. This enlarges the bandwidth significantly and enables the use of higher modulation frequencies.

Although optical transmission through fibers is an established technology, the processing of optical signals (routing, filtering, amplification, etc.) is still in an early stage of development. In conventional fiber-optic networks, optical signals are therefore converted into electronic signals for processing. To avoid these electronic bottlenecks in telecommunication networks and to transform optics from a transport technology into a real networking technology, it is necessary to create devices that are able to perform the predefined operations in the optical domain instead of the electronic domain.

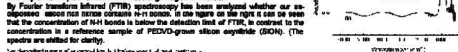
In the context of these developments, high-density integrated optics is a vital concept to realize advanced and low-cost optical devices for telecommunication systems.



Network performance can be improved by exchanging the bottlenecks in network junctions and replace them by optical devices.

FTIR analysis

FTIR spectra are an important tool for measuring the composition of materials. They can be used to identify the chemical composition of a material. In this work, FTIR is used to analyze the composition of SRN waveguides.



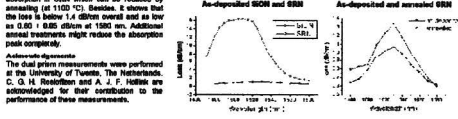
* An absorption peak is observed at 1100 cm⁻¹ and 780 cm⁻¹.

Loss in slab waveguides

The propagation loss in SRN slab waveguides has been analyzed by using the dual prism coupling method. The dual prism coupling method is based on the in- and out-coupling of light in a slab waveguide in which a waveguide is embedded. Advantages of using this method to determine propagation loss are:

- Losses due to direct coupling in channel waveguides are excluded. This implies that the dual prism coupling method can help to identify loss mechanisms.
- The in- and out-coupling are very reproducible. This implies that the error that is induced by repeated in- and out-coupling is very small and that the loss can be determined accurately.

For various wavelengths in the region between 1400 and 1500 nm the propagation loss in SRN and BDN slab waveguides has been determined by measuring the prism-coupled transmission. The results are displayed in the graphs below. The left graph shows that the SRN material exhibits a low propagation loss. The right graph shows that there is still a certain amount of H₂ related absorption in SRN which can be reduced by annealing (at 1100 °C). Besides, it shows that the loss is below 1.4 dB/cm overall and as low as 0.05 ± 0.03 dB/cm of 1500 nm. Additional anneal treatments might reduce the absorption peak completely.

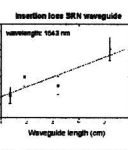


Loss in channel waveguides

Propagation loss measurements were carried out on SRN channel waveguides by using the indirect method. In the indirect method the optical transmission through a waveguide is measured. Subsequently, the waveguide is cut back and the transmission is measured again. In this step, propagation loss can be determined from coupling loss.

The height of the investigated waveguides was 1.3 μm and the width was 8 μm. Because this is relatively large, in relation to the high refractive index, the waveguides are multimode. The insertion loss coupling loss + propagation loss is plotted in the figure on the right. The obtained value for the propagation loss, which is the slope in the graph, is 0.7 ± 0.3 dB/cm. The large uncertainty is due to variations in the 3-to-2-μm coupling.

It should be able to determine the propagation loss in single mode waveguides in the near future. Single-mode waveguides are required for device applications.



Conclusion

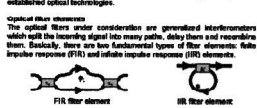
In the context of the developments in telecommunication, high-density integrated optics is a technology with various applications in network performance. The material silicon rich nitride (SRN) has some unique properties, which include high refractive index, low mechanical stress and compatibility with semiconductor processing technology, that enable it to become an important waveguide material for high-density integrated optics.

In this work, the propagation loss in SRN slab and channel waveguides has been investigated. The FTIR analysis shows that the concentration of H₂ bonds in SRN is very low (below the detection limit of the equipment). The dual prism coupling analysis gives a very accurate picture of the losses. The propagation loss, measured below 1.4 dB/cm and 0.6 ± 0.3 dB/cm at 1500 nm, is promising for applications. The obtained loss value for multi-mode waveguides, in which sidewall roughness doesn't play an important role, is in agreement with the dual prism coupling measurements.

- Key advantages that make the SRN technology more attractive include:
- Realization of high-quality single-mode waveguides (cross-sectional dimensions are ~ 0.8 x 0.6 μm).
 - Improvement of the fiber-to-chip coupling efficiency.

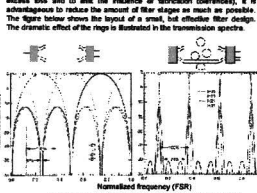
Applications

An application that illustrates the potential of the SRN technology is the incorporation of ring resonators in optical fibers. Optical fibers are best building blocks for modern telecommunication networks. They are invaluable to help extend the intrinsically large capacity of optical networks. Example of functions that are fulfilled by fibers are long-haul transport, dispersion compensation and gate applications. The first two functions are described to emphasize that importance for optical telecommunications and to point out the added value of the SRN technology compared to established optical technologies.

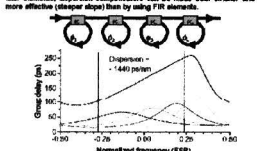


Fiber elements are characterized by an amplitude response and a phase response which both depend on parameters n and a (coupling coefficient and phase difference). Fiber responses can be tailored by varying these parameters. Coupling and combining fiber elements give more design freedom and can be used to realize an arbitrary fiber response. The combination of incorporating both pairs of elements in a fiber design response are generally not achieved with fiber shape.

Bandpass filters
 Bandpass filters are the basic building blocks for adding multiplexers in wavelength division multiplexing (WDM) systems. Ideal bandpass filters have 100% transmission in the passband and 0% transmission outside the passband. This can be achieved by using an infinite number of filter elements. Because of practical reasons (area reduction, reduction of cost) and to keep the response of filter elements, it is advantageous to reduce the amount of filter stages as much as possible. Many filter designs have shown the impact of a real, flat-topped filter design. The characteristic of the filter is illustrated in the transmission spectra.



Chromatic dispersion in optical fiber networks results in pulse broadening in time and distance. Compensation of chromatic dispersion becomes increasingly important with increasing bit rates in order to prevent individual pulses that carrying each other (temporal interference) by using SRN fiber elements, dispersion compensation can be made both smaller and more effective (lower slope) than by using FIR elements.



Advantages of SRN technology
 The main advantage of the SRN technology for the implementation of filters in optical devices is the fact that the bending radius of waveguides can be reduced to such an extent that filter resonators can be incorporated in high-density integrated devices.

The effect of the index step difference in refractive index between core and cladding on the bending radius of waveguides is summarized and compared to other technologies in the table below. Besides, the table shows that a propagation loss of 0.6 dB/cm is low considering the loss per stage is larger. This is positive for the number of devices that are compatible with current telecommunication standards.

Technology	Deposited Films (nm)	Silicon nitride (nm)	Silicon rich nitride (nm)
State of the art	Established	Established/new	New
Index step (Δn)	0.02	0.05	0.5
Bending radius	~10 mm	~1 mm	~40 μm
Propagation loss	0.01 dB/cm	0.05 dB/cm	0.6 dB/cm
Loss per ring	0.00 dB	0.03 dB	0.02 dB

DTU



Optical Loss Analysis of Silicon Rich Nitride Waveguides

H. Mertens (1), K. N. Andersen (2), W. E. Svendsen (3)

COM, Technical University of Denmark, Building 345 west, DK-2800 Kgs. Lyngby, Denmark

1: hm@com.dtu.dk, 2: ka@com.dtu.dk, 3: ws@com.dtu.dk

Abstract An analysis of the propagation loss in high-index LPCVD-grown silicon rich nitride (SRN) slab waveguides and channel waveguides is presented. A propagation loss as low as 0.6 dB/cm has been achieved.

Introduction

For applications of optical waveguides, it is essential to minimize propagation loss. The low propagation loss is one of the reasons for the success of integrated optics based on doped silica [1]. Other advantages of this technology include polarization-independent operation and the fact that device fabrication relies on scalable technologies that have been developed in semiconductor industry. However, a significant drawback is the low integration density of components. This drawback is caused by the inevitably low index contrast between core and cladding of doped silica waveguides, which does not permit reduction of bending radii of waveguides below ~ 10 mm.

Alternative material systems have been proposed to overcome the mentioned drawback, while maintaining the positive features of the doped silica technology. An example is the silicon oxynitride (SiON) technology [2], which permits bending radii of ~ 1 mm. A further increase in integration density is to be expected in the near future. In this context, the use of silicon rich nitride (SRN) as core waveguiding material opens up possibilities beyond the reach of silicon oxynitride.

This paper presents an analysis of the propagation loss in SRN slab waveguides and channel waveguides on the basis of different characterization methods.

Silicon rich nitride properties

Silicon rich nitride is deposited by low-pressure chemical vapor deposition (LPCVD), using SiCl_2H_2 and NH_3 as precursors. The material is characterized by a high refractive index and low mechanical stress.

The high refractive index of SRN, compared to silica, enables the realization of small bending radii. The index contrast of our waveguides ($\Delta n=0.6$) permits bending radii of ~ 40 μm without radiation losses [3]. A consequence of the high-index contrast is the fact that the cross-sectional dimensions of single-mode waveguides are submicron ($\sim 0.6 \times 0.6$ μm).

Low mechanical stress is important to omit material birefringence and to facilitate device fabrication. Ultralow stress values (<10 MPa) have been reported [4]. This is significantly less than the very high stress value (1.2 GPa [5]) of stoichiometric silicon nitride (Si_3N_4), which grounds the interest in SRN for optical waveguide applications. The mechanical stress in our

layers is below 100 MPa.

Details on our fabrication process have been published elsewhere [6].

FTIR analysis

Material layers that are deposited using precursors that incorporate both hydrogen and nitrogen may contain significant amounts of N-H bonds. This is the case for both plasma-enhanced and low-pressure chemical vapor deposition [7]. N-H bonds have their intrinsic infrared absorption at a wavenumber of 3350 cm^{-1} . The first overtone of this frequency is found at a wavelength of 1510 nm. The tail of this peak leads to absorption losses in the wavelength region of interest. Annealing of the layers at high temperatures can be used to largely remove the N-H bonds [7, 8].

Fourier transform infrared spectroscopy (FTIR) was applied to investigate whether our as-deposited SRN layers incorporate N-H bonds and to see what the influence of annealing is. An FTIR spectrum of an as-deposited SRN layer is shown in figure 1.

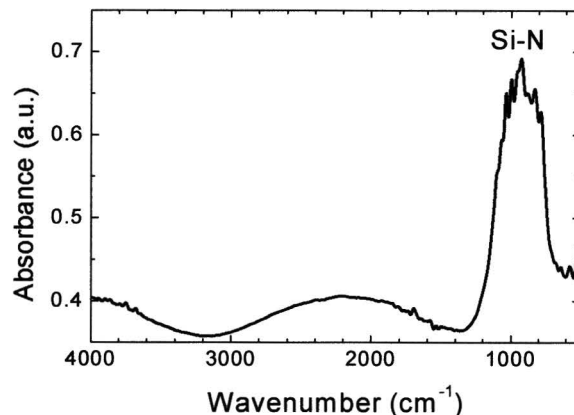


Figure 1: FTIR spectrum of a 1.2- μm -thick as-deposited SRN layer. Note that there is no N-H related absorption at 3350 cm^{-1} . The sinusoidal shape is due to etalon effects in the measurement setup.

The FTIR analysis shows that the amount of N-H bonds in our as-deposited SRN layers is lower than the detection limit of FTIR. This observation is in agreement with published results [4].

Dual prism coupling analysis

Optical loss spectra around the wavelength region of interest of slab SRN waveguides have been measured using dual prism coupling [9]. This

characterization method provides detailed information about N-H related absorption and gives an absolute number for the propagation loss in slab waveguides. This information is useful since losses due to sidewall roughness are excluded, which helps to identify loss mechanisms.

1.2- μm -thick SRN layers deposited onto thermally oxidized silicon wafers were used for this analysis. 2- μm -thick as-deposited PECVD-grown SiON layers with a refractive index of 1.52 on similar wafers were used as a reference.

Figure 2 shows a wavelength spectrum of the propagation loss of both an as-deposited SRN layer and an as-deposited SiON layer. The vertical scale is obtained by varying the prism separation [9].

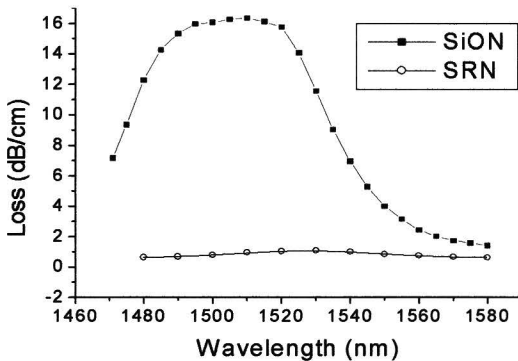


Figure 2: Propagation loss spectrum of an as-deposited SRN slab waveguide and an as-deposited SiON slab waveguide.

Figure 2 confirms that the N-H related absorption in SRN is negligible compared to as-deposited PECVD-grown SiON. The propagation loss in SRN is shown on an expanded scale in figure 3. A small absorption peak can be seen. The height of the peak decreases by annealing at 1100 °C, although it doesn't disappear completely.

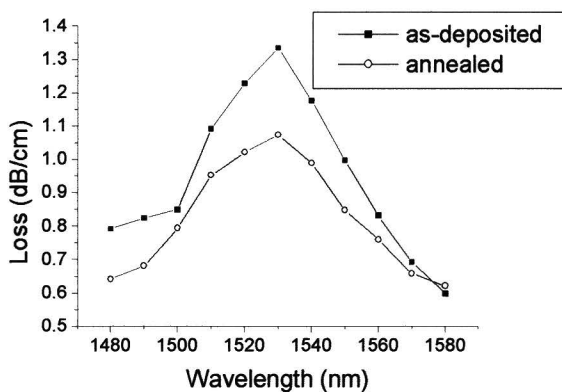


Figure 3: Propagation loss spectrum of an as-deposited SRN slab waveguide and an SRN slab waveguide that has been annealed at 1100 °C.

The propagation loss at a wavelength of 1580 nm is 0.60 ± 0.05 dB/cm.

Propagation loss in channel waveguides

The cutback method was used to determine the propagation loss in multi-mode SRN channel waveguides (1.3 x 8 μm) [6]. The obtained value is 0.7 ± 0.3 dB/cm. The fact that this value is close to the propagation loss in slab waveguides can be understood by the fact that sidewall roughness doesn't play an important role for multi-mode waveguides of these dimensions.

We expect to be able to determine the propagation loss in single-mode waveguides in the near future.

Conclusions

The analysis of the propagation loss in SRN slab waveguides points out that as-deposited SRN exhibits a small degree of N-H related absorption, which can be reduced by annealing at 1100 °C.

We achieved a propagation loss in high-index SRN slab waveguides as low as 0.60 ± 0.05 dB/cm at a wavelength of 1580 nm, which is a value that is in agreement with loss measurements of multi-mode waveguides. It leads us to conclude that SRN is a promising candidate for applications in high-density integrated optics

Acknowledgements

The dual prism measurements were performed at the University of Twente, The Netherlands. We would like to thank C. G. H. Roeloffzen and A. J. F. Hollink for their contribution to the performance of these measurements.

References

- 1 M. Kawachi, Opt. Quant. Electron., Vol 22 (1990), pp. 391-416.
- 2 G.-L. Bona, et al., Opt. Eng., Vol. 37 (1998), pp 3218-3228.
- 3 Private communications with Hugh Philipp.
- 4 M.-C. Cheng, et al., Sensor Mater., Vol. 11 (1999), pp. 349-358.
- 5 B. C. S. Chou, et al., IEEE Electron. Dev. Lett., Vol. 18 (1997), pp 599-601.
- 6 K. N. Andersen, et al., Accepted for Integrated Photonics Research 2002.
- 7 K. Wörhoff, et al., Journ. Lightwave Tech., Vol 17 (1999), pp. 1401-1407.
- 8 R. Germann, et al., Journ. Electrochem. Soc., Vol. 147 (2000), pp. 2237-2241.
- 9 P. Dannberg, et al., SPIE 2212 (1994), pp 478-483.

78

Bibliography

- [1] D. A. B. Miller, *Physical reasons for optical interconnection*, International Journal of Optoelectronics **11** (3), 155–168 (1997).
- [2] C.H. Fine and L.C. Kimerling, *Biography of a killer technology: optoelectronics drives industrial growth with the speed of light*, OIDA Future Vision Program, (Optoelectronics Industry Development Association), Washington, D.C., USA, 1997.
- [3] C. E. Shannon, *A mathematical theory of communication*, The Bell System Technical Journal **27**, 379–423, 623–656 (1948).
- [4] G.-L. Bona, W. E. Denzel, B. J. Offrein, R. Germann, H. W. M. Salemkink and F. Horst, *Wavelength division multiplexed add/drop ring technology in corporate backbone networks*, Optical Engineering **37** (12), 3218–3228 (1998).
- [5] J. Refi, *Optical Fibers for Optical Networking*, Bell Labs Technical Journal, January-March 1999, 246–261.
- [6] P. P. Mitra and J. B. Stark, *Nonlinear limits to the information capacity of optical fibre communications*, Nature **411**, 1027–1030 (2001).
- [7] B. E. A. Saleh and M. C. Teich, *Fundamentals of photonics*, John Wiley & Sons, New York, USA, 1991, ISBN: 0-471-83965-5.
- [8] G. P. Agrawal, *Fiber-optic communication systems*, John Wiley & Sons, New York, USA, 1997, ISBN: 0-471-17540-4.
- [9] –, *Technology trends on the website of the IST Thematic Network project OPTIMIST: www.ist-optimist.org* (consulted in July 2002).
- [10] A. W. Snyder and J. D. Love, *Optical waveguide theory*, Chapman and Hall, London, UK, 1983, ISBN: 0-412-09950-0.
- [11] F. Ladouceur and J. D. Love, *Silica-based buried channel waveguides and devices*, Chapman and Hall, London, UK, 1996, ISBN: 0-412-57930-8.
- [12] K. Okamoto, *Fundamentals of optical waveguides*, Academic Press, San Diego, USA, 2000, ISBN 0-12-525095-9.
- [13] J. D. Jackson, *Classical electrodynamics*, 3rd ed., John Wiley & Sons, New York, USA, 1999, ISBN: 0-471-30932-X.
- [14] D. J. Griffiths, *Introduction to quantum mechanics*, Prentice Hall, New Jersey, USA, 1995, ISBN: 0-13-124405-1.
- [15] J. D. Joannopoulos, R. D. Meade and J. N. Winn, *Photonic crystals, molding the flow of light*, Princeton University Press, New Jersey, USA, ISBN: 0-691-03744-2.
- [16] M. F. Crommie, C. P. Lutz, D. M. Eigler, *Confinement of electrons to quantum corrals on a metal-surface*, Science **262** (5131): 218–220 (1993).
- [17] C. K. Madsen and J. H. Zhao, *Optical filter design and analysis, a signal processing approach*, John Wiley & Sons, New York, USA, 1999, ISBN: 0-471-21375-6.
- [18] L. Eldada, *Advances in telecom and datacom optical components*, Optical Engineering, **40** (7), 1165–1178 (2001).

- [19] W. Deelman and C. Herben, *Integrated optoelectronics in Indium Phosphide Technology*, whitepaper ThreeFivePhotonics, 2002 available from www.threefivephotonics.com (consulted in July 2002).
- [20] L. Eldada, *The promise of polymers*, SPIE's OE Magazine **2** (5), 26–29 (2002).
- [21] –, *Project information APPTECH (All Polymer Photonic Technologies)* on the website of the IST Thematic Network project OPTIMIST: www.ist-optimist.org (consulted in July 2002).
- [22] H. W. M. Salemink, private communications.
- [23] C. G. P. Herben, D. H. P. Maat, X. J. M. Leijtens, M. R. Leys, Y. S. Oei, and M. K. Smit, *Polarization Independent Dilated WDM Cross-Connect on InP*, IEEE Photonics Technology Letters **11** (12), 1599–1601 (1999).
- [24] J. H. den Besten, R. G. Broeke, M. van Geemert, J. J. M. Binsma, F. Heinrichsdorff, T. van Dongen, T. de Vries, E. A. J. M. Bente, X. J. M. Leijtens and M. K. Smit, *A compact digitally tunable seven-channel ring laser*, IEEE Photonics Technology Letters **14** (6), 753–755 (2002).
- [25] J. Broeng, S. E. Barkou, A. Bjarklev, T. Søndergaard and E. Knudsen, *Review paper: crystal fibre technology*, News from The Danish Optical Society (DOPS-NYT) (2), 22–28 (2000), online available from www.crystal-fibre.com (consulted in July 2002).
- [26] M. Kawachi, *Silica waveguides on silicon and their application to integrated-optic components*, Optical and Quantum Electronics **22**, 391–416 (1990).
- [27] K. Wörhoff, P. V. Lambeck and A. Driessen, *Design tolerance analysis and fabrication of silicon oxynitride based planar optical waveguides for communication devices*, Journal of Lightwave Technology **17** (8), 1401–1407 (1999).
- [28] P. V. Bulkin, P. L. Swart and B. M. Laquet, *Properties and applications of electron cyclotron plasma deposited SiO_xN_y films with graded refractive index profiles*, Journal of Non-Crystalline Solids **187**, 484–488 (1995).
- [29] P. R. Herman, R. S. Marjoribanks, A. Oetl, K. Chen, I. Konovalov and S. Ness, *Laser shaping of photonic materials: deep-ultraviolet and ultrafast lasers*, Applied Surface Science **154-155**, 577–586 (2000).
- [30] Alcatel Optronics: *Selene Stress & Temperature*, version 4.3.00 for Windows NT, Alcatel, Enschede, The Netherlands, (see www.alcatel-optronics.nl, consulted in July 2002).
- [31] C. K. Madsen, G. Lenz, A. J. Bruce, M. A. Cappuzzo, L. T. Gomez, T. N. Nielsen, L. E. Adams and I. Brenner, *An all-pass filter dispersion compensator using planar waveguide ring resonators*, OFC 1999, **4**, 99–101 (1999).
- [32] H. Ou and J. Hübner, *Silica-on-silicon waveguide fabrication*, News from The Danish Optical Society (DOPS-NYT) (2), 39–42 (2001).
- [33] Cisilias, www.cisilias.com (consulted in July 2002).
- [34] R. J. Mears, L. Reckie, I. M. Jauncy and D. N. Payne, *Low-noise erbium-doped fibre amplifier operating at 1.54 μm*, Electronics Letters **23**, 1026–1028 (1987).
- [35] R. Germann, H.W.M. Salemink, R. Beyeler, G.L. Bona, F. Horst, I. Massarek, and B.J. Offrein. *Silicon oxynitride layers for optical waveguide applications*, Journal of the Electrochemical Society, **147**(6): 2237–2241, 2000

- [36] M. M. Spühler, B. J. Offrein, G.-L. Bona, R. Germann, I. Massarek and D. Erni, *A very short planar silica spot-size converter using a nonperiodic segmented waveguide*, *Journal of Lightwave Technology* **16** (9), 1680–1685 (1998).
- [37] B. J. Offrein, R. Germann, F. Horst, H. W. M. Salemink, R. Beyeler and G.-L. Bona, *Resonant coupler-based tunable add-after-drop filter in silicon-oxynitride technology for WDM networks*, *IEEE Journal of Selected Topics in Quantum Electronics* **5** (5), 1400–1406 (1999).
- [38] K. K. Lee, D. R. Lim, L. C. Kimerling, J. Shin and F. Cerrina, *Fabrication of ultralow-loss Si/SiO₂ waveguides by roughness reduction*, *Optics Letters* **26** (23), 1888–1890 (2001).
- [39] J. S. Foresi, D. R. Lim, L. Liao, A. M. Agarwal and L. C. Kimerling, *Small radius bends and large angle splitters in SOI waveguides*, *Proceedings of the SPIE* **3007**, 112–118 (1997).
- [40] K. N. Andersen, P. C. Nielsen, W. E. Svendsen, *Silicon rich nitride films and waveguides*, Integrated Photonics Research, Vancouver, Canada, July 14–19, 2002, IThA4.
- [41] H. T. Philipp, private communications.
- [42] W. D. Callister, *Materials science and engineering: an introduction*, 4th ed., John Wiley & Sons, New York, USA, 1997, ISBN: 0-471-13459-7.
- [43] K. N. Andersen, private communications.
- [44] M.-C. Cheng, C.-P. Chang, W.-S. Huang and R.-S. Huang, *Ultralow-stress silicon rich nitride films for microstructure fabrication*, *Sensors and Materials* **11** (6), 349–358 (1999).
- [45] B. C. S. Chou, J.-S. Shie, C.-N. Chen, *Fabrication of low-stress dielectric thin-film for microsensor applications*, *IEEE Electron Device Letters* **18** (12), 599–601 (1997).
- [46] –, *ITU-T Recommendation G.692 - Optical Interfaces for Multichannel Systems with Optical Amplifiers*, 1998 (www.itu.int, consulted in July 2002).
- [47] C. K. Madsen, *Tunable dispersion compensators based on optical allpass filters*, *IEEE LEOS Newsletter*, **15** (5), 2001, online available from www.ieee.org (consulted in July 2002).
- [48] F. Horst, C. Berendsen, R. Beyeler, G.-L. Bona, R. Germann, H. W. M. Salemink and D. Wiesmann, *Tunable ring resonator dispersion compensators realized in high-refractive-index contrast SiON technology*, ECOC 2000, post-deadline paper.
- [49] F. C. Blom, D. R. van Dijk, H. J. W. M. Hoekstra, A. Driessen and Th. J. A. Popma, *Experimental study of integrated-optics microcavity resonators: Toward an all-optical switching device*, *Applied Physics Letters* **71** (6), 747–749 (1997).
- [50] J. E. Heebner and R. W. Boyd, *Enhanced all-optical switching by use of a nonlinear fiber ring resonator*, *Optics Letters* **24** (12), 847–849 (1999).
- [51] E. Snoeks, G. N. van den Hoven and A. Polman, *Optimization of an Er-doped silica glass optical waveguide amplifier*, *IEEE Journal of Quantum Electronics* **32** (9), 1680–1684 (1996).
- [52] S. Park, S.-S. Kim, L. Wang and S.-T. Ho, *Single-mode lasing operation using a microring resonator as a wavelength selector*, *IEEE Journal of Quantum Electronics* **38** (3), 270–273 (2002).
- [53] C. Manolatou, S. G. Johnson, S. Fan, P. R. Villeneuve, H. A. Haus and J. D. Joannopoulos, *High-density integrated optics*, *Journal of Lightwave Technology* **17** (9), 1682–1692 (1999).

- [54] –, *IBM announces world's fastest silicon-based transistor*, Press release, East Fishkill, New York, USA, June 25, 2001.
- [55] M.J.W. Rodwell, M. Urteaga, Y. Betser, T. Mathew, P. Krishnan, D. Scott, S. Jaganathan, D. Mensa, J. Guthrie, R. Pullela, Q. Leex, B. Agarwal, U. Bhattacharya and S. Long, *Scaling of InGaAs/InAlAs HBTs for high speed mixed-signal and mm-wave ICs*, International Journal of High Speed Electronics and Systems **11** (1), 159–215 (2001).
- [56] T. F. Krauss and R. M. De La Rue, *Photonic crystals at optical wavelengths - past, present and future*, Progress in Quantum Electronics **23** (2), 51–96 (1999).
- [57] J. Sajeew, M. Florescu, *Photonic bandgap materials: towards an all-optical micro-transistor*, Journal of Optics A **3**, S103–S120 (2001).
- [58] L. C. Kimerling, *Photons to the rescue: microelectronics becomes microphotonics*, The Electrochemical Society Interface **9** (2), 28–31 (2000).
- [59] D. A. B. Miller, *Rationale and challenges for optical interconnects to electronic chips*, Proceedings of the IEEE **88** (6), 728–749 (2000).
- [60] C.H. Henry, R. F. Kazarinov, H. J. Lee, K. J. Orlowski and L. E. Katz, *Low loss Si_3N_4 - SiO_2 optical waveguides on Si*, Applied Optics **26** (13), 2621–2624 (1987).
- [61] F. H. P. M. Habraken and A. E. T. Kuiper, *Silicon nitride and oxynitride films*, Materials Science and Engineering **R12** (3), 123–175 (1994).
- [62] Tempres Systems, Inc., Heerde, The Netherlands (see www.tempres.nl, consulted in July 2002).
- [63] K. E. Mattsson, *Silica-on-silicon fabrication technology for telecommunication*, Ph. D. thesis, Mikroelektronik Centret (MIC), DTU, Denmark (1994).
- [64] Metricon Corporation, Pennington, New Jersey, USA (see www.metricon.com, consulted in July 2002).
- [65] P. C. Nielsen, private communications.
- [66] W. A. P. Claassen, H. A. J. Th. W. Pol and A. H. Goemans and A. E. T. Kuiper, *Characterization of silicon-oxynitride films deposited by plasma-enhanced CVD*, Journal of the Electrochemical Society **133** (7), 1458–1464 (1986).
- [67] P. R. Griffiths and J. A. de Haseth, *Fourier transform infrared spectroscopy*, John Wiley & Sons, New York, USA, 1996, ISBN: 0-471-09902-3.
- [68] Oriel Instruments, Stratford, Connecticut, USA (see www.oriel.com, consulted in July 2002).
- [69] –, *MIR 8000TM Modular infrared Fourier transform spectrometer, instruction manual*, Oriel Instruments, Stratford, Connecticut, USA (see www.oriel.com, consulted in July 2002).
- [70] P. Dannberg and A. Bräuer, *Precise waveguide loss measurement by a modified two prism method*, Proceedings of the SPIE **2212**, 478–483 (1994).
- [71] L. Liao, D. R. Lim, A. M. Agarwal, X. Duan, K. K. Lee and L. C. kimerling, *Optical transmission losses in poly crystalline silicon strip waveguides: effects of waveguide dimensions, thermal treatment, hydrogen passivation and wavelength*, Journal of Electronic Materials **29** (12), 1380–1386 (2000).

- [72] H. Nagel, A. G. Aberle and R. Hezel, *Determination of optical constants of semitransparent films and substrates for silicon solar cell applications*, Conference Record, 2nd World Conference on Photovoltaic Energy Conversion (Vienna, Austria, 1998), 1422 - 1425.
- [73] M. Svalgaard, C. V. Poulsen, A. Bjarklev and O. Poulsen, *Direct UV-writing of buried singlemode channel waveguides in Ge-doped silica films*, *Electronic Letters* **30**, 1401–1402 (1994).
- [74] Y. Shani, C. H. Henry, R. C. Kistler, R. F. Kazarinov and K. J. Orlowsky, *Integrated optic adiabatic devices on silicon*, *IEEE Journal of Quantum Electronics* **27** (3), 556–566 (1991).
- [75] –, *IQ-200 Optical Test System*, EXFO, Vanier, Quebec, Canada, 2000 (see www.exfo.com, consulted in July 2002)
- [76] S. M. Sze, *VLSI Technology*, 2nd edition, McGraw-Hill, New York, USA, 1988, ISBN: 0-07-100347.
- [77] –, *Process theory* on the Virtual Cleanroom website of the Georgia Institute of Technology: www.ece.gatech.edu/research/labs/vc (consulted in July 2002).
- [78] –, *Selene, 2D mode solver for integrated optics, software documentation*, version 4.2, Kymata software, Enschede, The Netherlands, 2000 (see www.alcatel-optonics.nl, consulted in July 2002).
- [79] D. A. Zauner, *Integrated optical devices for wavelength division multiplexing using PECVD and direct UV-writing techniques*, Ph. D. thesis, COM, Technical University of Denmark, 2000, ISBN: 87-974-02-6.
- [80] C. Laurent-Lund, *Multilevel integration of optical waveguides*, Ph. D. thesis, MIC, Technical University of Denmark, 1997, ISBN: 87-89935-10-1.
- [81] –, *Labview, graphical programming language*, version 6, National Instruments, Austin, Texas, USA, 2000 (see www.ni.com/labview, consulted in July 2002)
- [82] R. T. Kersten, *A New Method for Measuring Refractive Index and Thickness of Liquid and Deposited Solid Thin Films*, *Optical Communications* **13**, 327 (1975).
- [83] W. E. Svendsen, private communications.